INFORMATION TO USERS

This reproduction was made from a copy of a document sent to us for microfilming. While the most advanced technology has been used to photograph and reproduce this document, the quality of the reproduction is heavily dependent upon the quality of the material submitted.

The following explanation of techniques is provided to help clarify markings or notations which may appear on this reproduction.

1. The sign or "target" for pages apparently lacking from the document photographed is "Missing Page(s)". If it was possible to obtain the missing page(s) or section, they are spliced into the film along with adjacent pages. This may have necessitated cutting through an image and duplicating adjacent pages to assure complete continuity.

2. When an image on the film is obliterated with a round black mark, it is an indication of either blurred copy because of movement during exposure, duplicate copy, or copyrighted materials that should not have been filmed. For blurred pages, a good image of the page can be found in the adjacent frame. If copyrighted materials were deleted, a target note will appear listing the pages in the adjacent frame.

3. When a map, drawing or chart, etc., is part of the material being photographed, a definite method of "sectioning" the material has been followed. It is customary to begin filming at the upper left hand corner of a large sheet and to continue from left to right in equal sections with small overlaps. If necessary, sectioning is continued again–beginning below the first row and continuing on until complete.

4. For illustrations that cannot be satisfactorily reproduced by xerographic means, photographic prints can be purchased at additional cost and inserted into your xerographic copy. These prints are available upon request from the Dissertations Customer Services Department.

5. Some pages in any document may have indistinct print. In all cases the best available copy has been filmed.

University Microfilms International
300 N. Zeeb Road
Ann Arbor, MI 48106

King, Thomas Adrian

COMPUTER ANALYSIS OF LITHOLOGIC AND HYDROTHERMAL ALTERATION ASSEMBLAGES USING MULTISCANNER DATA: SILVER BELL MINING DISTRICT, PIMA COUNTY, ARIZONA

The University of Arizona M.S. 1986

PLEASE NOTE:

In all cases this material has been filmed in the best possible way from the available copy. Problems encountered with this document have been identified here with a check mark ✓.

1. Glossy photographs or pages ✓
2. Colored illustrations, paper or print ✓
3. Photographs with dark background _____
4. Illustrations are poor copy _____
5. Pages with black marks, not original copy _____
6. Print shows through as there is text on both sides of page _____
7. Indistinct, broken or small print on several pages ✓
8. Print exceeds margin requirements _____
9. Tightly bound copy with print lost in spine _____
10. Computer printout pages with indistinct print _____
11. Page(s) _____ lacking when material received, and not available from school or author.
12. Page(s) _____ seem to be missing in numbering only as text follows.
13. Two pages numbered _____. Text follows.
14. Curling and wrinkled pages _____
15. Dissertation contains pages with print at a slant, filmed as received _____
16. Other _____

_____

_____

University
Microfilms
International

COMPUTER ANALYSIS OF LITHOLOGIC AND HYDROTHERMAL ALTERATION ASSEMBLAGES USING MULTISCANNER DATA: SILVER BELL MINING DISTRICT, PIMA COUNTY, ARIZONA

by

THOMAS ADRIAN KING

A Thesis Submitted to the Faculty of the

DEPARTMENT OF MINING AND GEOLOGICAL ENGINEERING

In Partial Fulfillment of the Requirements
For the Degree of

MASTER OF SCIENCE
WITH A MAJOR IN GEOLOGICAL ENGINEERING

In the Graduate College

THE UNIVERSITY OF ARIZONA

1 9 8 6

STATEMENT BY AUTHOR

This thesis has been submitted in partial fulfillment of requirements for an advanced degree at The University of Arizona and is deposited in the University Library to be made available to borrowers under the rules of the Library.

Brief quotations from this thesis are allowable without special permission, provided that accurate acknowledgement of source is made. Requests for permission for extended quotation from or reproduction of this manuscript in whole or in part may be granted by the copyright holder.

SIGNED: Thomas A. King

APPROVAL BY THESIS DIRECTOR

This thesis has been approved on the date shown below:

Charles E. Glass

C. E. GLASS
Professor of Geological Engineering

2/18/86
DATE

TABLE OF CONTENTS

TABLE OF CONTENTS--Continued

LIST OF ILLUSTRATIONS

LIST OF ILLUSTRATIONS -- Continued

LIST OF ILLUSTRATIONS -- Continued

LIST OF TABLES

ABSTRACT

A qualitative technique has been developed for detecting hydrothermal alteration and lithologic units in a Color-Ratio Composite (CRC) image. The technique involves combining mulitscanner data into a single data set and determining color association with rock/alteration type in a CRC prior to image formation.

The technique was developed using data from a NS-001, 8 channel scanner and a M^2S, 11 channel scanner. By combining two multispectral data sets, the analyst has increased flexibility in choosing spectral bands for optimum detection of materials.

The qualitative technique determines spectral separability of materials and optimizes CRC image compilation based upon in situ reflectance values, ratio values, ternary diagrams, chromaticity diagrams and color science theory. The best CRC images corresponded to ternary/chromaticity diagrams that showed optimum separation of the field samples. Also, this technique defines a relationship between rock/alteration type with color in a CRC image.

CHAPTER 1

INTRODUCTION

The use of remotely sensed data in mineral identification and discrimination of hydrothermal alteration assemblage has steadily increased over the past decade. Modern multiple detector scanners are able to acquire vast quantities of spectral reflectance data from earth materials. These spectral reflectance data are commonly acquired by satellite or aircraft scanners; an operation referred to as remote sensing. In the search for minerals and possible ore deposits, remote sensing data consist of wavelength-intensity information, acquired by measuring the intensity of electromagnetic radiation leaving an object at specific wavelengths (Siegal and Gillespie, 1980, p. 6).

This research investigates a technique for combining two digital imagery airborne-scanner data sets to detect hydrothermal alteration assemblages and discriminate lithologies within an ore deposit. The project has several objectives. The first objective is to determine the feasibility of combining two digital imagery data sets from different airborne-multispectral scanners into a single, better data set. The second objective is to use the combined data to detect hydrothermal alteration zones associated with iron-bearing and clay mineralization. The third objective is to develop a qualitative method to uniquely define a relationship between rock/alteration type with color in a Color-Ratio Composite (CRC). This method requires use of normalized

ratio values from spectral reflectance field data, plotting of the results in ternary diagrams, and correlating the results to color spectrum divisions in color triangles or chromaticity diagrams used in color science. The final objective is to determine whether ratios of ratioed spectral bands can be utilized for lithologic discrimination. One can use these methods as a preliminary tool in an exploration program for initial detection of areas of iron-bearing and clay mineralization. The detection of such mineralized areas may indicate that a potential ore deposit lies at or beneath the mineralized surface.

CHAPTER 2

REMOTE SENSING MODEL

Every material has a distinct spectral signature. "By spectral signature is meant a single feature or a pattern of features whose shapes, locations and relative intensities are completely characteristic of a particular material" (Siegal and Gillespie, 1980, p. 27). Therefore, remote sensing is based upon the ability to discriminate among materials by their spectral differences.

Spectral Properties of Materials

The spectral reflectance curves for soil, vegetation (healthy), and water are shown in Figure 2.1 on page four. The shapes, locations and intensities of each curve are evident. Vegetation exhibits a very distinctive spectral signature. A small peak centered at 0.52 micrometers (um) represents chlorophyll absorption by plant leaves. The region form 0.70 - 1.30 um represents a plants general health and internal structure. The steeper the curve form 0.70 - 0.80 um, the healthier the plant. In a false color IR photo this wavelength region is color coded red and is referred to as the "red edge". Finally, three water absorption bands are noted at 1.4, 1.9 and 2.7 um (Goetz, Rock and Rowan, 1983, p. 577).

The soil reflectance curve exhibits little variation. Factors that influence soil spectral signatures are moisture content, texture, surface roughness, iron-oxide presence and organic matter. Reflectance

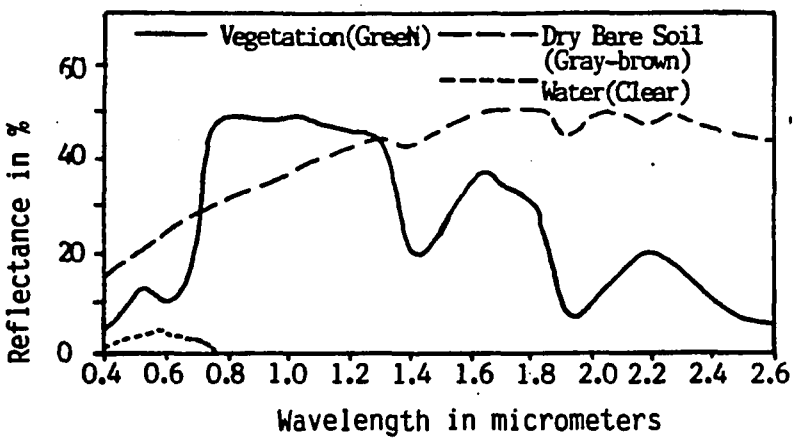

Figure 2.1 Typical spectral reflectance curves for soil, vegetation and water (from Lillesand and Kieffer, 1979, p. 18).

curves for soils are reduced with increased surface roughness, organic material and iron-oxide staining (Lillesand and Kieffer, 1979, p. 19).

Water is highly absorbed in the reflected infrared region. Therefore, locating water bodies within an image can be easily done in the reflected infrared. Clear water appears blue/green as energy below the 0.60 micrometer wavelength is transmitted (Lillesand and Kieffer, 1979, p. 20).

Spectral Properties of Rocks and Minerals

The spectral emittance of minerals and rocks are different for each wavelength region due to varying physical and chemical properties. The physical properties that produce the spectra of rocks and minerals are those of electronic or vibrational processes (Siegal and Gillespie, 1980, p. 28). Electronic processes are prevalent in the visible spectral region while vibrational processes dominate within the near-

infrared, mid-infrared and far-infrared. The electronic and vibrational processes take place within a transition element's crystalline structure (Goetz, et al., 1983, p. 576). "Absorption or emission of specific wavelengths of EM radiation takes place as changes from one energy state to another occur. These changes are referred to as transitions" (Hunt, 1977, p. 503). The electronic transitions found in transition elements result from energy changes in the D-shell electrons within a crystal field of the mineral, and therefore results in absorption features that are characteristic for each particular mineral. These absorption features can be detected through remote sensing operations (Goetz, et al., 1983, p. 576). "It is important to realize that the most common and necessary ingredients of minerals and rocks, namely silicon, aluminum and oxygen do not possess energy levels located in such a way that transitions between them can yield spectral features in the visible and near-infrared range" (Siegal and Gillespie, 1980, p. 29). But, one should not be too alarmed. Iron is a transition element whose electrical properties allow for detection by remote sensing scanners. Iron is "the most common cause of charge transfer and electronic transition absorption features seen in rock and soil reflectance spectra" (Goetz, et al, 1983, p. 576). Iron is ubiquitous, naturally occurring and is the fourth most abundant element on earth. Most of the spectral information determined for geologic materials is due to the presence or absence of iron (Siegal and Gillespie, 1980, p. 29).

Rock and Mineral Spectral Signatures

The main emphasis for the exploration geologist is in applying remote sensing data for defining lithologic units, especially those of hydrothermally altered rocks. Assessment studies have been conducted on specific areas of the spectral region that are useful for detecting lithologic units. "Spectral features that occur in altered rocks derive from both electronic and vibrational processes, principally involving iron or the hydroxyl group" (Hunt and Ashley, 1979, p. 1613). The electronic transitions in the visible and near-infrared range of iron-bearing minerals "produce diagnostic minima near 0.43, 0.65, 0.85 and 0.93 micrometers" (Hunt and Ashley, 1979, p. 1613). The iron-bearing minerals that produce these transitions are hematite, goethite and jarosite. Figure 2.2 on page seven shows the spectral signatures for iron-bearing minerals. The vibrational transitions are developed in clay and water bearing constituents of rocks and minerals, exhibiting spectral features near 1.4, 1.6, 1.75, 1.9 and 2.2 um (Figure 2.3, page seven). The clay minerals of kaolinite, potassium micas, pyrophylite, montmorillonite, diaspore and gypsum are some of the minerals that produce these spectral features.

Hematite and goethite occur in both altered and unaltered areas. The oxide minerals in altered rocks form principally from the weathering of iron sulfides, specifically pyrite. So, the presence of hematite and goethite by themselves does not indicate an area of hydrothermal alteration (Buckingham and Sommer, 1983, p. 664).

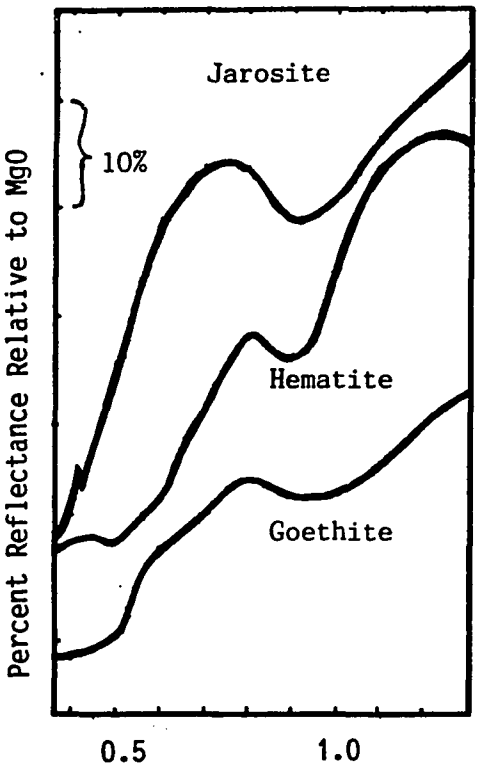

Figure 2.2 Iron-bearing mineral spectra. Features due to electronic transitions in the spectra of iron-bearing minerals common in hydrothermally altered rocks. Spectra displaced vertically for clarity. (adapted from Hunt and Ashley, 1979, p. 1616).

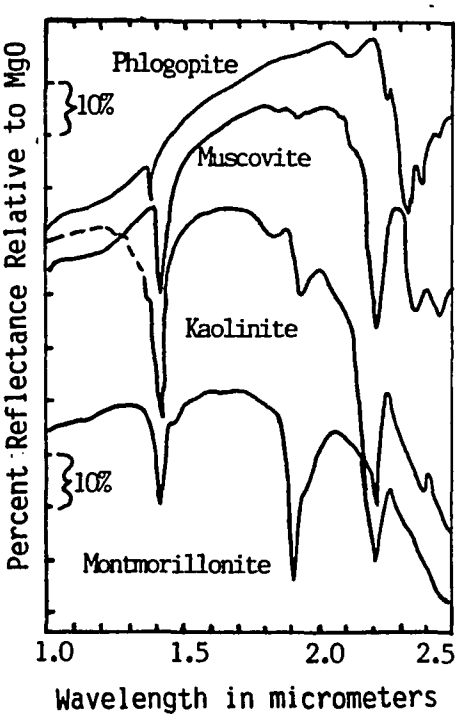

Figure 2.3 Clay mineral spectra. Features due to vibrational processes in the spectra of four hydroxyl-bearing minerals commonly present in hydrothermally altered rocks. Spectra displaced vertically. (adapted from Hunt and Ashley, 1979, p. 1617).

Altered rocks contain higher concentrations of clay minerals than unaltered rocks. Clays form from the break down of feldspars and silicates due to hydrothermal alteration fluids and regular chemical weathering processes. Clay minerals have intense absorption features due to bending and stretching of Al-OH bonds, thus allowing detection of the alteration clays by their unique spectral signatures.

Jarosite and alunite occur in altered regions. When jarosite and alunite are found, they can be considered as diagnostic indicators that the area has undergone some form of hydrothermal alteration. However, the non-occurrence does not indicate non-alteration. Therefore, remote sensing studies in suspected areas of hydrothermal alteration should concentrate on detection of iron forming oxide minerals and the Al-OH clay minerals.

CHAPTER 3

GEOLOGY OF NORTH SILVER BELL

The Silver Bell mining district, located 50 km to the northwest of Tucson, Arizona, contains a large porphyry copper deposit (Figure 3.1, page ten). Two open pit mining operations extracted large quantities of disseminated copper-molybdenum ore, and lesser amounts of silver.

Mineralogically, the area was mainly influenced by events of the Laramide orogeny (Richard and Courtright, 1966, p. 160). The Laramide time was one of active volcanism, base and precious metal mineralization and hydrothermal alteration. The Cu, Mo, and Ag mineralization occurred between 69 and 73 million years ago, and was accompanied by a hydrothermal alteration event (Abrams, et al., 1983, p. 596). Host rocks for copper ore consist of intrusive bodies of alaskite, dacite porphyry and quartz monzonite porphyry. A geologic map of the area is located in Figure 3.2, page eleven.

Lithologically, the north Silver Bell area consists of igneous and sedimentary rocks. Paleozoic limestones (Abrigo Fm) and quartzites (Bolsa) are present in the El Tiro area. The limestones were mined for their thick skarn deposits. The dominant Mesozoic rocks are the ore hosts. Alaskite underlies the western half of El Tiro pit and is host to chalcocite ore. The dacite porphyry underlies the eastern portion of El Tiro pit and is host to some low-grade supergene ore. The Quartz

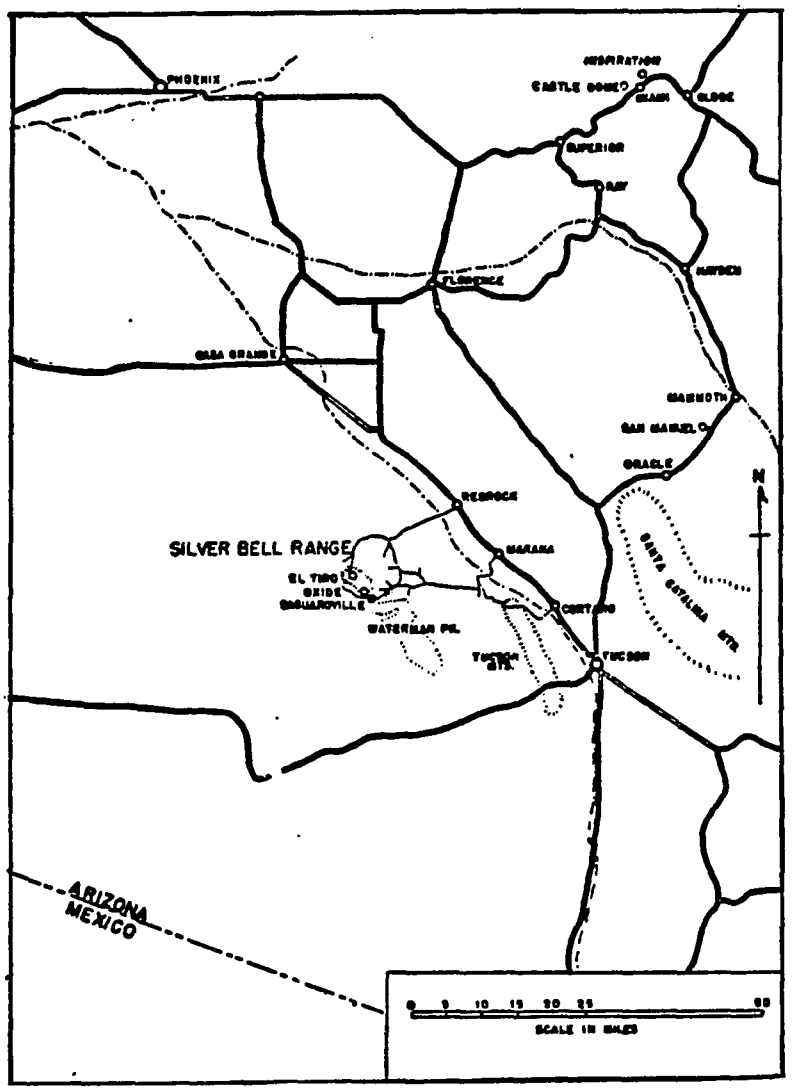

Figure 3.1 Location map. Silver Bell mining district, Southern Arizona (Kerr, 1951, p. 454).

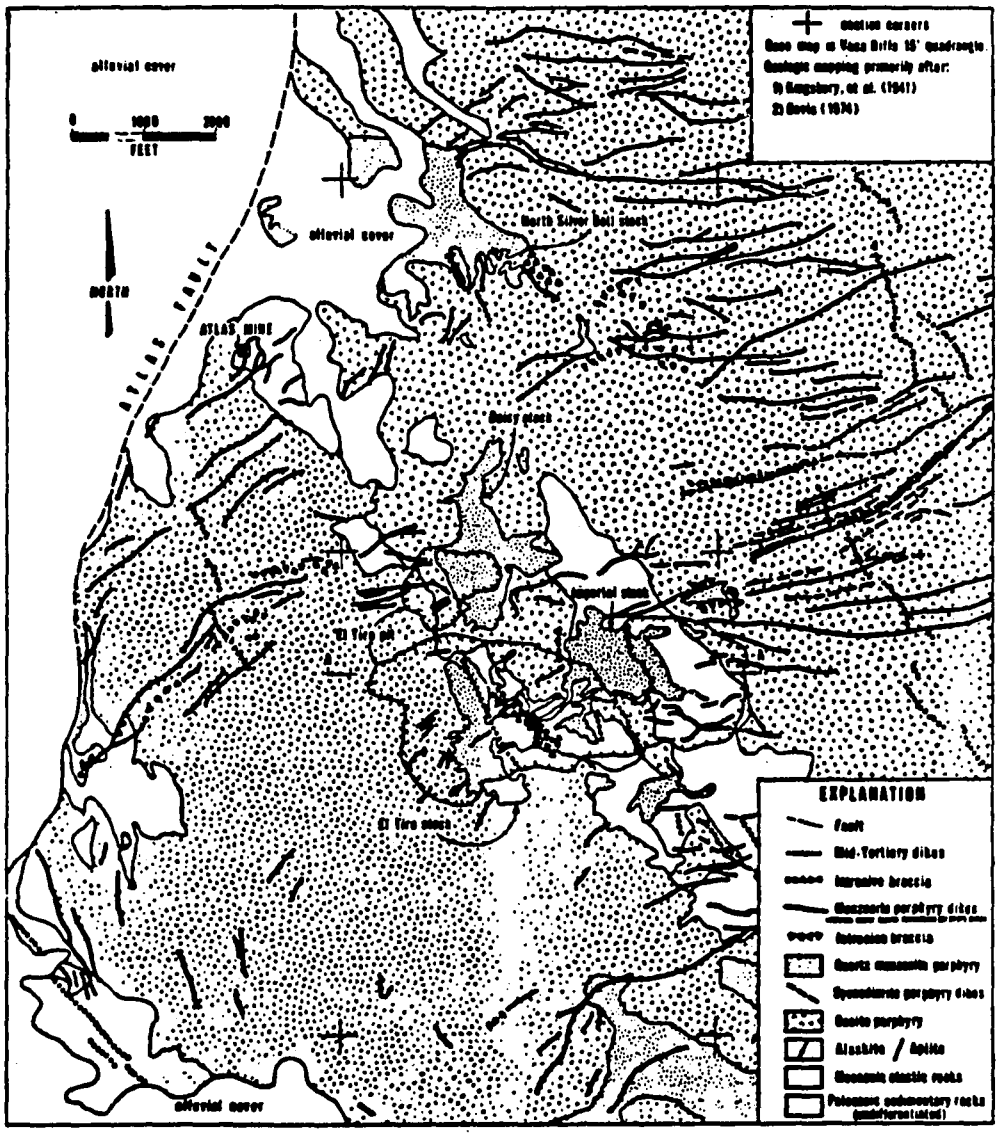

Figure 3.2 Geologic map. El Tiro open pit mine and surrounding area, Silver Bell mining district (geology projected through dump areas)(from Graybeal, 1982, p. 489).

monzonite porphyry is located both in and around El Tiro pit and is host to important hypogene and supergene ore (Graybeal, 1982, p. 490). Cenozoic rocks include volcanic extrusives and sedimentary conglomerates.

The alteration assemblages associated with the hydrothermal event form an elongate zone trending north-northwest. An outer propylitic alteration sequence envelopes the more intense potassic and phyllic alteration zones (Figure 3.3, page 13). The propylitic alteration zone is characterized by the mineral assemblage of epidote-chlorite, with calcite, albite and pyrite. The phyllic zone is characterized by the mineral assemblage of quartz, sericite and pyrite. The phyllic zone overprints the potassic zone. The potassic assemblage is characterized by the minerals of biotite-chalcopyrite, with quartz and pyrite (Graybeal, 1982, p. 493-495). Graybeal stated that the "potassic and propylitic alteration minerals occur largely as selective replacements of mafic minerals and plagioclase" (1982, p. 493). The altered mineral assemblages in the Silver Bell area consist of hydroxyl-bearing minerals, those of kaolinite, sericite, white-mica and montmorillonite. Weathering of the host ore rocks has yielded significant quantities of hematite and goethite gossans (Loghry, 1972).

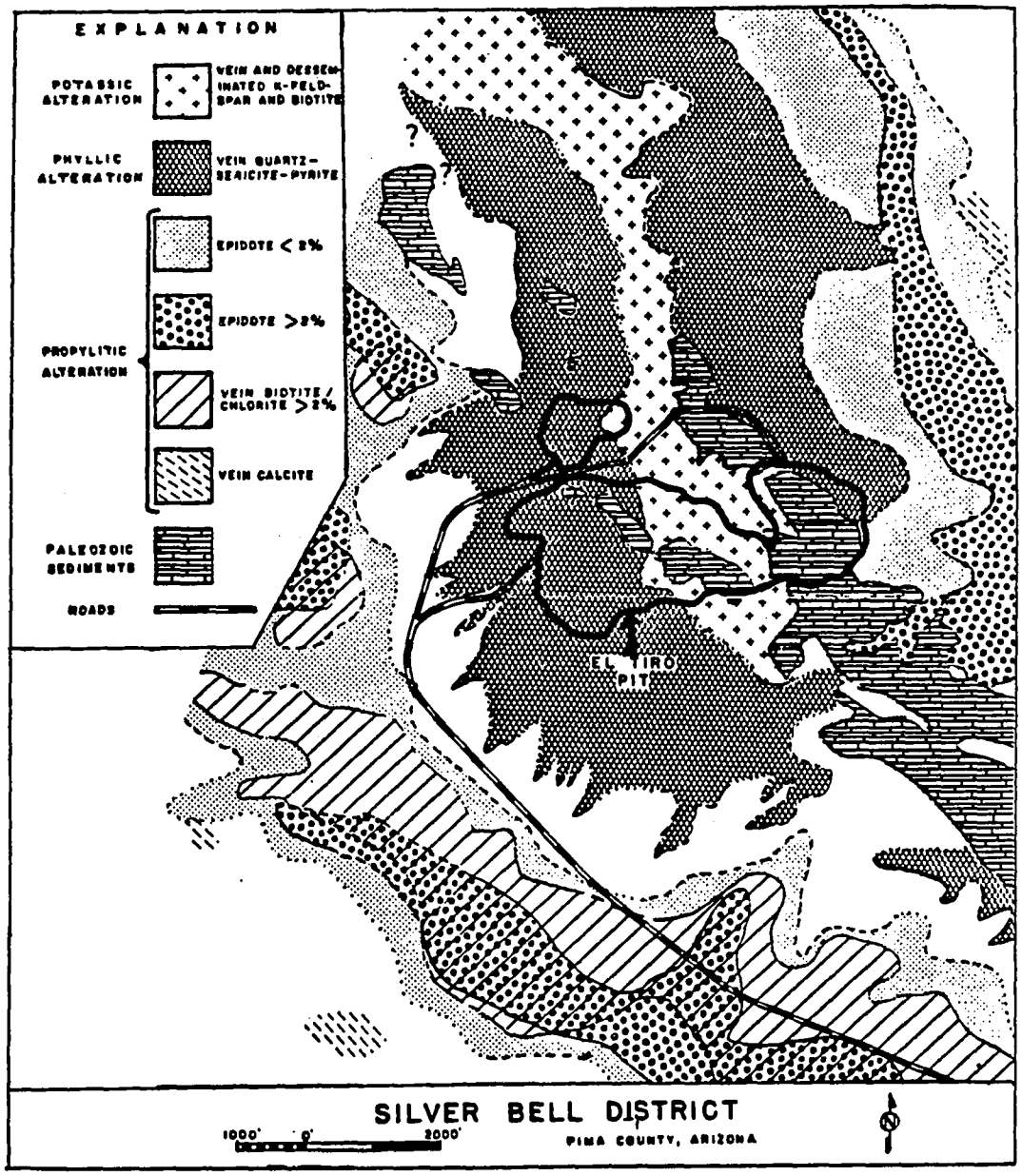

Figure 3.3 Alteration map. North Silver Bell, Silver Bell mining district (from ASARCO, 1985, personal communication).

CHAPTER 4

PROJECT MODEL

Airborne multispectral digital imagery forms the data base for this project. The airborne data were acquired in 1977 and 1978 as part of the NASA/Geosat test case study. The NASA study areas consisted of three porphyry copper deposits, one of which was the Silver Bell mine and surrounding area (Abrams, et al., 1983, p. 592). The study area for this project is the north Silver Bell area of the Silver Bell mining district, encompassing the areas in and around El Tiro open pit mine. The multispectral imagery scenes consist of two data sets: an 8 channel, NS-001 aircraft Thematic Mapper (TM) simulator scanner, and an 11 channel, M^2S aircraft scanner.

Implementation of the objectives, as stated in the introduction, required many steps. First a study area was defined. El Tiro open pit mine was chosen as the study area for several reasons: 1) good alteration and geologic maps for correlation, 2) availability of aerial photographs, 3) availability of an orthophotoquad for ground truth data, and 4) the area shows good lithologic and alteration variation. Second, images of the area were extracted from the original image sets. Each spectral band was extracted to create images with an approximate size of 512 pixels by 512 lines. Third, the two data sets were registered. The two data sets were acquired on different scanning systems, at different altitudes, at different times of the year and at different spatial

resolutions. These differences prohibit non-registered use of the two data sets in computer analyses. Both 8 and 11 channel data sets were registered to an orthophotoquad reference map. The use of the orthophotoquad allowed for accurate geometric registration of the two data sets. The fourth and final step involves the analysis process. Analyses included: 1) Spectral band selection, 2) Atmospheric correction, 3) Computation of spectral band ratios, 4) Selection of ratio pairs from ternary diagrams for alteration detection in Color-Ratio Composites (CRC), and 5) Compute ratios of ratio values for specific enhancement of lithologic units. Three ratio/ratio images were combined in a CRC image for detection of the rock units.

CHAPTER 5

PRE-PROCESSING ANALYSES

The two data sets used in this study were acquired from the original NASA/Geosat data sets. The original data tapes were copied onto new magnetic tapes for permanent inclusion in the Department of Mining and Geological Engineering's digital imagery library. The field data were acquired with the assistance of Ray Sadowski, a geologist affiliated with AMAX Corporation. The field data were recorded as part of the NASA/Geosat test case study in 1978.

Area Subsampling

Once chosen, the study area was located in the image scenes and extracted. The NS-001 (8 channel) data were extracted into images that were 512 pixels by 512 lines. The M^2S (11 channel) data were extracted into images that were 512 pixels by 452 lines. The 11 channel scanner has a lower spatial resolution (approximately 15 meters) than the 8 channel scanner (12 meters), therefore the same area covered by the 11 channel scanner requires less lines than the same area covered by the 8 channel scanner.

Data Set Combination

The use of both data sets was necessary for optimum detection of the alteration assemblages in the study area. The narrow spectral bandwidths of the 11 channel scanner afford better detection of absorb-

tion bands and reflectance peaks of iron-bearing minerals within the visible and near-infrared regions of the electromagnetic (EM) spectrum (Figure 5.1, page 18). The 8 channel scanner can detect reflectance peaks and absorption bands of clay minerals in the near- to far-infrared regions of the EM spectrum (Figure 5.1). The spectral bands and bandwidths for each scanning system are given in Figure 5.2, page 19).

Most previous alteration studies utilized data from only one scanning system. By combining two scanner data sets, the analyst has the opportunity to select the best spectral bands from each data set to combine into a single, better data set. Also this allows the analyst freer reign in design of an analysis program.

Spectral Band Selection

The spectral bands were chosen based upon several criteria: 1) previous research work with spectral reflectance curves of minerals, 2) geology of the study area, and 3) field data. The spectral bands were selected to preferentially enhance areas of iron-bearing and clay mineralization within the alteration zones of El Tiro pit and the surrounding area.

Previous research work proved that specific spectral bands were better than others for hydrothermal alteration detection in mineralized areas. Hunt and his coworkers (1971a and b, 1973a and b, 1974, 1976a and b) have compiled a large listing of spectral reflectance curves for rocks and minerals (for examples, see Figures 2.2 and 2.3). The reflectance curves show absorption bands (0.43, 0.85 and 0.93um for iron-bearing minerals, and 2.20um for clay minerals) and reflectance peaks

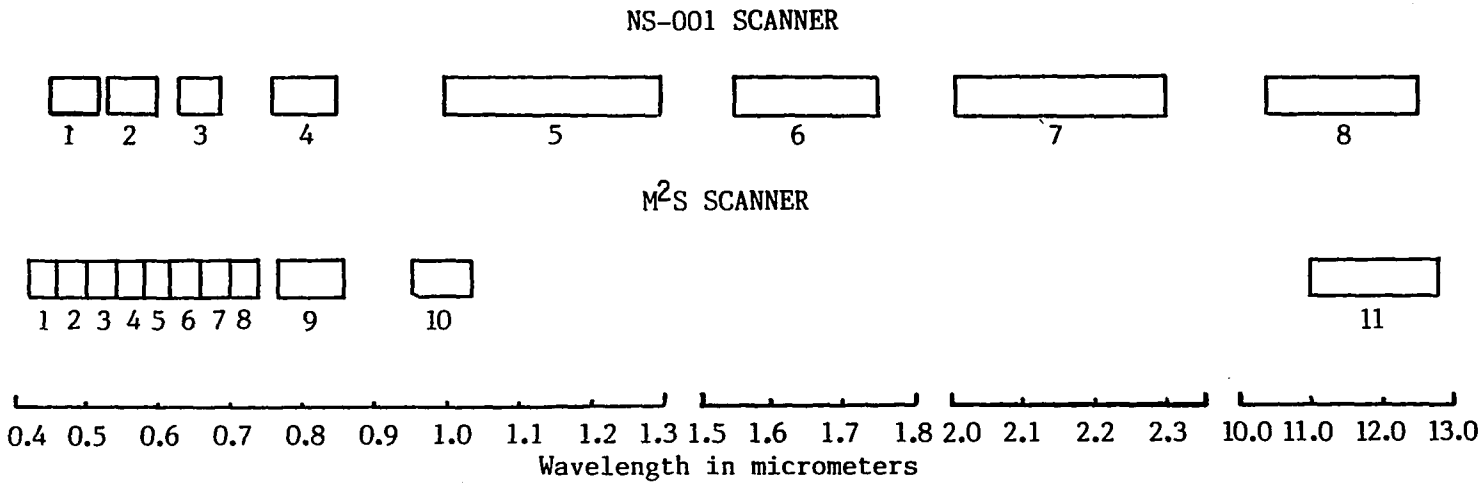

Figure 5.1 Spectral bandwidths for the NS-001 and M^2S scanners.

NS-001		M^2S	
Channel	Bandwidth (um)	Channel	Bandwidth (um)
1	0.45-0.52	1	0.419-0.456
2	0.53-0.60	2	0.457-0.498
3	0.63-0.69	3	0.502-0.541
4	0.76-0.90	4	0.543-0.581
5	1.00-1.30	5	0.581-0.618
6	1.55-1.75	6	0.618-0.658
7	2.08-2.30	7	0.657-0.697
8	10.4-12.5	8	0.699-0.741
		9	0.768-0.861
		10	0.956-1.037
		11	11.00-12.80

Figure 5.2 Spectral bands and bandwidths for the scanners used in the study. Data for NS-001 from Slater, 1985, p.95. Data for the M^2S scanner recorded from image labels. (um = micrometers)

(0.72 and 0.80um for iron-bearing minerals, and 1.65um for clay minerals) that can be utilized in an analysis program for detection of iron-bearing and clay minerals. Rowan, Goetz and Ashley (1977) successfully classified zones of hydrothermal alteration using spectral band ratios to detect absorption bands for iron-bearing minerals (0.90um) of hematite, goethite and jarosite, and for clay minerals (2.20um) of kaolinite and montmorillonite.

The lithology of the study area dictates what mineral species are present. In areas of hydrothermal alteration, clay minerals of kaolinite, illite, montmorillonite and the sulfate alunite are common, along with weathering mineral products of sulfides, such as hematite,

along with weathering mineral products of sulfides, such as hematite, goethite and jarosite. The alteration associated minerals as mentioned above are found in the study area (refer to Ch 3 for alteration minerals). Therefore, spectral bands were selected to detect these particular mineral species, specifically to detect the absorption bands and reflectance peaks that characterize these minerals.

Finally, field data were obtained for the major rock types within the study area. The data consisted of spectral reflectance curves (Refer to Appendix C). The altered rocks display unique spectral reflectance curves different from unaltered rocks. Absorption bands (0.43 and 2.20um) and reflectance peaks (0.73 and 1.65um) are noted in areas of the spectrum that would indicate the presence of iron and clay bearing minerals. Therefore, based upon all the above criteria, eight spectral bands were selected for use in the study, and are given in Figure 5.3.

Scanner System	Channel	Bandwidth (um)
M^2S	1	0.419-0.456
M^2S	4	0.543-0.581
M^2S	7	0.657-0.697
M^2S	8	0.699-0.741
M^2S	9	0.768-0.861
M^2S	10	0.956-1.037
NS-001	6	1.55-1.75
NS-001	7	2.08-2.30

Figure 5.3 Spectral Bands used in the study. (um = micrometers)

CHAPTER 6

DIGITAL IMAGE PROCESSING

After the spectral bands were selected, the data sets were registered and atmospherically corrected. First, the 8 channel data set had to be geometrically corrected. This data set was reversed with respect to east and west, due to preprocessing done on the original data set at Johnson Space Center (Realmuto, 1985, p. 36). A reversal program, RVERSE, for use on Geosat images, was written by a fellow graduate student working with the 8 channel data (see Appendix A). Permission was obtained to use the program (Realmuto, 1985).

Image Registration

A method for geometric registration of the two data sets involved warping both data sets to a reference map. The reasons for warping the data sets were: 1) spatial registration was needed prior to computer processing, and 2) the data sets can be warped for geometric fidelity with respect to actual ground surface points. An orthophotoquad was selected as the reference map (Figure 6.1, page 22). Utilization of an orthophotoquad allows for accurate image warping and unique pixel representation of the data points. Therefore, the corrected data sets will represent a planimetric map of the study area.

The warping process involved selecting and digitizing unique points in the orthophotoquad. The points were assigned (x,y) coordinate values for use as reference control points. In performing the digitiza

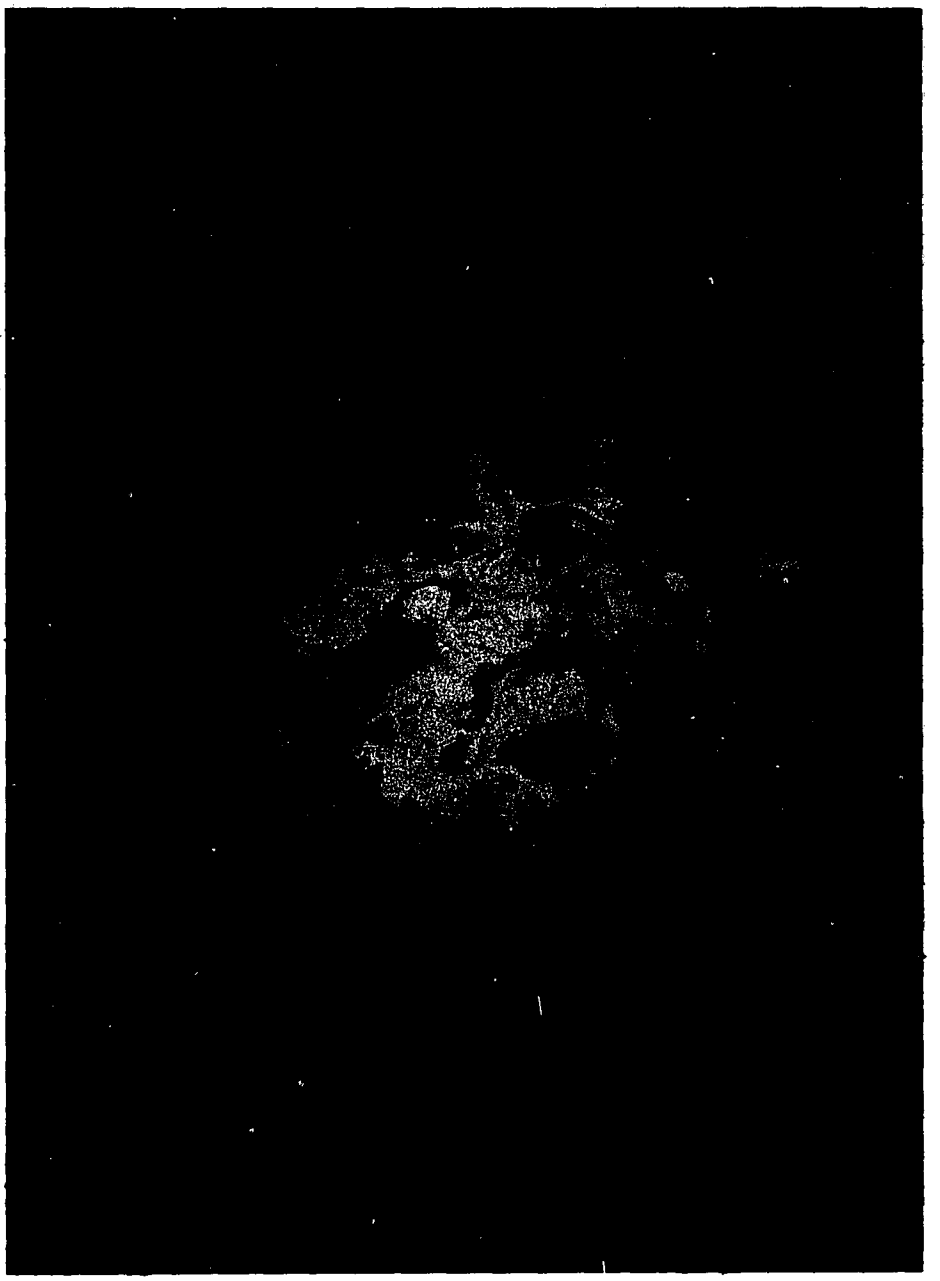

Figure 6.1 Subsection of the Orthophotoquad used as a reference map (from Vaca Hills NE, Ariz., N3222.5-W11130/7.5, Orthophotoquad, 1972).

tion, the reference map was oriented northward. Therefore, the original data sets would undergo an angular, clockwise rotation, from southeast to due north, in the warping process. Control points consisted of unique landmarks within the three data sets, such as crossroads, ridge crests, mine workings and stream confluences.

Over 50 control points were selected from which only 18 were used in the warping process. More control points than necessary were selected to provide the best possible selection and spacing of the control point pairs. A widely spaced control point pattern provides a truer transformation of the data sets to the reference coordinates of the orthophotoquad.

Once the reference control points were selected and digitized, they were located in the data sets. Pixel coordinates were determined through use of the computer program "POINTS". The POINTS program is part of a computer package in the S511 processing system available at the Digital Image Analysis Laboratory (DIAL) on the University of Arizona campus. Then, after the control point coordinate pairs were recorded for each image, a two step computer program analysis was used to warp the original data sets to the new coordinates of the reference map.

The first step in the warping process involves a program that performs a correctness of fit upon image and reference control point pairs. The program is called SCOEFF, and is a SADIE 3.0 subroutine program. The program determines image control point coordinates from the reference control points. Many program runs were necessary, changing the selected control points between runs, to sufficiently

reduce errors in image control point pair coordinate calculations. The errors are in terms of pixel unit variations between the actual input image control point coordinates and the calculated control point coordinates from a polynomial distortion model. Refinements of image control point coordinates, for each data set, will reduce the overall Root Mean Square Error (RMSE) between the data sets. The lower the RMSE value, the better the match between the two control point coordinate sets. A low RMSE value (+ or - one) will result in a very good warp or transformation of the original image orientation to the new orientation of the refernce map. The final RMSE value for the 8 channel data set is 1.138 pixels, and the final RMSE value for the 11 channel data set is 1.041 pixels (Refer to Appendix B for control point calculations and RMSE values). The final, refined image control point pairs were then used to transform, or warp, the images to the new reference coordinates.

The second step involved using the final control point pairs in the warping procedure using the SADIE 3.0 subroutine program GEOM. The GEOM subroutine converts the data sets to the reference coordinates. Refer to Appendix A for the computer programs SCOEFF and GEOM.

Warping Analysis

First, the rotation of the images from southeast to due north occurred with very little distortion. Second, the warped images were very small when displayed on the monitor. The images had been reduced in size from their original spatial resolutions (Figures 6.2 to 6.5, pages 25 and 26). Doubling the reference control point coordinates doubled the size of the warped data sets, thus overcoming the image size

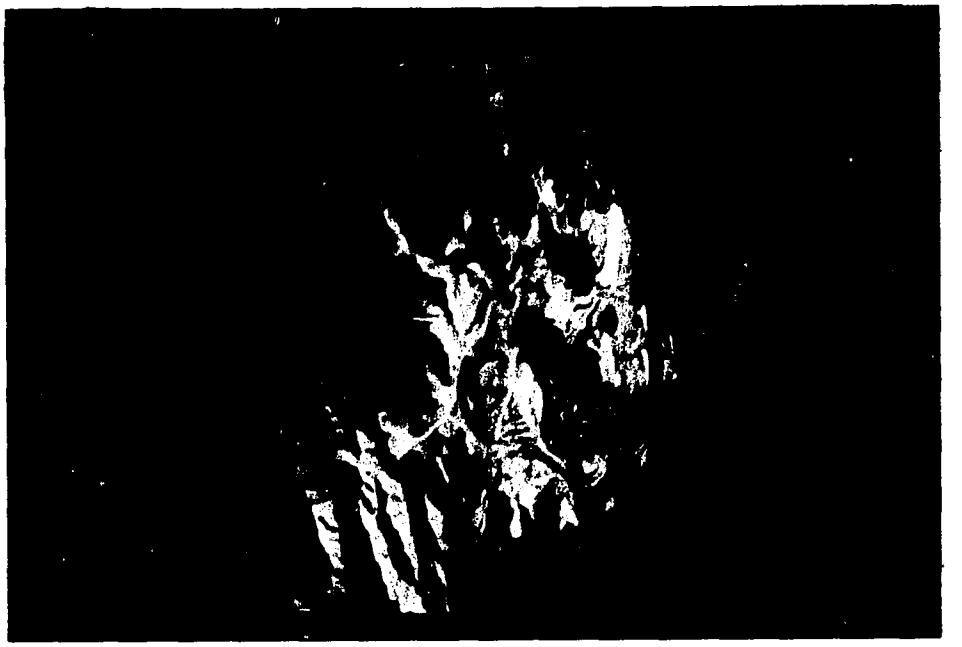

Figure 6.2 Original image: 1.65 um. North Silver Bell area, El Tiro open pit mine.

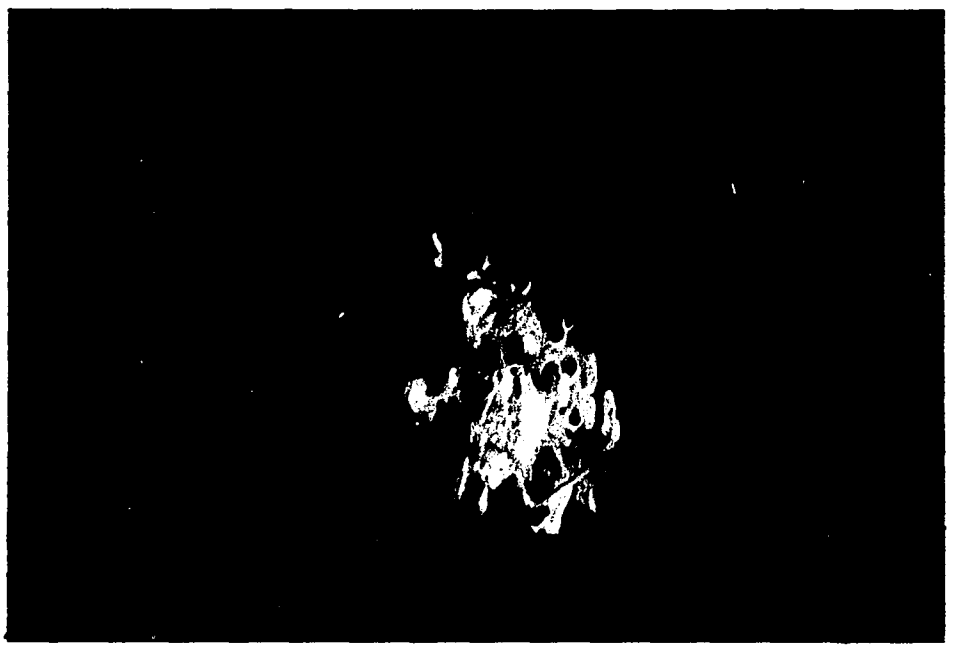

Figure 6.3 Original image: 0.44 um. North Silver Bell area, El Tiro open pit mine.

Figure 6.4 Warped image: 1.65 um. North Silver Bell, El Tiro open pit mine. Original control point pairs used in the registration process.

Figure 6.5 Warped image: 0.44 um. North Silver Bell, El Tiro open pit mine. Original control point pairs used in the registration process.

problem. However the larger images had to be shifted into the display space of the monitor. This was accomplished by selectively determining x and y values to subtract from the doubled reference control point pairs. The new doubled-shifted reference control point pairs were used to warp the data sets.

The final warping results proved excellent. This is seen when one compares the original images to the final warped images (Figures 6.6 to 6.7, pages 28 and 29). Pixel loss from the original images is estimated at 1/4 of the original scene, with the main areas of loss occurring at the edges. One other facet that proved beneficial was that the 11 channel images, originally 512 X 452, were transformed into 512 X 512 images due to the doubling of the control points in the warping routine. Therefore, all the warped images are 512 pixels by 512 lines.

Radiometric Corrections

Radiance values derived from spectral bands of multispectral scanners do not directly relate to the "true" ground reflectance levels. Several factors are known to effect the radiance values, such as electronic sensor bias and atmospheric scatter bias (Lillesand and Kieffer, 1979, p. 558). The bias factors are recorded along with reflectance values by the scanner's sensors and will create inaccurate gray level values (higher) for each image scene. In certain types of image processing, these bias effects can be effectively removed. However, in the case of spectral band ratios, the radiance bias is not removed in the ratio process (Schowengerdt, 1983, p. 152). Therefore, a radiometric correction was performed on the warped images prior to

Figure 6.6 Final warped image: 1.65 um. North Silver Bell, El Tiro open pit mine. Doubled control point pairs used in the registration process.

Figure 6.7 Final warped image: 0.44 um. North Silver Bell, El Tiro open pit mine. Doubled control point pairs used in the registration process.

further analytical processing programs. An assumption was made that the lowest gray level values in each spectral band corresponded to the bias factors.

Atmospheric scattering affects the visible wavelength radiation emitted from an electromagnetic energy source, such as the sun. The atmospheric scatter bias will cause an increase in gray level values in the visible and near infrared spectral region, while it will have little effect on the spectral bands in the mid infrared (1.65 and 2.20 um). The electronic bias, different for different bands of the sensor, could also cause an increase in gray level values. Both bias factors cause constant gray level value increases in each spectral band. Therefore, both bias factors were removed from the image scenes simultaneously. The correction procedure involved subtracting the lowest gray level value from each pixel in each spectral band.

Reflectance values for water in an image scene should exhibit irradiance values of zero in the NIR. Images acquired in the NIR spectral region usually have some pixels with gray levels at or very near zero if a water body is present in the scene (Schowengerdt, 1983, p. 152). Deep and clear water bodies provide the best sites for evaluating atmospheric scattering effects upon multispectral imagery scenes. Two areas of water are located in the study area. The water bodies consist of deep leaching ponds. Intensity values (gray levels) were recorded for the ponds. Similar gray level values for pixels within the ponds denoted a uniformity of reflectance and clarity of the water. Also, gray level values for water pixels in each image matched the lowest gray level values for each images histogram (Figure 6.8, page 31).

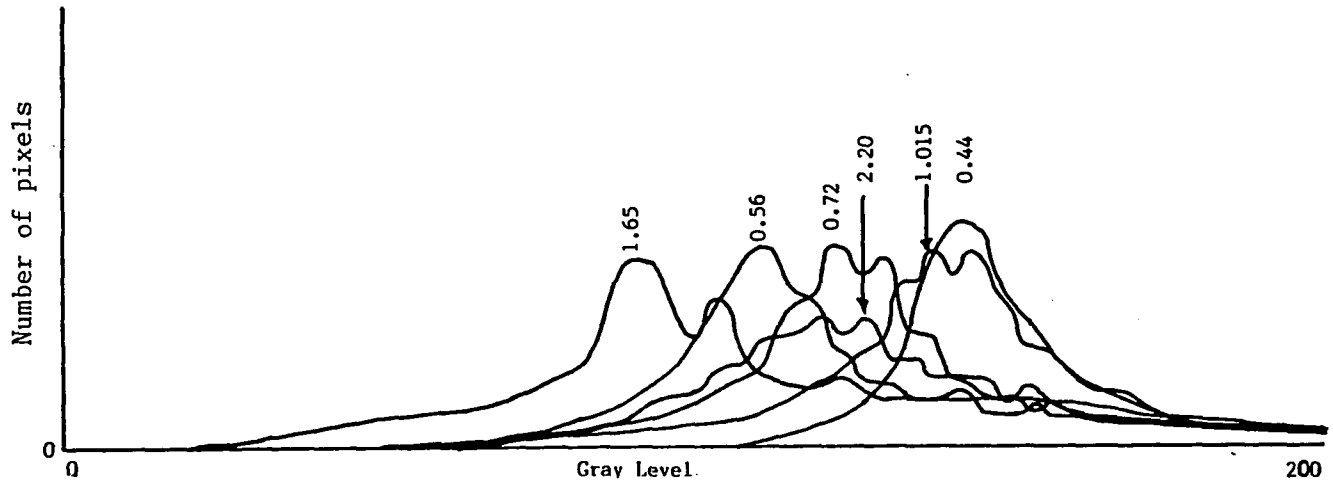

Figure 6.8 Original histograms of the spectral bands used in the study.

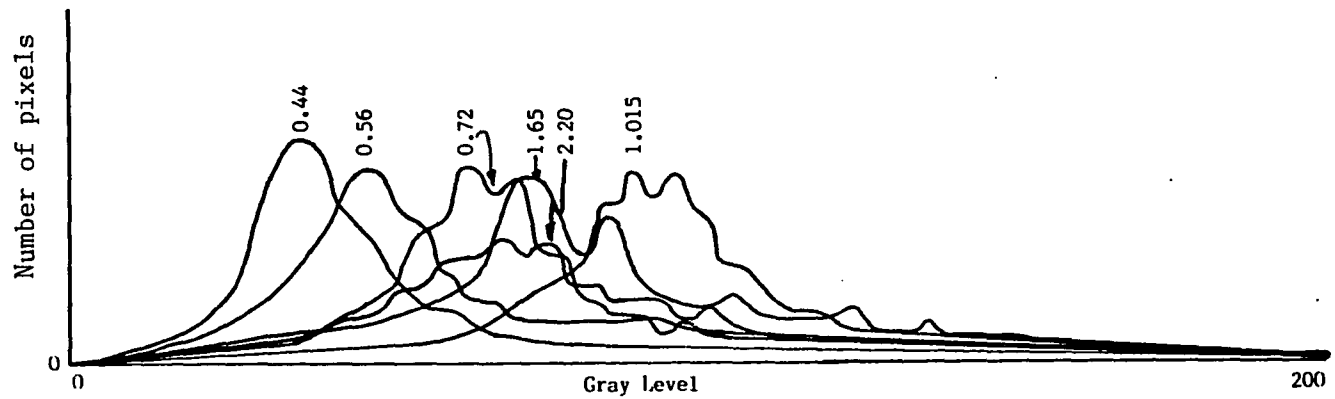

Figure 6.9 Radiometrically corrected histograms.

The displacement of the low end of the histogram from the zero gray level value is therefore assumed to be caused by electronic sensor bias and/or atmospheric scatter. Therefore, the minimum pixel gray level value in each image was subtracted from all pixels in each image. A constant scattering level was assumed for each scene for each spectral scanner at the time of the recordings (Schowengerdt, 1983, p. 153). The new, corrected histograms of each image are shown in Figure 6.9, page 31.

CHAPTER 7

DIGITAL IMAGE PROCESSING

The use of spectral band ratios was first developed as a preclassification technique in remote sensing. By calculating ratios of spectral bands, variations in radiance can be used to preferentially enhance one material over another. Processing of this type can:

1) Remove temporally or spatially-varying gain and bias factors. This is accomplished only if these factors are the same in the bands used in the ratio.

2) Suppress radiance variations arising from topographic slope and aspect.

3) Enhance radiance differences between soils and vegetation. (Schowengerdt, 1983, p. 154)

Ratios of spectral bands are calculated by dividing one spectral band by another, pixel by pixel, to produce a new ratio image. The ratio image typically has a low dynamic range in brightness. Therefore, a contrast stretch can be applied for visual enhancement of surficial material variations produced in the ratio process.

Spectral ratios are useful in mineral and/or alteration discrimination if the materials in question exhibit reflectance variations in their spectral curves. For unique mineral discrimination, a ratio of two spectral bands must "show values which are significantly different for different mineral species and quite similar for all samples of a particular mineral" (Whitney, Abrams and Goetz, 1983, p. 694).

Selection of the best ratio pair can be determined by computing ratios and evaluating the results. Reflectance curves for the rocks and vegetation in the study area are necessary for ratio evaluation. Then, a qualitative judgement can be made as to the value of a ratio "by plotting the average ratio values for different ratios for several important minerals (rocks) and noting the variability" (Whitney, et al., 1983, p. 694). Actual numerical values are not of main importance, rather it is the variability of ratio values that will aid in the spectral separation of rocks, vegetation and alteration zones.

Ratio Selection Criteria

The first criterion dealt with combining spectral bands that would effectively suppress gain factors arising from topographic slope and aspect. Ratio pairs from one scanner were selected to eliminate these radiance variations. The variations can be effectively removed in the ratio process if it is the same for both bands (as stated in number one on page 33). Effective elimination of the gain factors can not be accomplished if the ratio pairs consist of spectral bands from both data sets. The two data sets were acquired at different times of the day and at different times of the year. Therefore, scene illumination would be different for both data sets and the resulting ratio image would not effectively remove the gain factors from both spectral bands.

The second criterion dealt with determining ratio pairs that would highlight certain mineral assemblages associated with areas that have undergone hydrothermal alteration and mineralization processes. The two major assemblages that can be detected through ratio techniques

are the hydroxyl bearing minerals (clays) and the iron-bearing minerals. The clay minerals of kaolinite, sericite and montmorillonite and the sulfate alunite are characterized by a reflectance peak at 1.65 um and an absorption band at 2.20 um. Past research work has shown that the ratio pair of 1.65/2.20 can successfully detect clay minerals (Rowan, et al., 1977). The ferric iron minerals, specifically hematite and goethite are characterized by reflectance peaks at 0.73 um and minima at 0.85 and 0.90 um. The ratio pair of 0.73/0.56 has been successfully used for detection of ferric iron mineralization due to surficial iron-oxide staining (Prost, 1980, p. 897).

Field Data Analysis

The use of field data from the north Silver Bell area was the key in determining which spectral bands would provide the most information concerning rock and alteration units. The field data consisted of spectral reflectance curves for rocks in the study area. Initial analysis of the reflectance curves showed absorption bands and reflectance peaks for rock and alteration detection. The reflectance curves for the altered rocks appear very similar to reflectance curves for other altered rocks (Figures 7.1 and 7.2, page 36). Therefore, the altered rocks at north Silver Bell should be detectable through proper spectral band ratio selection.

Tabular and graphical representations of ratio value data were used to determine the best ratio pairs. Spectral reflectance curves used in the project include: 1) three alaskite samples, 2) two dacite porphyry samples, 3) one quartz monzonite sample, 4) a paleozoic

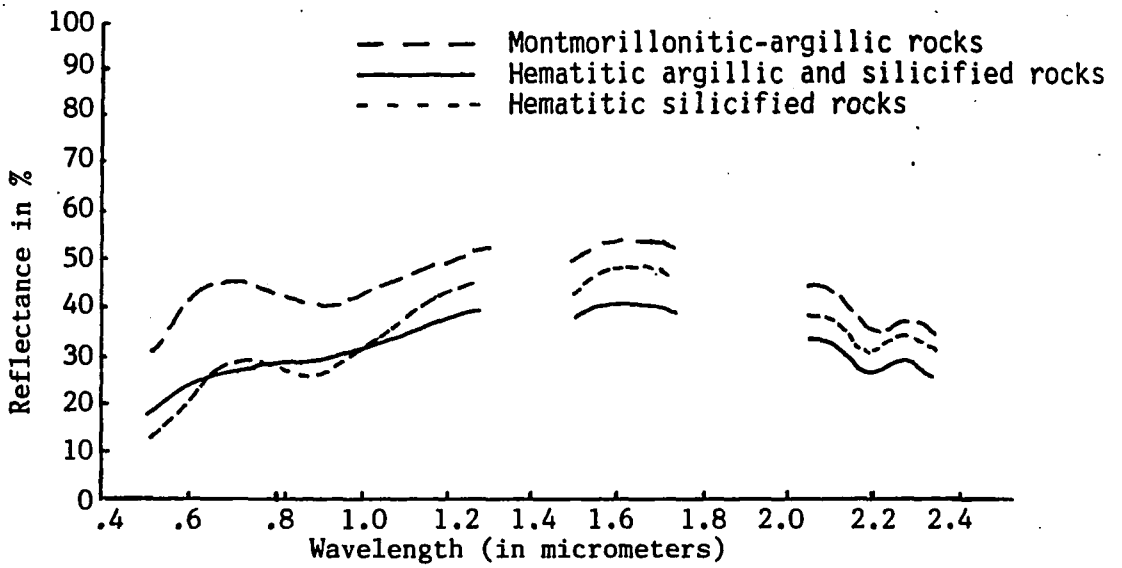

Figure 7.1 In-situ reflectance spectra for altered rocks in the Goldfield, Nevada mining district (Rowan, et al., 1977, p. 525).

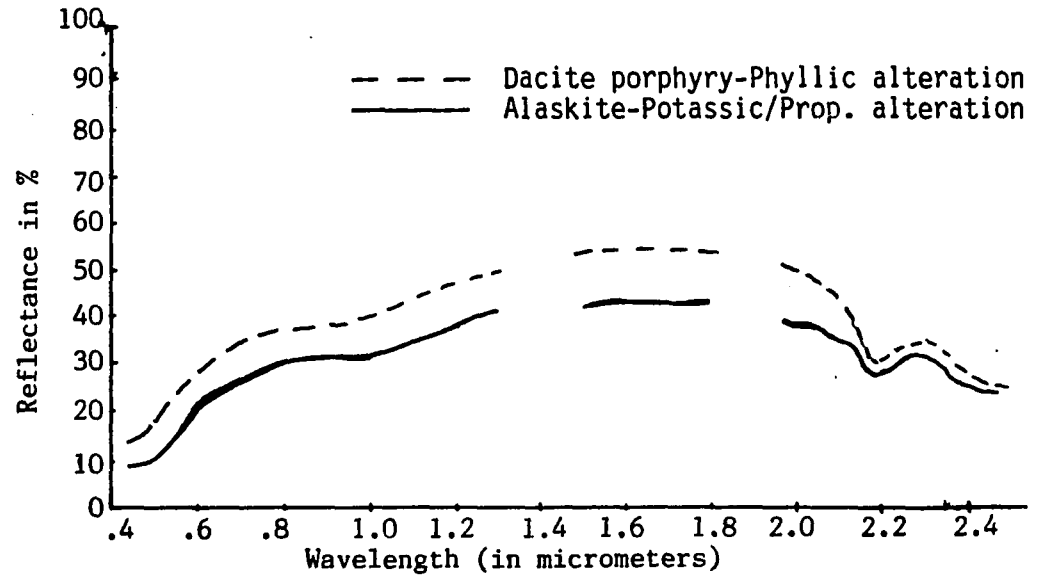

Figure 7.2 In-situ reflectance spectra for two altered rocks in the north Silver Bell mining district.

limestone sample and 5) vegetation samples. Examples of the reflectance curves are given in Appendix C, figures 1 - 8.

Ratio Selection

Reflectance values from eight spectral bands were recorded for each rock/vegetation sample. Ratios for each material were computed from these reflectance values. The spectral band ratios were selected to enhance areas of clay and iron-oxide mineralization (see Appendix D, for percentage reflectance values).

Iron-oxide mineral detection requires use of shorter wavelength spectral bands of the 11 channel scanner. Ratio pairs were selected with similar denominator spectral bands. This was done to provide optimum ratio value variation in discriminating iron-bearing rocks. The spectral bandwidths centered at 0.56 and 1.015 um were selected for denominator bands. Therefore, the spectral band ratio pairs used for possible detection of iron-bearing minerals were:

$$1)\ \frac{\text{Ch } 1,11}{\text{Ch } 4,11} = \frac{0.44}{0.56}, \quad 2)\ \frac{\text{Ch } 8,11}{\text{Ch } 4,11} = \frac{0.72}{0.56}, \quad 3)\ \frac{\text{Ch } 9,11}{\text{Ch } 4,11} = \frac{0.815}{0.56},$$

$$4)\ \frac{\text{Ch } 10,11}{\text{Ch } 4,11} = \frac{1.015}{0.56}, \quad 5)\ \frac{\text{Ch } 1,11}{\text{Ch } 10,11} = \frac{0.44}{1.015}, \quad 6)\ \frac{\text{Ch } 4,11}{\text{Ch } 10,11} = \frac{0.56}{1.015},$$

$$7)\ \frac{\text{Ch } 7,11}{\text{Ch } 10,11} = \frac{0.68}{1.015}, \quad 8)\ \frac{\text{Ch } 8,11}{\text{Ch } 10,11} = \frac{0.72}{1.015}, \quad 9)\ \frac{\text{Ch } 9,11}{\text{Ch } 10,11} = \frac{0.815}{1.015}.$$

Also, three other ratio pairs were selected:

$$10)\ \frac{\text{Ch } 1,11}{\text{Ch } 8,11} = \frac{0.44}{0.72}, \quad 11)\ \frac{\text{Ch } 8,11}{\text{Ch } 1,11} = \frac{0.72}{0.44} \quad \text{and} \quad 12)\ \frac{\text{Ch } 6,8}{\text{Ch } 7,8} = \frac{1.65}{2.20}.$$

Ratio pairs 10 and 11 were chosen based on reflectance peaks at 0.72 um and an absorption band at 0.44 um (Hunt and Ashley, 1979, pp. 1619-20). Ratio pair 12 was chosen for clay mineral detection. Ratio pair values were tabulated for all the field data and are given in Appendix E.

Once the ratio process was complete and the values tabulated, an average value for each ratio pair from each rock/vegetation sample was calculated (Table 1, page 39). Numerical comparison of ratio values can aid in determining rock separability due to spectral reflectance characteristics. If the values are vastly different, then there should be an unique discrimination between the rocks for that particular ratio pair.

Ratio Pairs and CRC Selection

The next step was to determine which ratio pairs could be effectively combined into a Color-Ratio Composite (CRC) for alteration detection. A CRC is an image that combines three ratio images into a colored image, with each ratio image assigned a primary color. Combining three ratio images in a CRC should uniquely define or separate rocks and/or alteration assemblages. Two methods of data representation were employed to determine the best three ratio set for compiling a CRC image: Graphical plots and Ternary Diagrams.

Graphical Method

Initial ratio pair selection was based upon a graphical representation of ratio values (Figure 7.3, page 40). Ratio pairs were combined so that the numerator would have (if possible) a larger reflectance value than the denominator. Therefore, high ratio values, indicated by peaks in the ratio pair graphs, would indicate minerals or

Table 1. Average ratio values for rocks/vegetation samples from the study area. Letters represent specific ratio pairs. Numbers represent actual ratio values.

$1 = \frac{0.44}{0.56}$, $2 = \frac{0.72}{0.56}$, $3 = \frac{0.815}{0.56}$, $4 = \frac{1.015}{0.56}$, $5 = \frac{0.44}{1.015}$, $6 = \frac{0.56}{1.015}$,

$7 = \frac{0.68}{1.015}$, $8 = \frac{0.72}{1.015}$, $9 = \frac{0.815}{1.015}$, $10 = \frac{0.44}{0.72}$, $11 = \frac{0.72}{0.44}$, $12 = \frac{1.65}{2.20}$.

	Ratio Values											
Material	1	2	3	4	5	6	7	8	9	10	11	12
Alaskite:												
52405	0.60	1.78	1.85	2.08	0.29	0.48	0.78	0.85	0.89	0.33	3.01	1.37
52406	0.65	1.62	1.74	1.91	0.34	0.52	0.80	0.87	0.91	0.39	2.55	1.35
52603	0.63	1.57	1.66	1.78	0.36	0.57	0.83	0.88	0.93	0.41	2.49	1.08
Dacite Porphyry:												
52604	0.61	1.59	1.68	1.88	0.33	0.54	0.79	0.85	0.90	0.38	2.61	1.55
52605	0.66	1.59	1.69	1.95	0.34	0.52	0.76	0.82	0.87	0.41	2.43	1.55
Qtz. Mon. Porphyry:												
52602	0.67	1.37	1.44	1.53	0.44	0.65	0.85	0.89	0.94	0.50	2.01	1.17
Limestone:												
52403	0.78	1.23	1.31	1.40	0.57	0.72	0.85	0.89	0.93	0.64	1.57	1.12
Vegetation:												
Manzanita 98	0.80	2.00	3.00	3.30	0.24	0.30	0.30	0.61	0.91	0.40	2.50	1.38
Lt. Clrd. Bush 99	0.70	1.50	1.95	2.40	0.29	0.42	0.48	0.63	0.81	0.47	2.14	1.32
Palo Verde 911	0.67	1.90	2.57	2.38	0.28	0.42	0.32	0.80	1.08	0.35	2.86	1.73

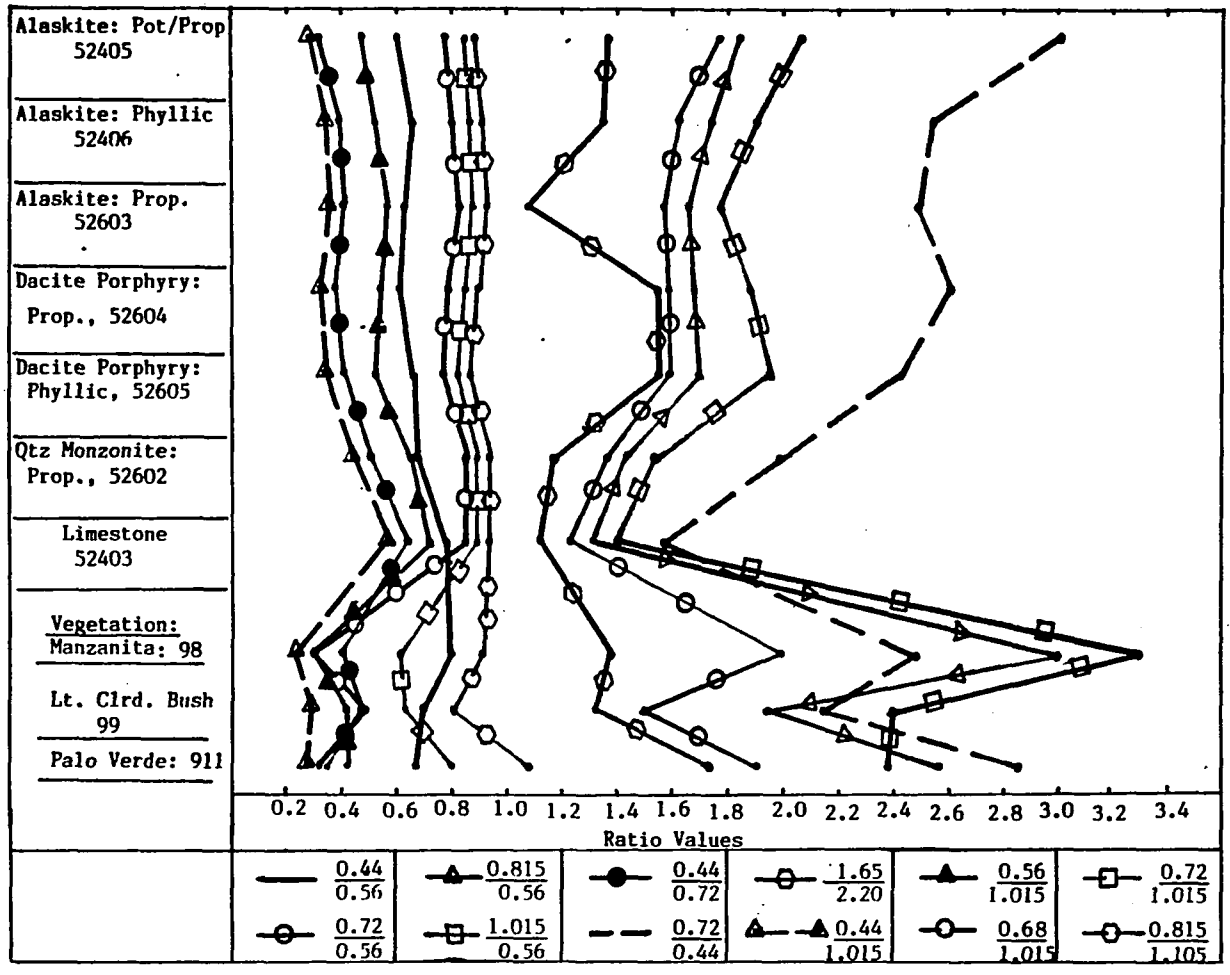

Figure 7.3 Graphical plot of average ratio values for field data. Spectral band ratios showing rock discrimination based on spectral differences.

rocks that could be detected in a ratio image. This representation of ratio values enables the analyst to visually compare different ratio pairs.

Ratio pair selection was based upon visual analysis of Figure 7.3. Ratio pairs were selected that highlighted one rock unit (ratio value peaks) over the rest. Therefore, nine ratio pairs out of twelve were initially selected (Figure 7.4, page 42). Three ratio pairs were not chosen because their ratio values were very similar to other ratio pair values.

The nine ratio pairs were then combined into sets of three ratio pairs. The sets were chosen to determine which three ratio pair set was best for discriminating rock and alteration units. Ratio pair combinations are given in Figures 7.5 to 7.9, pages 43 through 47. Visual analysis of these figures provided initial ratio set selection for CRC compilation. Peaks in the ratio plots indicate rocks that will be highlighted, flat lines indicate similar ratio values amongst different rocks. Therefore, one can determine from the graph those rocks or alteration assemblages that will be enhanced (peaks) through the use of a particular ratio pair for a particular ratio set.

Even in utilizing the graphical method, the process of determining which ratio sets were best for rock and alteration discrimination was still difficult. Therefore, a new method of representing the ratio values for a three ratio set was developed.

	Ratio Pair	Mineral Detection Capability
(1)	0.44/0.56	Jarosite
(2)	0.72/0.56	Iron-oxides
(4)	1.015/0.56	Hematite
(5)	0.44/1.015	Goethite and Jarosite
(6)	0.56/1.015	Iron-oxides
(8)	0.72/1.015	Goethite and Jarosite
(10)	0.44/0.72	Iron-oxides
(11)	0.72/0.44	Iron-oxides
(12)	1.65/2.20	Clay Minerals

Figure 7.4 Ratio pairs selected for use in the study. Numbers in ( ) designate each paricular ratio pair as stated in the text, page 35.

Ternary Diagram Method

Final ratio set selection was based upon a new method for determining spatial and spectral separation of rocks and alteration assemblages. This new qualitative method was developed for determining ratio pair selection, spectral separation of materials and color association with normalized ratio values plotted in a ternary diagram. The new method incorporates ratio values, ternary diagrams and color science theory.

The use of ternary diagrams is new in digital image processing analyses. A ternary diagram is a powerful tool for determining spatial relationships among three normalized data sets. Ternary diagrams have been widely used in geologic analyses to show relationships between chemical composition and mineralogy of rocks and minerals. In this

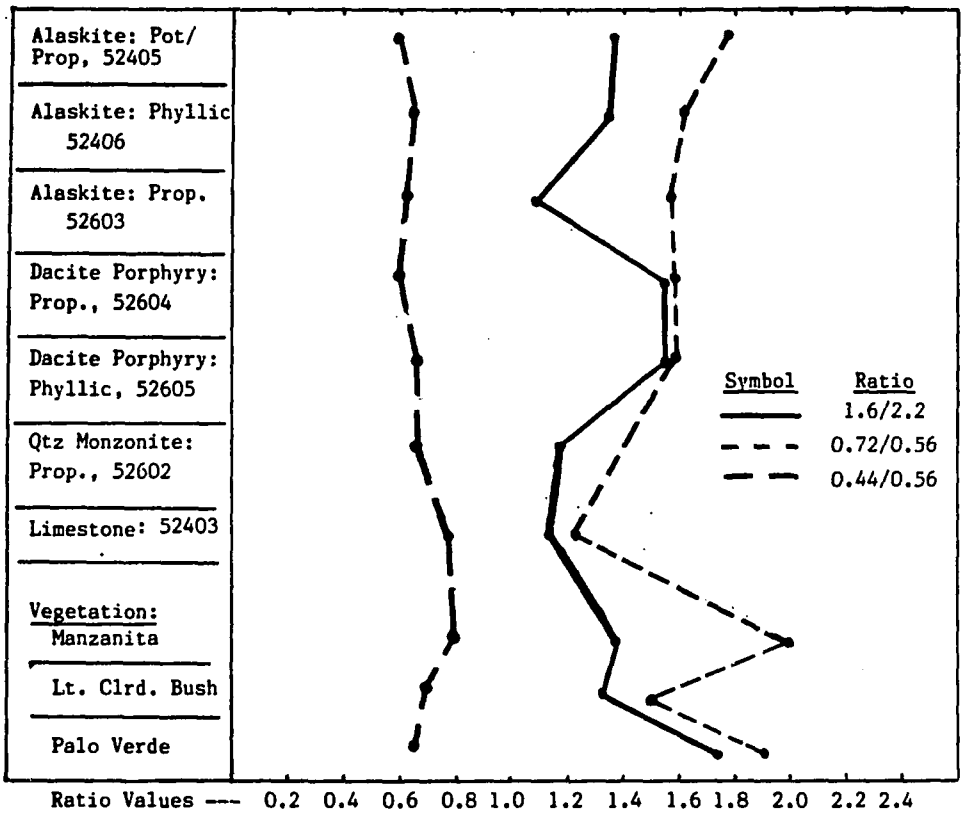

Figure 7.5 Graphical plot: Ratio Set 1. Average ratio values for samples. This ratio pair set shows good distinction between altered and unaltered rocks. Good for dacite detection, less for alaskite.

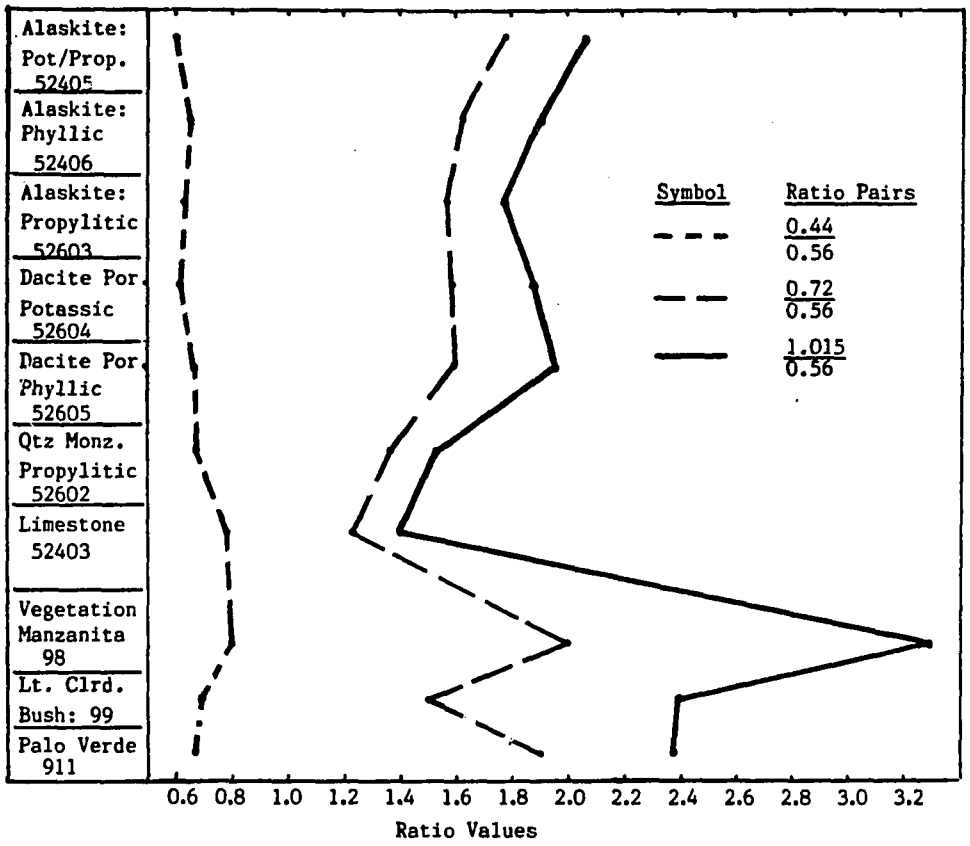

Figure 7.6 Graphical plot: Ratio Set 2. Ratio values for rock and vegetation samples. Vegetation and limestone detectable. Altered rocks non-discriminated with this ratio pair set.

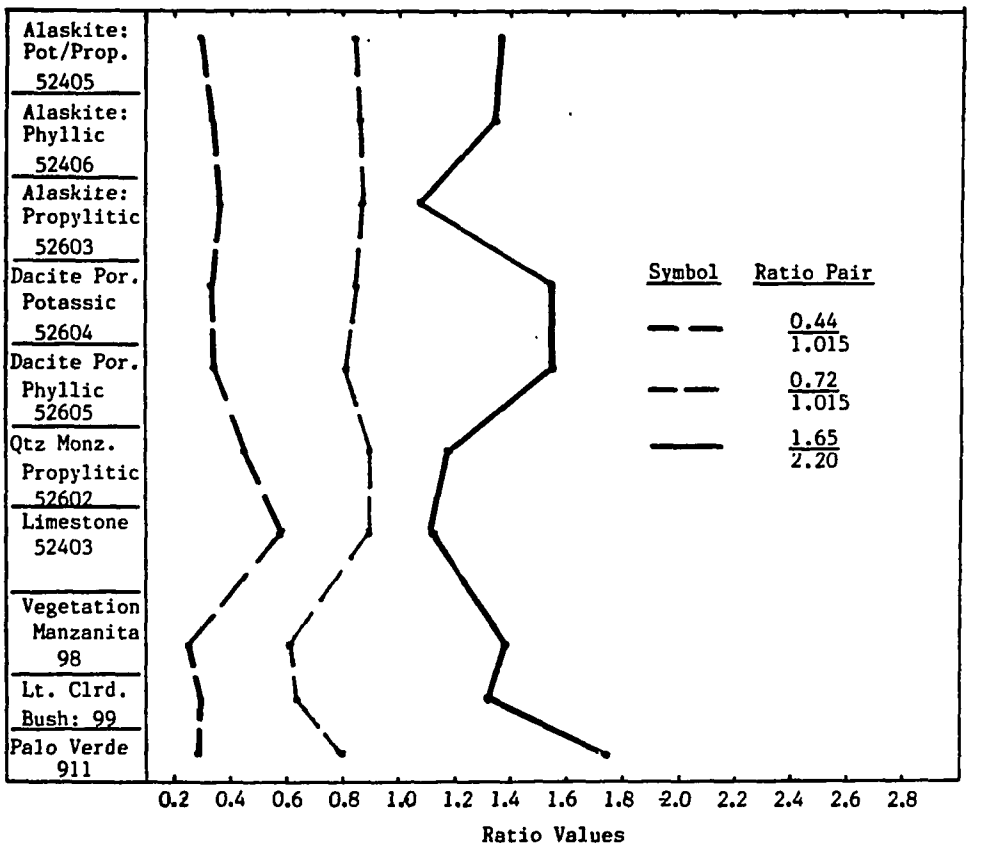

Figure 7.7 Graphical plot: Ratio Set 3. Ratio values for rock and vegetation samples. Excellent ratio set for clay mineral detection (peak in dacites). The potassic/phyllic altered rocks are distinguished from the propylitic altered rocks. Clays will appear bright in the image.

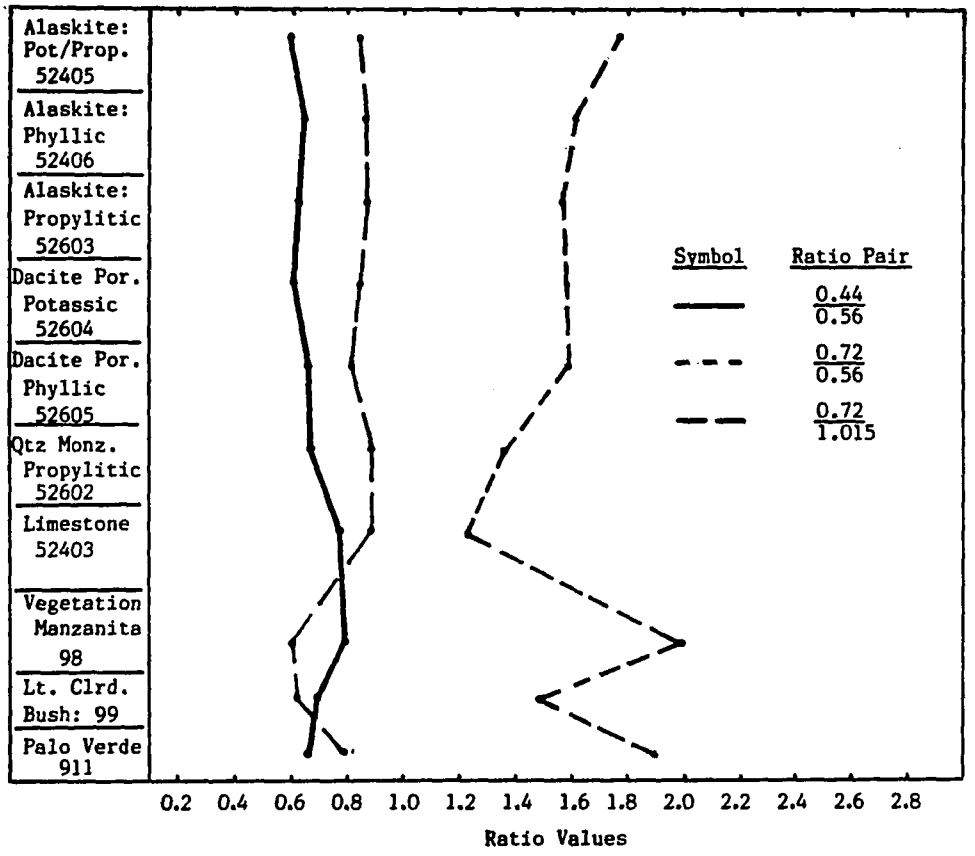

Figure 7.8 Graphical plot: Ratio Set 4. Ratio values for rock and vegetation samples. Good ratio pair set for distinguishing altered from unaltered rocks. Vegetation will appear bright in the image.

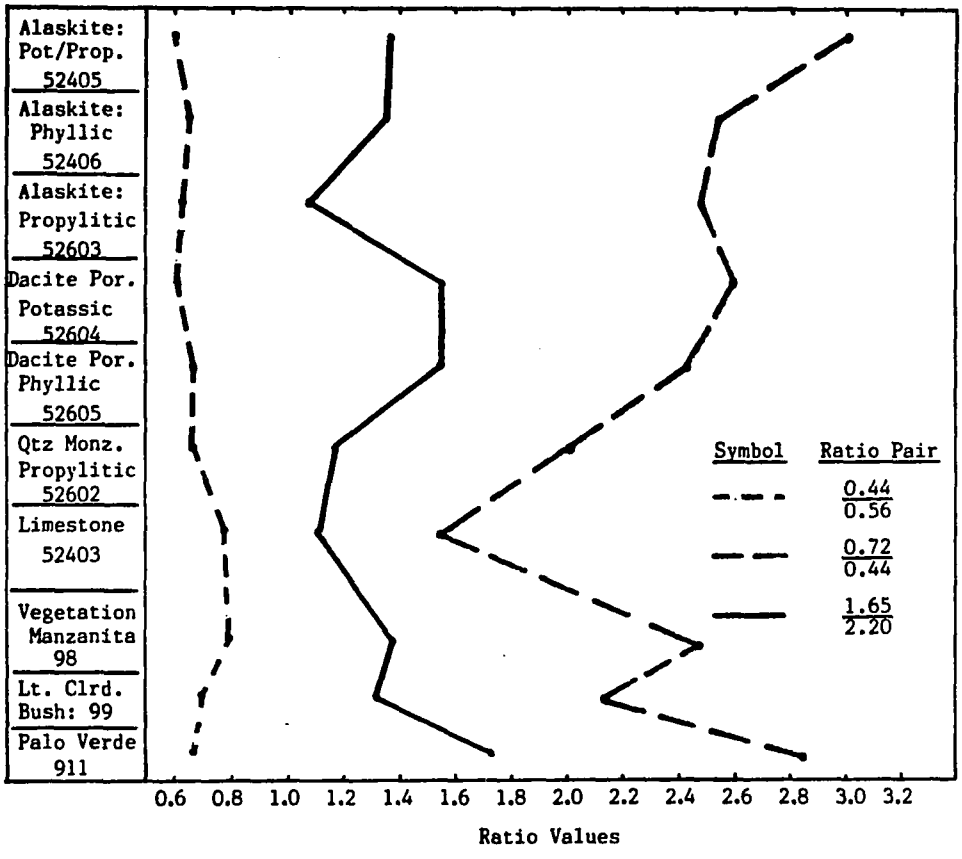

Figure 7.9 Graphical plot: Ratio Set 5. Ratio values for rock and vegetation samples. Excellent distinction between altered and unaltered rocks. The 0.72/0.44 ratio pair should prove useful for alaskite detection.

analysis, the ternary diagram provides an unique and useful method for displaying spectral separation of materials based upon normalized ratio values of three ratio pairs.

Ratio Values/Tristimulus Values. A direct relationship between plotting normalized ratio values in a ternary diagram to color representations in a CRC image is possible through the use of color science theory. First, ratio values computed for each ratio pair in a ratio set are analogous to tristimulus values used in color science. Tristimulus values are defined as "amounts of the three primary (or reference, or matching) stimuli required to give a color match with the color stimulus considered, in a trichromatic system" (Judd and Wyszechi, 1975, p. 377). So, one can define the ratio values as representing the amounts of the three primary stimuli required to make a specific color. The tristimulus values are defined by the symbols X, Y and Z (Clulow, 1972, p. 128). The X, Y and Z values are analogous to the ratio values for each ratio pair, and they will be defined as A, B and C for any given ratio set.

Normalized Ratio Values/Chromaticity Coordinates. Second, the tristimulus values are used in deriving the chromaticity coordinates that define a specific color when plotted in a color triangle. In color science a color triangle or unit color plane, called a chromaticity diagram, is used to represent the color spectrum. The form of the triangle depends on the initial choice of orienting the three primaries in the three-dimensional space (Judd and Wyszechi, 1975, p. 52). The choice is arbitrary and therefore any form of triangle will suffice to describe a chromaticity diagram. "The equilateral form has the

advantage of treating the three primaries in a symmetrical way (Judd and Wyszechi, 1975, p. 52). This is exactly the orientation of a ternary diagram (Figure 7.10, page 50).

The chromaticity coordinates are defined as:

$$x = \frac{X}{X + Y + Z}, \quad y = \frac{Y}{X + Y + Z}, \quad z = \frac{Z}{X + Y + Z}.$$

These coordinates represent the normalized tristimulus values, as their sum totals one: $x + y + z = 1$ (Clulow, 1972, p. 128). This is exactly what is done when ratio values are normalized. The normalization process for ratio values is defined as:

$$a = \frac{A}{A + B + C}, \quad b = \frac{B}{A + B + C}, \quad c = \frac{C}{A + B + C}.$$

Therefore, the process of normalizing ratio values for a ratio set and plotting the normalized values in a ternary diagram (see Figure 7.10) is analogous to determining the chromaticity coordinates from tristimulus values and plotting the coordinates in a chromaticity diagram (Figure 7.11, page 51).

Ternary Diagrams/Chromaticity Diagrams. The chromaticity diagram represents all the spectral colors defined by combinations of the three primary stimuli. By arbitrarily assigning each vertex of the triangle one of the primary stimuli, a spectral locus is defined. The spectral locus defines the color regions, and the area inside the spectral locus curve contains all the physical colors. So, how does this color science analysis relate to color in a CRC image? The ternary diagram has at its vertexes the ratios used for the CRC image. Then, by

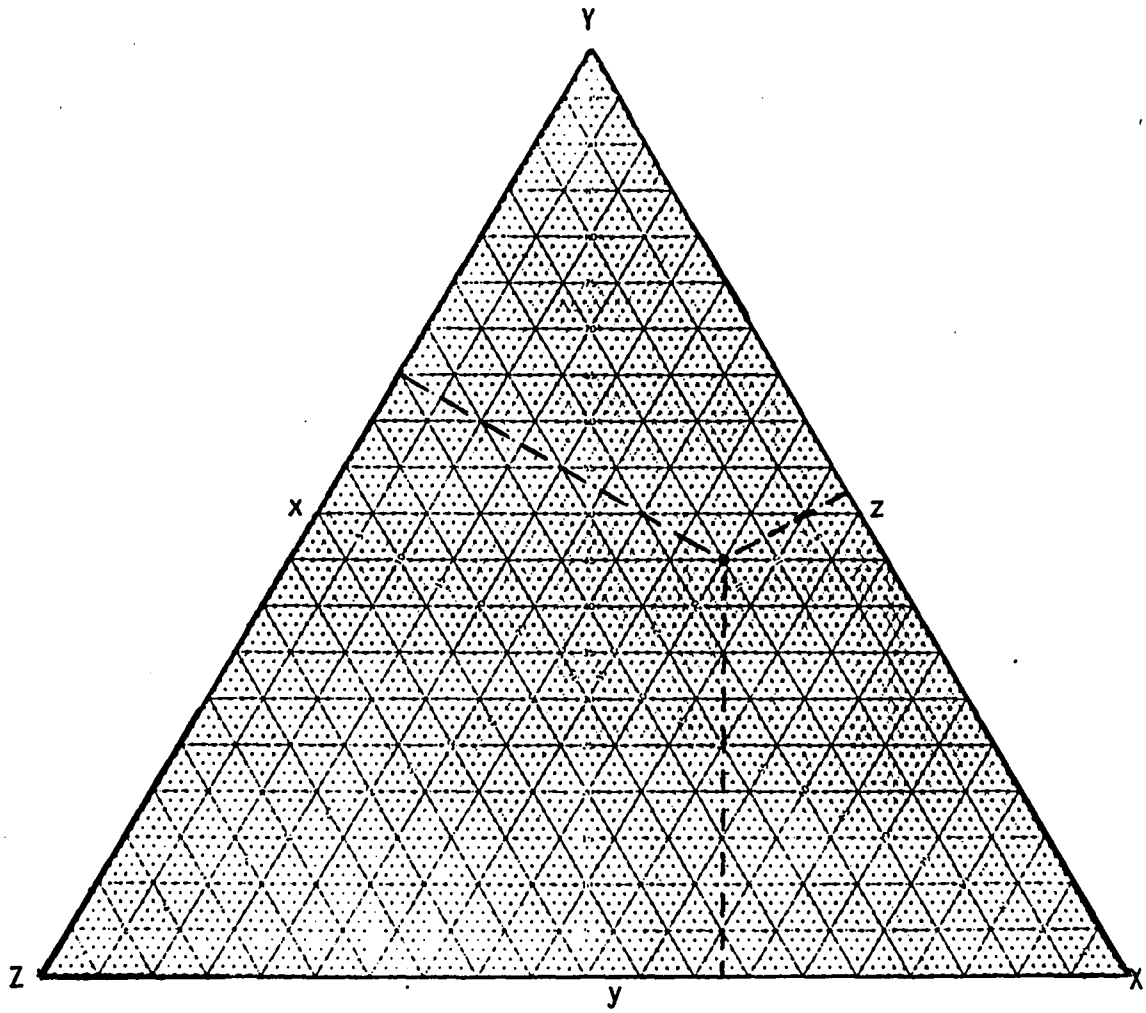

Figure 7.10 Ternary Diagram/Chromaticity Diagram.

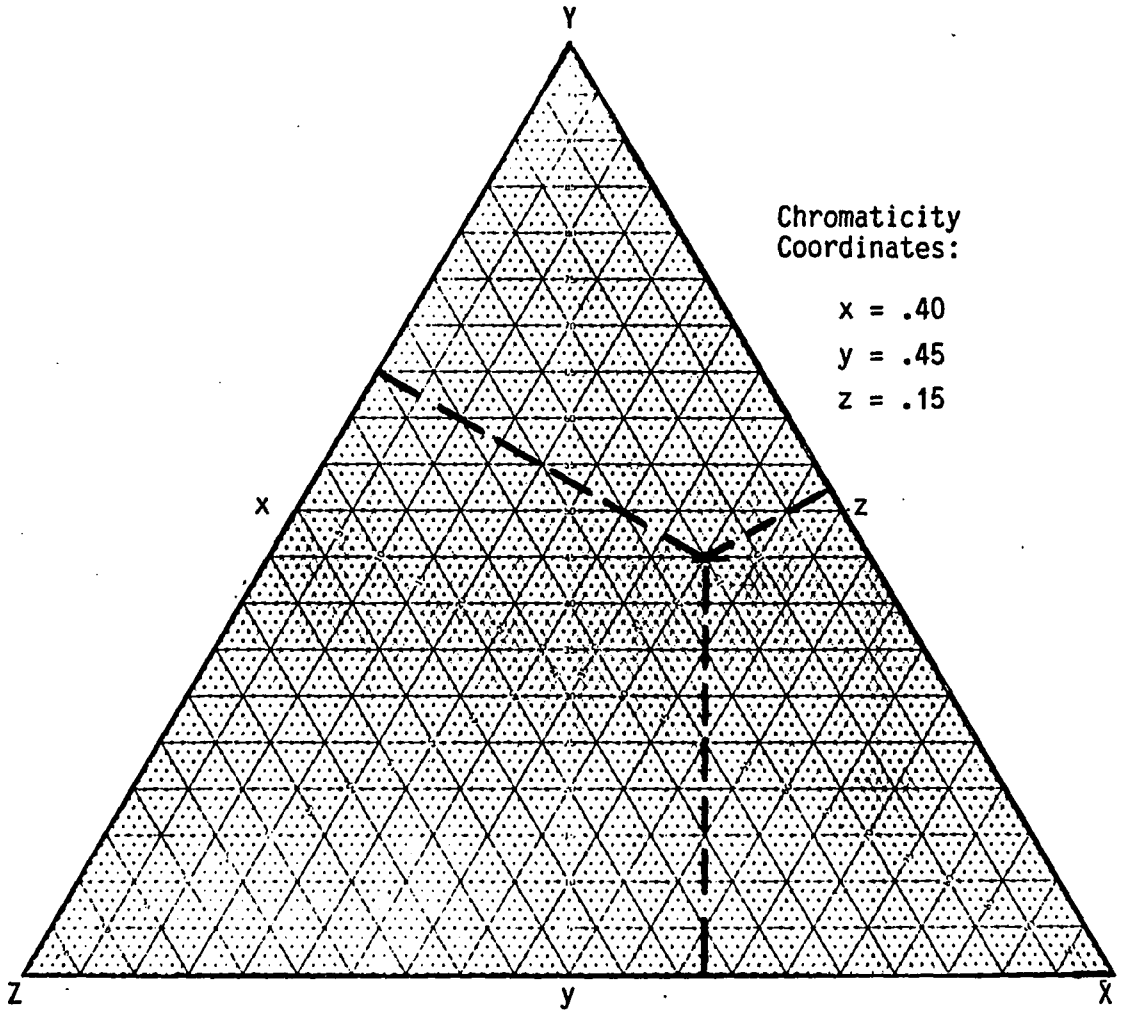

Figure 7.11 Chromaticity Diagram. Chromaticity coordinates: x, y and z. Tristimulus values or Color Coordinates: X, Y and Z (adapted from Bouma, 1971, p. 58).

assigning each ratio pair (each vertex) a primary color (stimuli), as is done when a CRC is compiled, one is transforming the ternary diagram into a chromaticity diagram. Therefore, the points in the diagram that represent normalized ratio values for a particular rock should now represent a unique color (Figure 7.12, page 53). And, colors are what make the CRC so useful in distinguishing rock types and alteration assemblages from other materials.

By using a ternary diagram, one can determine whether certain ratio sets will produce adequate separation of alteration assemblages and/or rock units in a CRC image. The analyst can eliminate ratio sets that produce single data clusters, which would indicate a uniform color distribution for all the materials, and therefore produce a very uniform, non-interpretable CRC image.

So, by assigning each ratio pair to a particular vertex, and then assigning each vertex a primary color (stimuli) corresponding to the color areas of the chromaticity diagram, rock types and alteration zones can be assigned colors by visual inspection of where the normalized ratio values plot in the diagram (Figure 7.12).

The ternary diagram plots provide the necessary information for spectral separation of the rocks. However, most chromaticity diagrams are expressed in a rectilinear-triangular form for ease of data plotting on ordinary rectilinear graph paper. The rectilinear form requires only two of the three coordinates for defining colors in the diagram. Therefore, all the ternary/chromaticity diagrams have been changed into the rectilinear form. Figure 7.13, page 54 shows the transformation

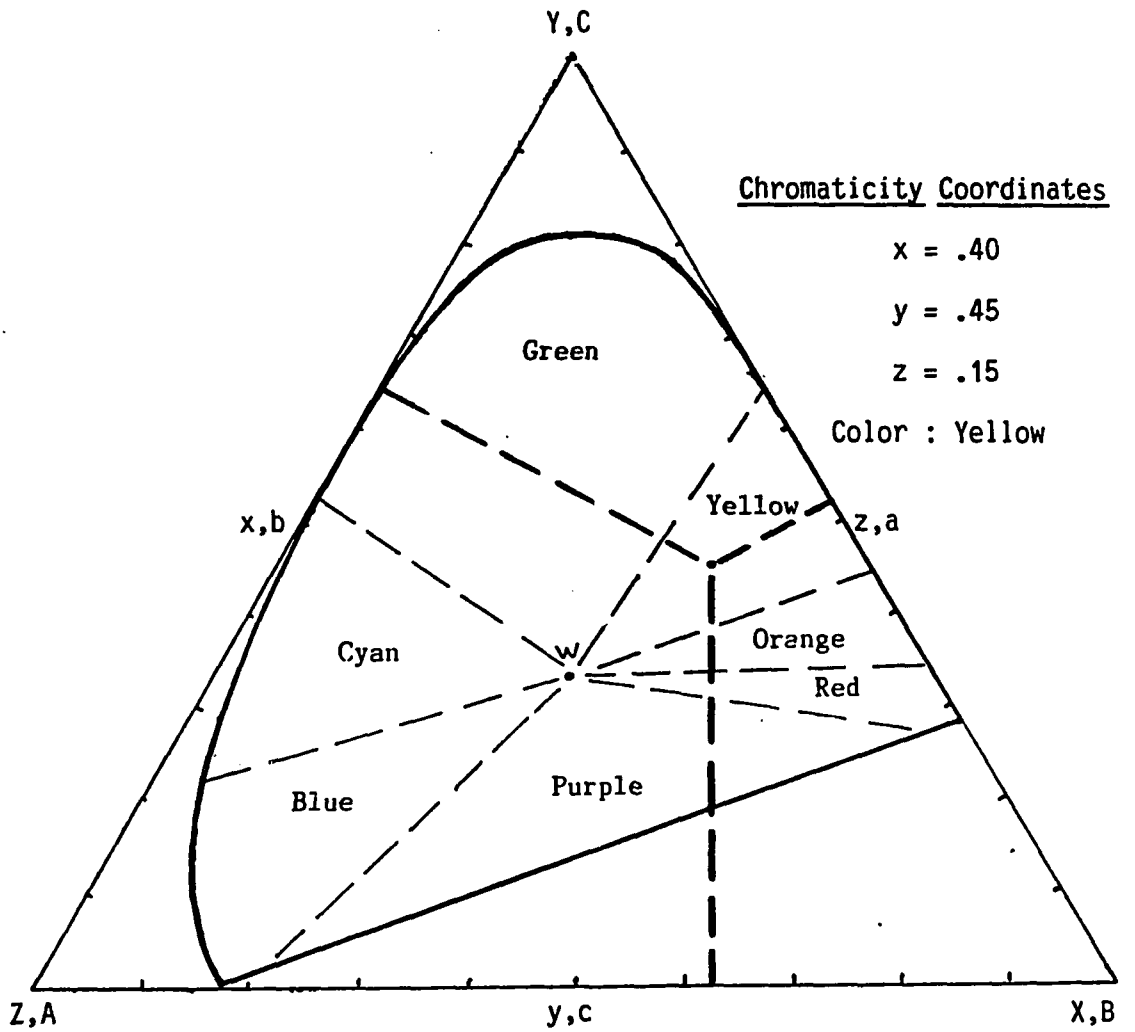

Figure 7.12 Chromaticity diagram with spectral locus. Chromaticity coordinates for a unique point, given by x, y and z (adapted from Bouma, 1971, p. 58).

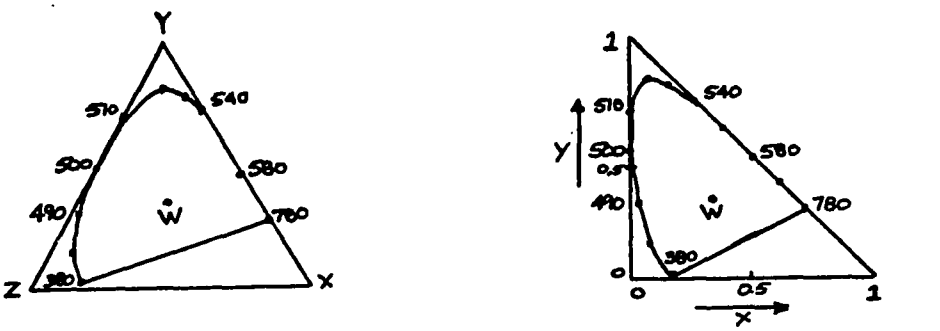

(a) Equilateral form (b) Rectilinear form

Figure 7.13 Chromaticity Diagrams (from Bouma, 1971, p. 58).

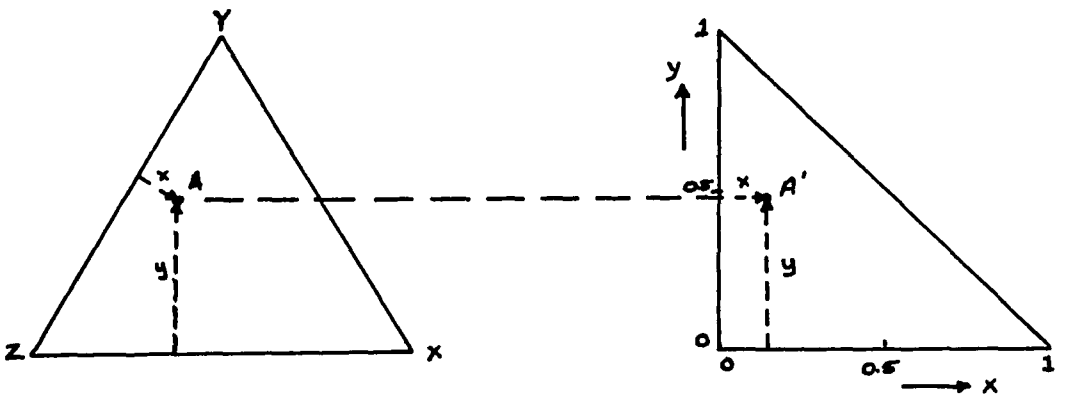

(a) Equilateral form (b) Rectilinear form

Figure 7.14 Transformation from equilateral to rectilinear form for a chromaticity diagram. Point A in (a) plots as A' in (b), where x and y are the chromaticity coordinates (from Bouma, 1971, p. 61).

from the equilateral to rectilinear form, while Figure 7.14, page 54 shows the conversion of data points from one form to the other.

The ternary diagram provides two important pieces of information: 1) it can be used to determine if a particular ratio set will yield spectral separation of rocks and alteration assemblages, and 2) it can aid in determining the colors that each material will exhibit in a CRC image, thus removing most of the awkwardness associated with assigning colors to rocks and alteration zones after the CRC has been formed.

However, there are limitations to this process. The major one concerns field data plotting. The ternary diagram will only show color and spectral separation for the materials represented by the given field data. So, the ternary diagram will qualitatively determine the approximate colorations for each rock and/or alteration type, as it represents an ideal color space, not the color space of the final CRC image.

Final CRC Selection

By combining ratio pairs in ratio sets and plotting the normalized ratio values in ternary diagrams, one can visually ascertain which ratio sets will provide the best spectral separation of materials. The final CRC sets were selected based upon the spread or clustering of data points in the ternary/chromaticity diagrams. Five ratio sets were analyzed (Figures 7.15 - 7.24, pages 56 - 65) and two proved best for optimizing spectral and color separation of lithologic and alteration units. The ratio values for the ratio sets are given in Appendix F.

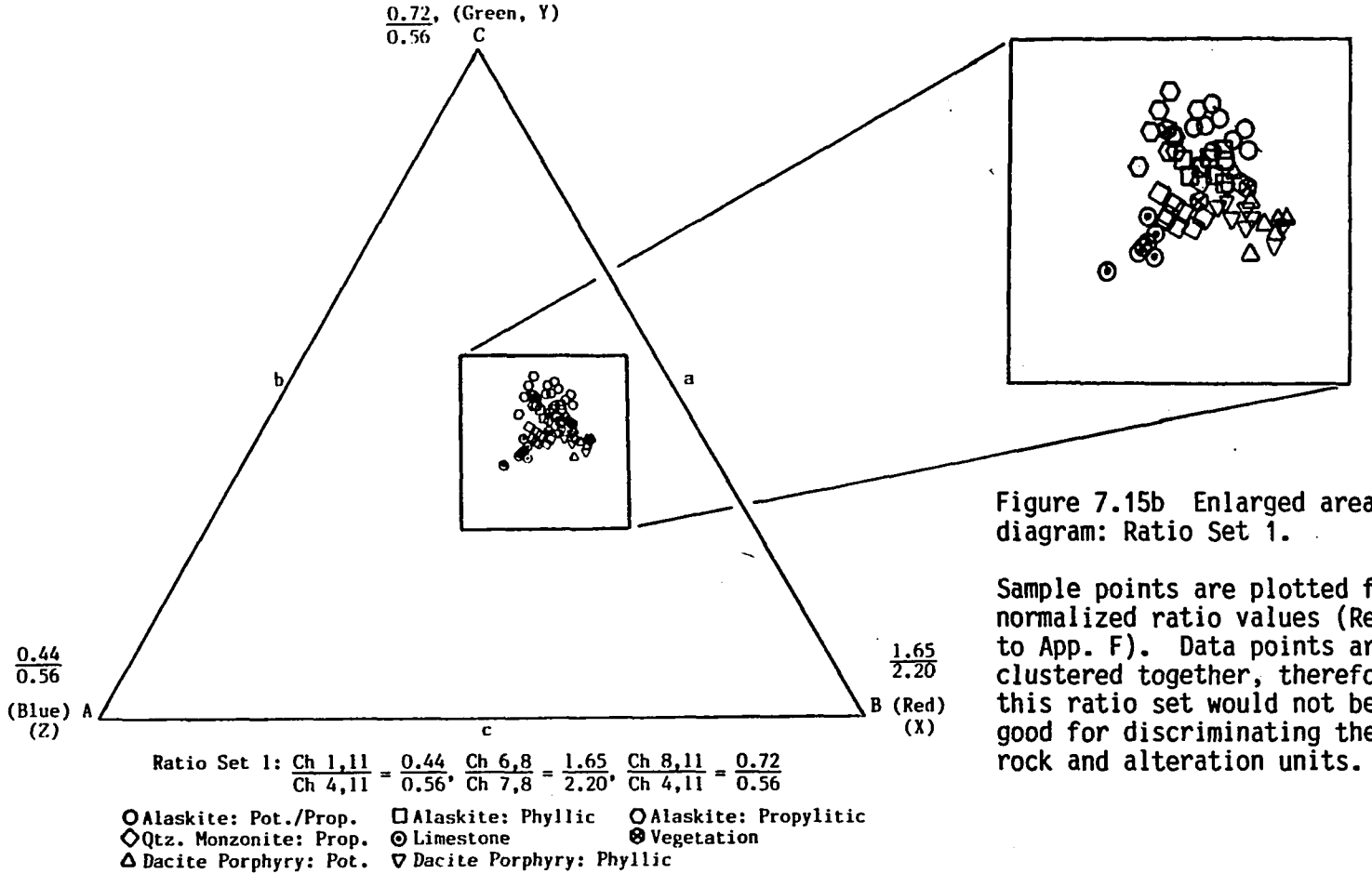

Figure 7.15a Ternary Diagram/Chromaticity Diagram: Ratio Set 1.

Figure 7.15b Enlarged area diagram: Ratio Set 1.

Sample points are plotted from normalized ratio values (Refer to App. F). Data points are clustered together, therefore this ratio set would not be good for discriminating the rock and alteration units.

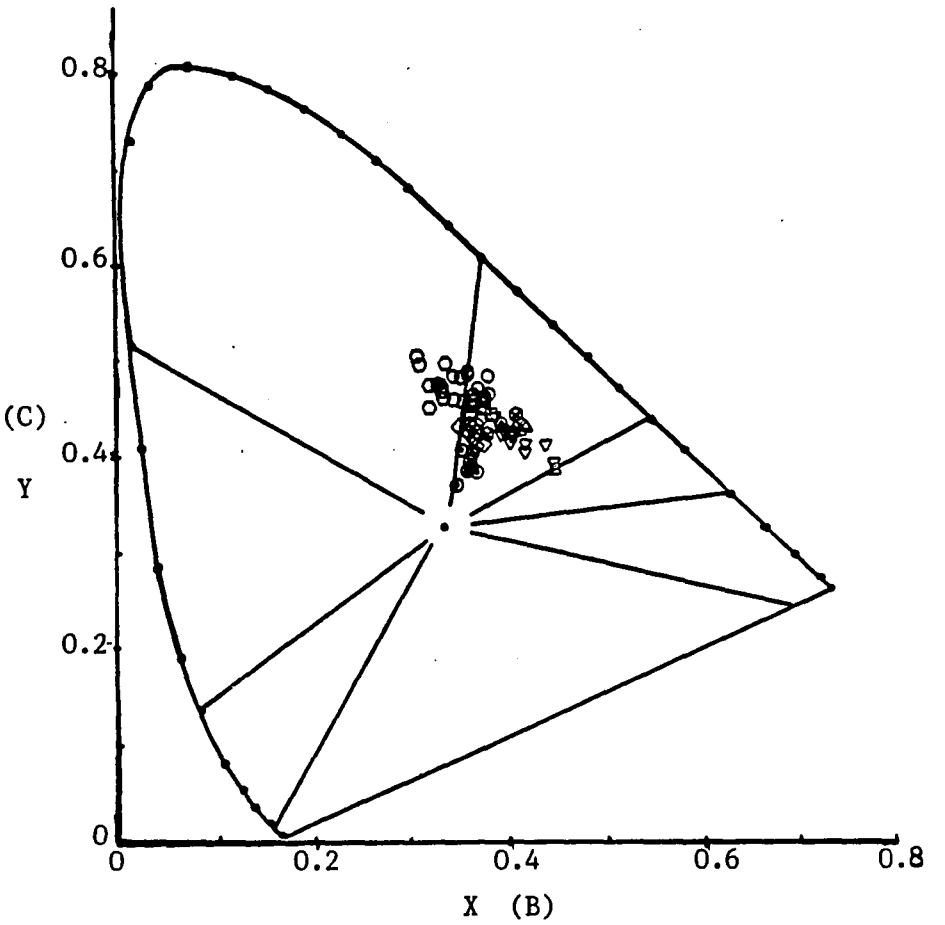

Ratio Set 1: $\frac{\text{Ch } 1,11}{\text{Ch } 4,11} = \frac{0.44}{0.56}$, $\frac{\text{Ch } 6,8}{\text{Ch } 7,8} = \frac{1.65}{2.20}$,

$\frac{\text{Ch } 8,11}{\text{Ch } 4,11} = \frac{0.72}{0.56}$.

○ Alaskite: Pot./Prop.	△ Dacite Porphyry: Potassic
□ Alaskite: Phyllic	▽ Dacite Porphyry: Phyllic
○ Alaskite: Propylitic	⊙ Limestone
◇ Qtz. Monzonite: Prop.	⊗ Vegetation

Figure 7.16 Rectilinear Chromaticity Diagram, Ratio Set 1. Data plotted from normalized ratio values (Refer to App. F).

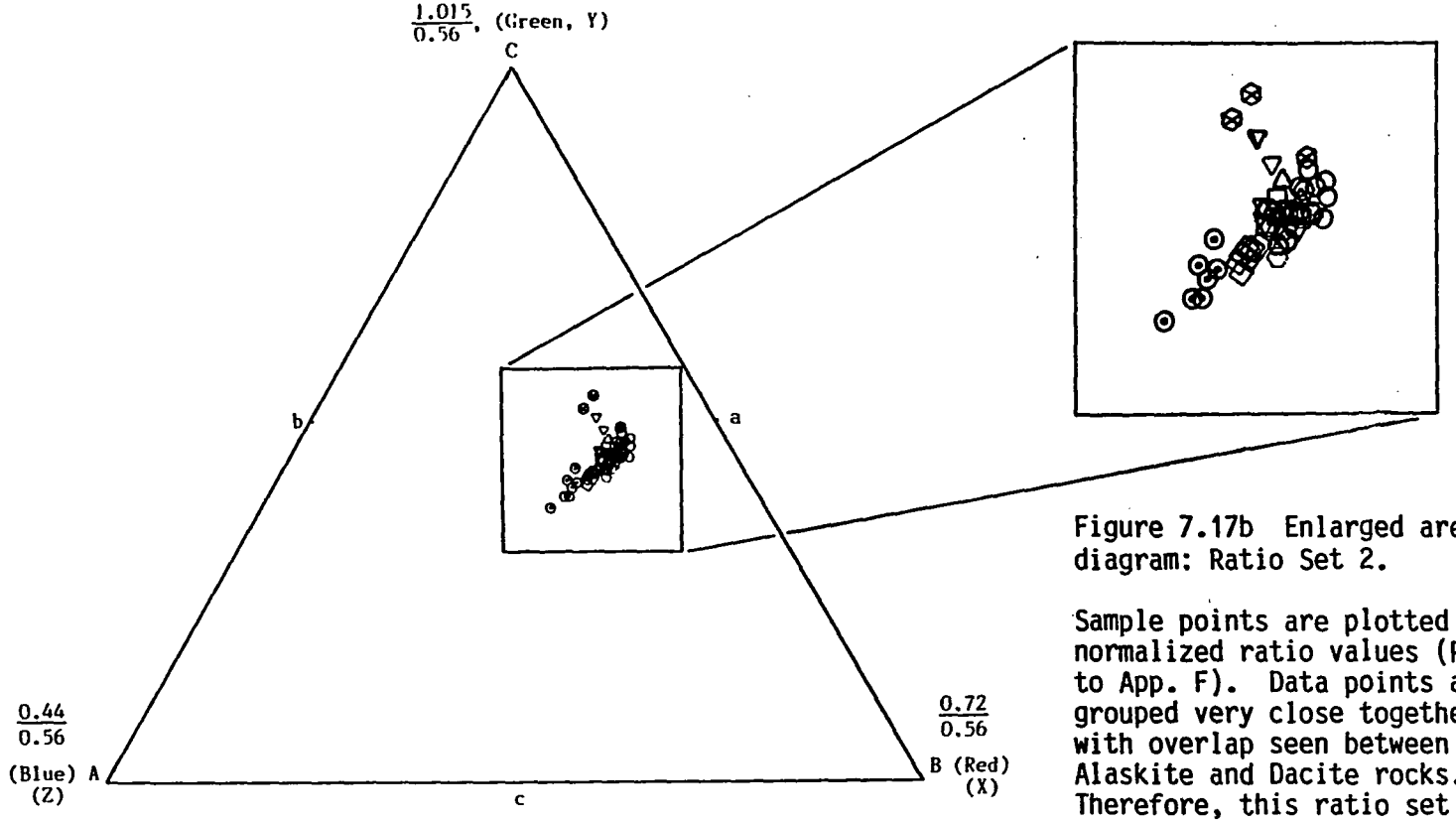

Ratio Set 2: $\frac{Ch\ 1,11}{Ch\ 4,11} = \frac{0.44}{0.56}$, $\frac{Ch\ 8,11}{Ch\ 4,11} = \frac{0.72}{0.56}$, $\frac{Ch\ 10,11}{Ch\ 4,11} = \frac{1.015}{0.56}$.

○ Alaskite: Pot./Prop. □ Alaskite: Phyllic ○ Alaskite: Propylitic
◇ Qtz. Monzonite: Prop. ⊙ Limestone ⊗ Vegetation
△ Dacite Porphyry: Pot. ▽ Dacite Porphyry: Phyllic

Figure 7.17a Ternary Diagram/Chromaticity Diagram: Ratio Set 2.

Figure 7.17b Enlarged area diagram: Ratio Set 2.

Sample points are plotted from normalized ratio values (Refer to App. F). Data points are grouped very close together, with overlap seen between the Alaskite and Dacite rocks. Therefore, this ratio set would not be good for discriminating the rocks.

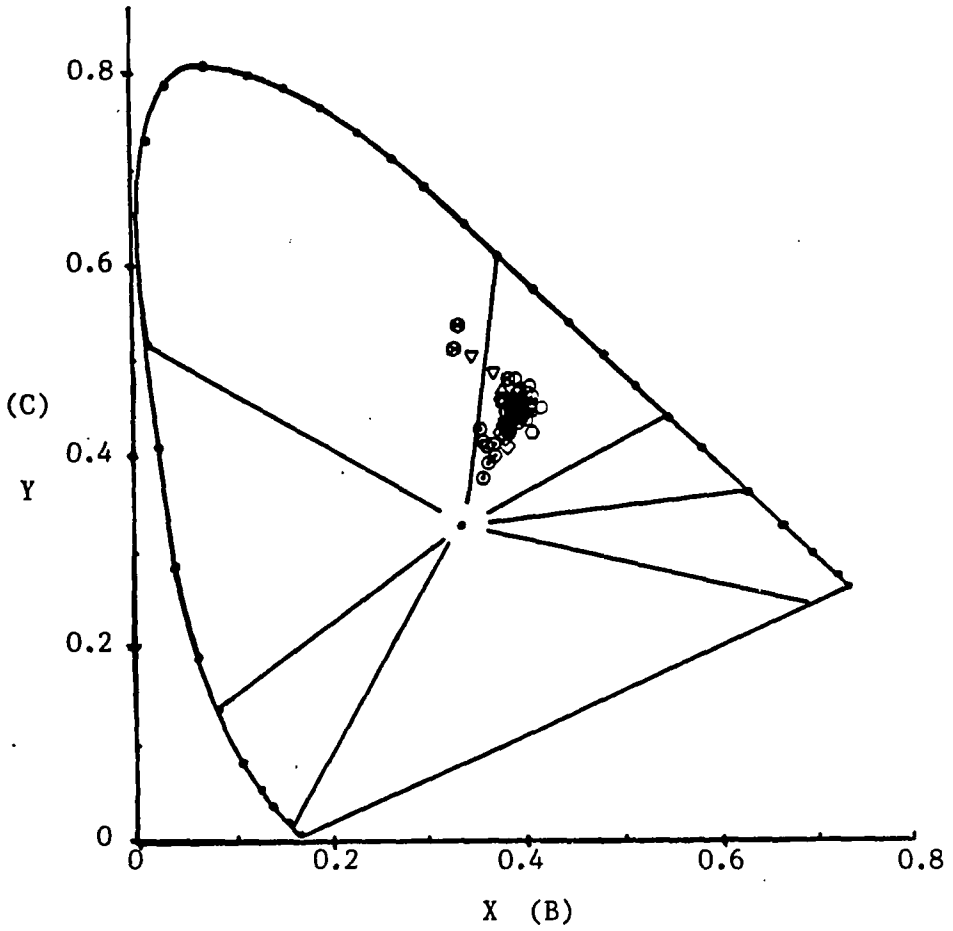

Ratio Set 2: $\frac{\text{Ch } 1,11}{\text{Ch } 4,11} = \frac{0.44}{0.56}$, $\frac{\text{Ch } 8,11}{\text{Ch } 4,11} = \frac{0.72}{0.56}$,

$\frac{\text{Ch } 10,11}{\text{Ch } 4,11} = \frac{1.015}{0.56}$.

○ Alaskite: Pot./Prop.	△ Dacite Porphyry: Potassic
□ Alaskite: Phyllic	▽ Dacite Porphyry: Phyllic
⬡ Alaskite: Propylitic	⊙ Limestone
◇ Qtz. Monzonite: Prop.	⊛ Vegetation

Figure 7.18 Rectilinear Chromaticity Diagram, Ratio Set 2. Data plotted from normalized ratio values (Refer to App. F).

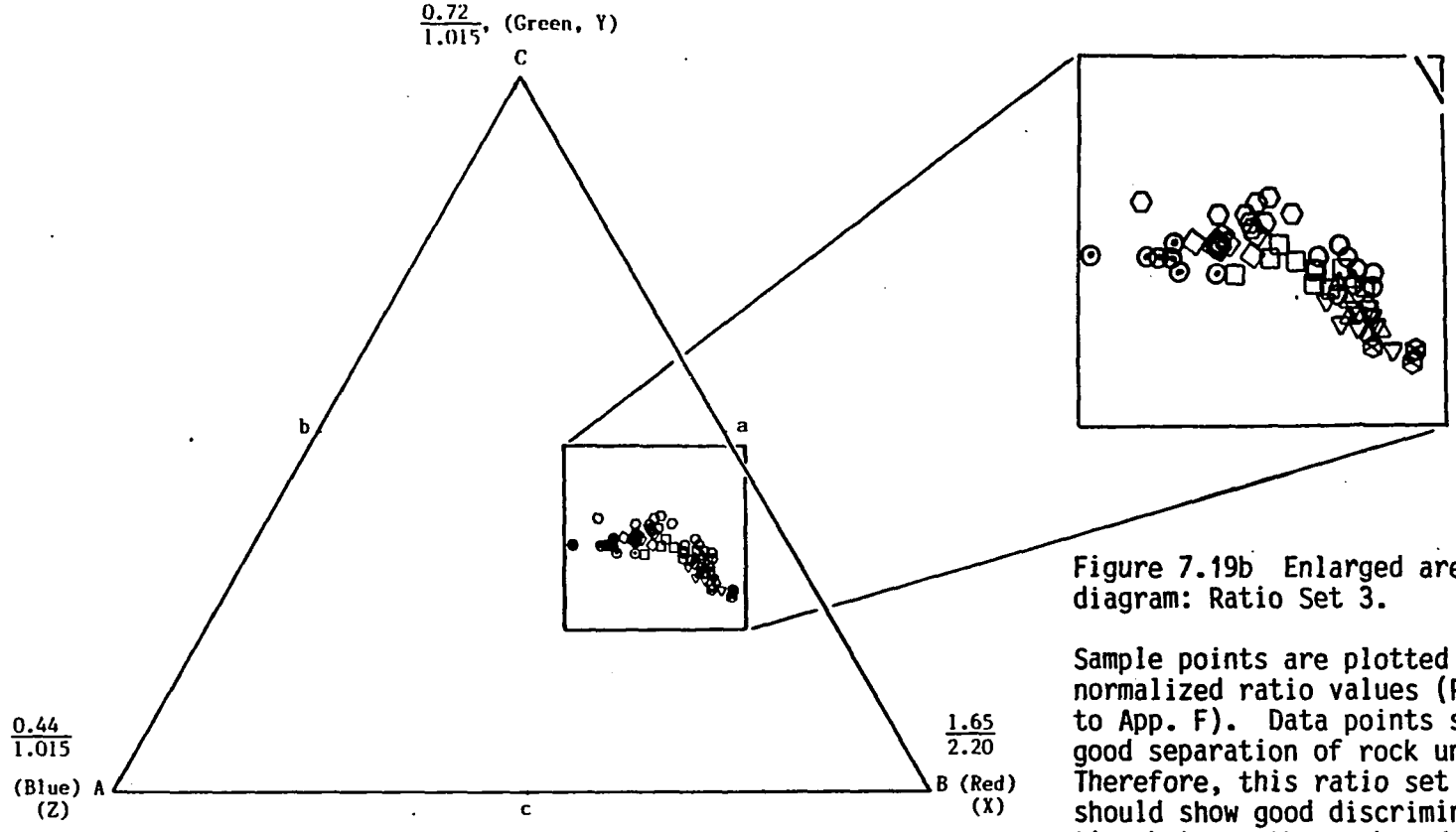

Ratio Set 3: $\frac{Ch\ 1,11}{Ch\ 10,11} = \frac{0.44}{1.015}, \frac{Ch\ 6,8}{Ch\ 7,8} = \frac{1.65}{2.20}, \frac{Ch\ 8,11}{Ch\ 10.11} = \frac{0.72}{1.015}$.

○ Alaskite: Pot./Prop. □ Alaskite: Phyllic ○ Alaskite: Propylitic
◇ Qtz. Monzonite: Prop. ◉ Limestone ⊗ Vegetation
△ Dacite Porphyry: Pot. ▽ Dacite Porphyry: Phyllic

Figure 7.19a Ternary Diagram/Chromaticity Diagram: Ratio Set 3.

Figure 7.19b Enlarged area diagram: Ratio Set 3.

Sample points are plotted from normalized ratio values (Refer to App. F). Data points show good separation of rock units. Therefore, this ratio set should show good discrimination between the rock and alteration units.

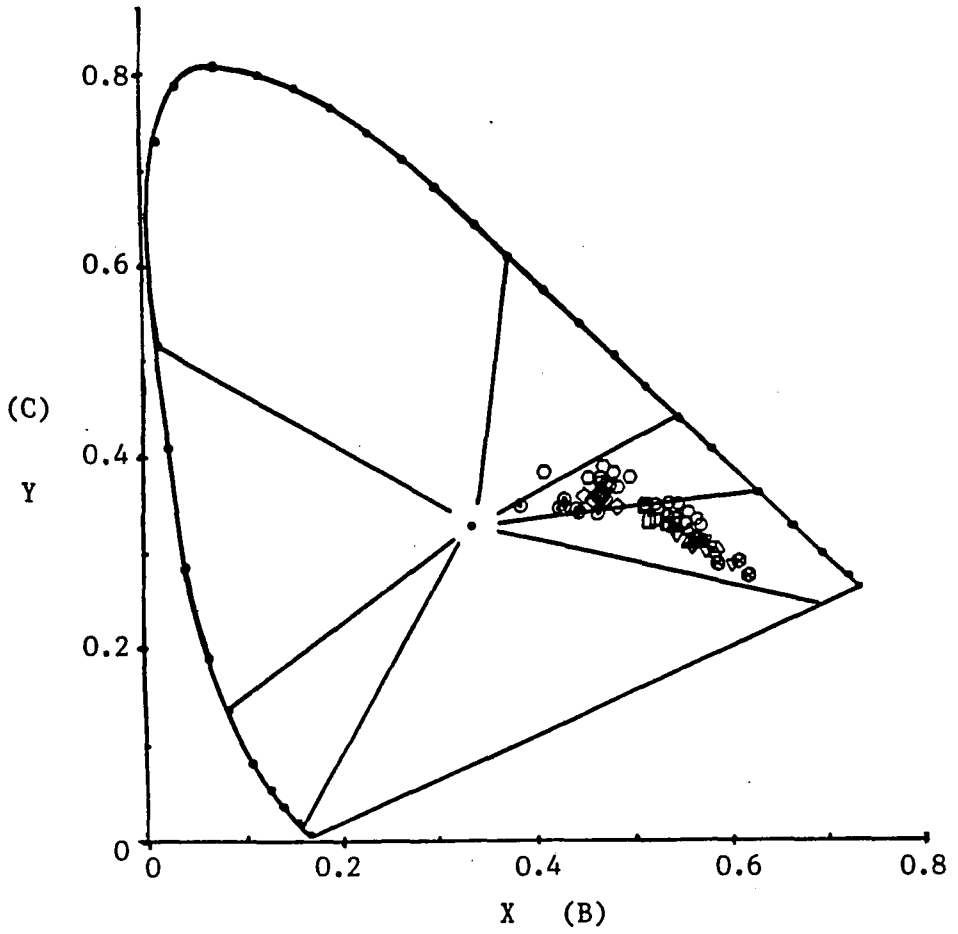

Ratio Set 3: $\frac{\text{Ch } 1,11}{\text{Ch } 10,11} = \frac{0.44}{1.015}$, $\frac{\text{Ch } 6,8}{\text{Ch } 7,8} = \frac{1.65}{2.20}$,

$\frac{\text{Ch } 8,11}{\text{Ch } 10,11} = \frac{0.72}{1.015}$.

○ Alaskite: Pot./Prop.	△ Dacite Porphyry: Potassic
□ Alaskite: Phyllic	▽ Dacite Porphyry: Phyllic
○ Alaskite: Propylitic	◉ Limestone
◇ Qtz. Monzonite: Prop.	⊗ Vegetation

Figure 7.20 Rectilinear Chromaticity Diagram, Ratio Set 3. Data plotted from normalized ratio values (Refer to App. F).

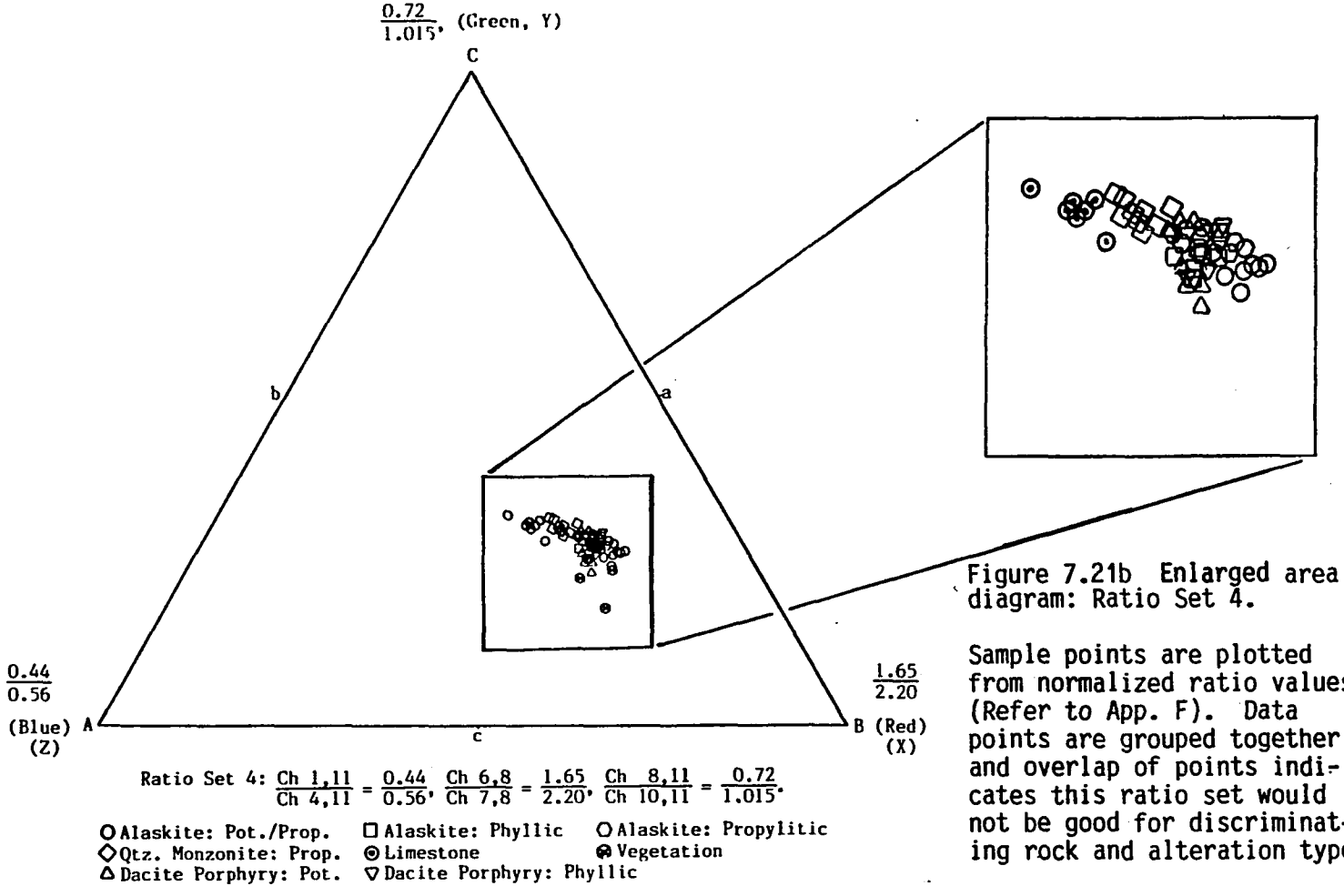

Figure 7.21a Ternary Diagram/Chromaticity Diagram: Ratio Set 4.

Figure 7.21b Enlarged area diagram: Ratio Set 4.

Sample points are plotted from normalized ratio values (Refer to App. F). Data points are grouped together and overlap of points indicates this ratio set would not be good for discriminating rock and alteration type.

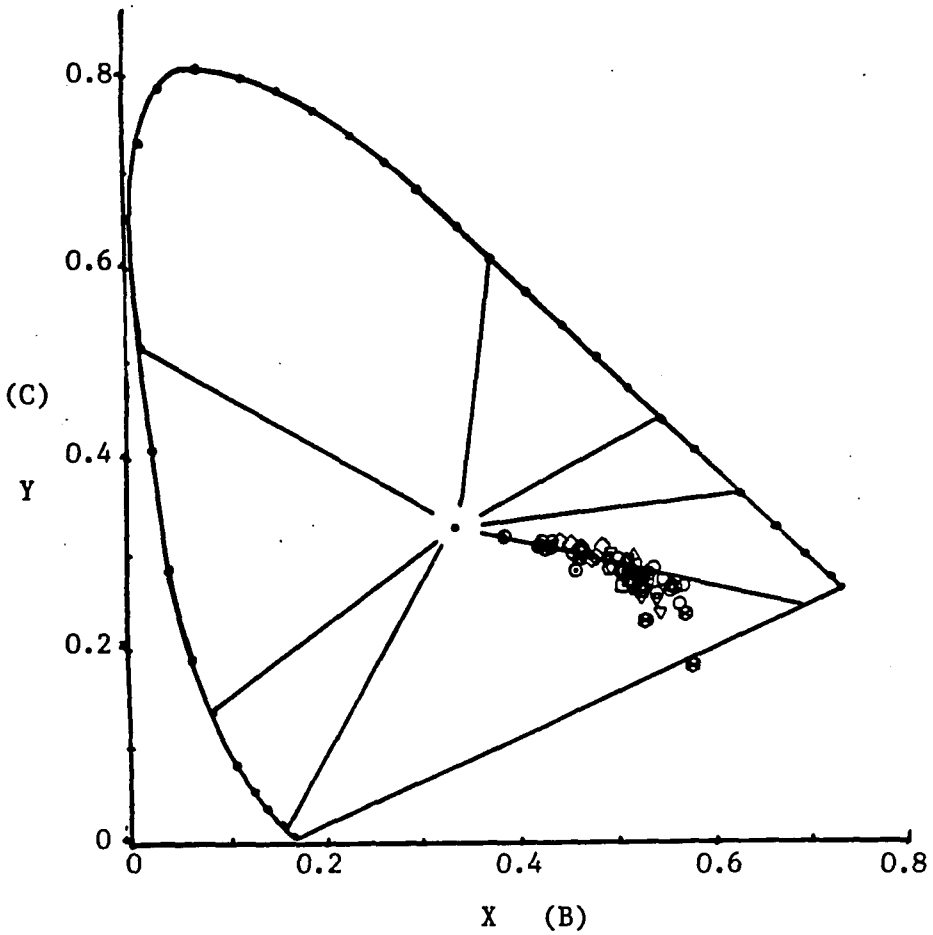

Ratio Set 4: $\frac{\text{Ch } 1,11}{\text{Ch } 4,11} = \frac{0.44}{0.56}$, $\frac{\text{Ch } 8,11}{\text{Ch } 4,11} = \frac{0.72}{0.56}$,

$\frac{\text{Ch } 8,11}{\text{Ch } 10,11} = \frac{0.72}{1.015}$.

- ○ Alaskite: Pot./Prop.
- □ Alaskite: Phyllic
- ⬡ Alaskite: Propylitic
- ◇ Qtz. Monzonite: Prop.
- △ Dacite Porphyry: Potassic
- ▽ Dacite Porphyry: Phyllic
- ⊙ Limestone
- ⊛ Vegetation

Figure 7.22 Rectilinear Chromaticity Diagram, Ratio Set 4. Data plotted from normalized ratio values (Refer to App. F).

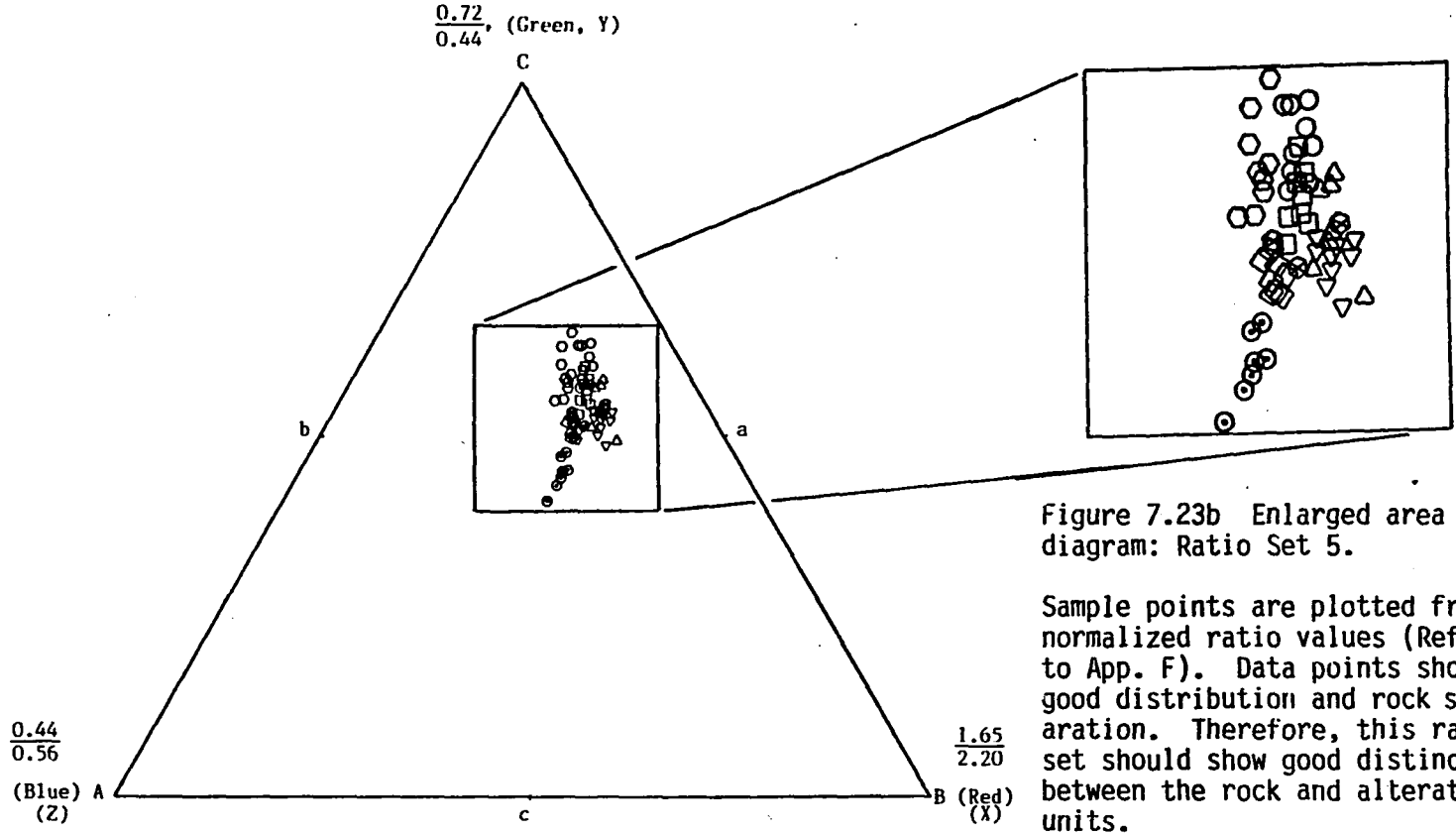

Ratio Set 5: $\frac{Ch\ 1,11}{Ch\ 4,11} = \frac{0.44}{0.56}$, $\frac{Ch\ 6,8}{Ch\ 7,8} = \frac{1.65}{2.20}$, $\frac{Ch\ 8,11}{Ch\ 1,11} = \frac{0.72}{0.44}$.

○ Alaskite: Pot./Prop. □ Alaskite: Phyllic ○ Alaskite: Propylitic
◇ Qtz. Monzonite: Prop. ⊙ Limestone ⊗ Vegetation
△ Dacite Porphyry: Pot. ▽ Dacite Porphyry: Phyllic

Figure 7.23a Ternary Diagram/Chromaticity Diagram: Ratio Set 5.

Figure 7.23b Enlarged area diagram: Ratio Set 5.

Sample points are plotted from normalized ratio values (Refer to App. F). Data points show good distribution and rock separation. Therefore, this ratio set should show good distinction between the rock and alteration units.

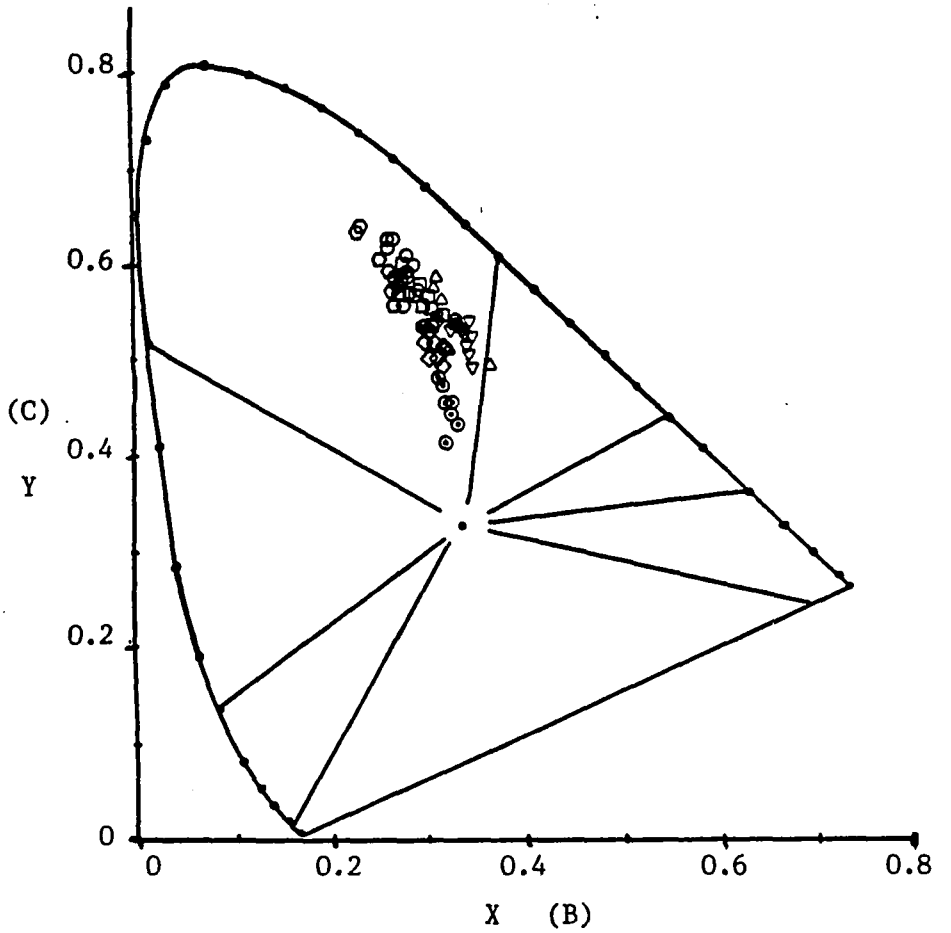

Ratio Set 5: $\frac{\text{Ch } 1,11}{\text{Ch } 4,11} = \frac{0.44}{0.56}$, $\frac{\text{Ch } 6,8}{\text{Ch } 7,8} = \frac{1.65}{2.20}$,

$\frac{\text{Ch } 8,11}{\text{Ch } 1,11} = \frac{0.72}{0.44}$.

○ Alaskite: Pot./Prop.	△ Dacite Porphyry: Potassic
□ Alaskite: Phyllic	▽ Dacite Porphyry: Phyllic
○ Alaskite: Propylitic	⊙ Limestone
◇ Qtz. Monzonite: Prop.	⊗ Vegetation

Figure 7.24 Rectilinear Chromaticity Diagram, Ratio Set 5. Data plotted from normalized ratio values (Refer to App. F).

The final ratio sets selected for combination into CRC images are:

1) $\frac{\text{Ch } 1,11}{\text{Ch } 10,11} = \frac{0.44\text{um}}{1.015\text{um}}$, $\frac{\text{Ch } 8,11}{\text{Ch } 10,11} = \frac{0.72\text{um}}{1.015\text{um}}$, and $\frac{\text{Ch } 6,8}{\text{Ch } 7,8} = \frac{1.65\text{um}}{2.20\text{um}}$;

2) $\frac{\text{Ch } 1,11}{\text{Ch } 4,11} = \frac{0.44\text{um}}{0.56\text{um}}$, $\frac{\text{Ch } 8,11}{\text{Ch } 1,11} = \frac{0.72\text{um}}{0.44\text{um}}$, and $\frac{\text{Ch } 6,8}{\text{Ch } 7,8} = \frac{1.65\text{um}}{2.20\text{um}}$;

3) $\frac{\text{Ch } 1,11}{\text{Ch } 4,11} = \frac{0.44\text{um}}{0.56\text{um}}$, $\frac{\text{Ch } 8,11}{\text{Ch } 4,11} = \frac{0.72\text{um}}{0.56\text{um}}$, and $\frac{\text{Ch } 6,8}{\text{Ch } 7,8} = \frac{1.65\text{um}}{2.20\text{um}}$.

The third ratio set was selected to show how data clustering of ratio values in a ternary diagram will yield a CRC image with uniform coloration and minimal material discrimination.

Ratio Process

The ratio procedure utilized the warped, atmospherically corrected images. A computer program, RATIO1, was written to use the SADIE 3.0 subroutine PROQUO to perform the image division (see Appendix A for computer programs). Visual enhancement of each ratio image was done during the ratio process by using a scale factor, incorporated in the PROQUO subroutine to perform a simple gray level transformation (multiplication) upon each ratioed pixel. The scale factor was used to enhance contrast of the ratio image and to preserve the radiance variations produced among materials in the ratio process. The scale factor does not alter the pixel distribution or the spread of the data in the ternary diagrams.

A unique scale factor was used for image enhancement. The scale factor was selected so that when each gray level value of each pixel was multiplied by the scale factor, $\leq 95\%$ of all data (pixels) fell within

the dynamic range of the display device (0 - 255). All other ratio values greater than the maximum gray level value defined were thresholded to the dynamic range of the system. Therefore, significantly large ratio values for materials will not be lost in the ratio process. A value of 75.0 was found satisfactory as a scale factor in the ratio process.

Therefore, two ratio analyses were performed. The first was conducted using a scale factor of 1.0. A histogram of each ratio image was analyzed to determine the proper scale factor for use in a final ratio process. Then, the ratio routine was run again with the final scale factor. Examples of the final ratio images are given in Figures 7.25 to 7.28 , pages 68 to 71. After the ratioing was complete, the CRC images were compiled using the computer program CRC2 (see Appendix A). The program compiled three ratio images into one in an interleaving process.

Figure 7.25 Ratio Image: 1.65/2.20. Bright/white areas indicate clay minerals created by alteration/weathering processes. El Tiro open pit mine.

Figure 7.26 Ratio Image: 0.72/0.56. Bright/white areas indicate the presence of ferric iron minerals of hematite, goethite and jarosite. Iron mineralization due to the weathering of sulfides in and around El Tiro open pit mine.

Figure 7.27 Ratio Image: 0.72/0.44. Bright/white areas indicate the presence of ferric iron minerals of hematite, goethite and jarosite. Iron mineralization due to the weathering of sulfides in and around El Tiro open pit mine.

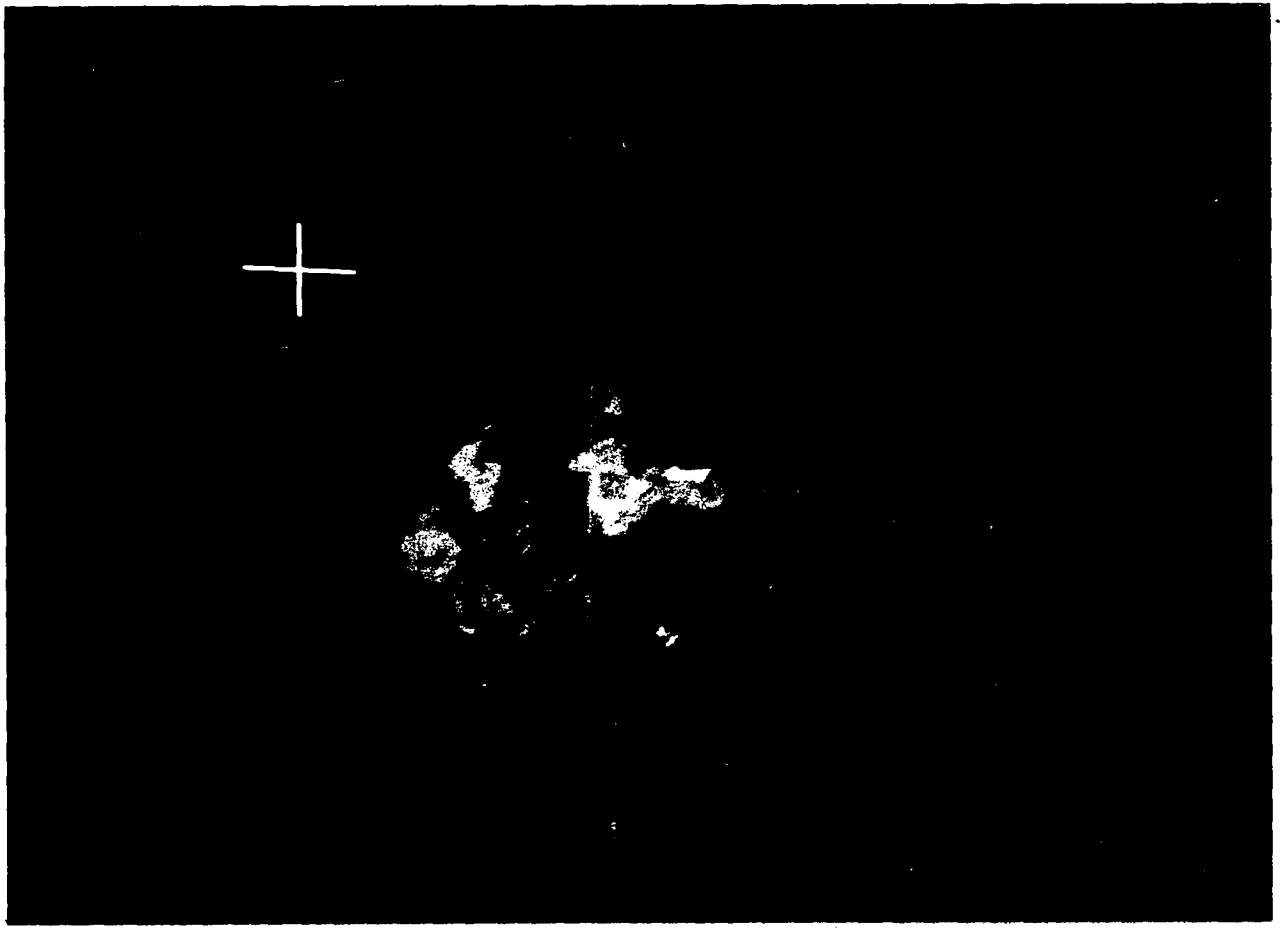

Figure 7.28 Ratio Image: 0.44/0.72. Dark areas indicate the presence of ferric iron minerals of hematite, goethite and jarosite. Iron mineralization due to the weathering of sulfides in and around El Tiro open pit mine.

CHAPTER 8

COLOR-RATIO COMPOSITES

The three CRC sets selected for analysis contain ratio images that distinguish alteration assemblages and rock units. The 1.65/2.20 ratio image is excellent for clay mineral detection and is used in all three CRC sets. The other ratio images feature 11 channel data for ferric-iron mineral detection. All three CRC sets distinguish altered from unaltered rocks, but only CRC sets 1 and 2 are useful for alteration zone delineation.

The analysis process was conducted in two stages. The first involved mapping the rock/alteration units in each CRC image. Units were mapped, based upon color, on an acetate overlay sheet. Direct comparisons were made between reference maps (Figures 3.2 and 3.3) and the CRC images. The reference maps served as ground truth data for analysis of the CRC images. The second stage involved: 1) verifying the use of the ternary/chromaticity diagrams for selection of ratio sets for CRC compilation, and 2) verifying the use of the ternary/chromaticity diagram for determining general color designations for rock units in a CRC image.

CRC SET 1 ANALYSIS

CRC Set 1 consists of the ratio pairs 0.44/1.015 (Ch 1,11/10,11), 0.72/1.015 (Ch 8,11/10,11) and 1.65/2.20 (Ch 6,8/7,8). The three primary colors assigned to the ratio pairs were: blue = 0.44/1.015, green = 0.72/1.015 and red = 1.65/2.20. Rock and alteration unit boundaries were determined for the CRC image, and are indicated on an acetate overlay. The overlay accompanies the CRC image (Figure 8.1, page 74).

CRC Set 1 shows excellent spectral separation of altered and unaltered rocks (Figure 8.1). The potassic and phyllic altered rocks are distinguished from the propylitic altered rocks. The potassic and phyllically altered areas, note B in the overlay, appears reddish to red-orange in the image. The propylitically altered rocks are bluish-green to green (A). Areas of clay mineralization (phyllically altered zones) are displayed in reds, oranges and pinks. However, vegetation (E) also appears reddish in the image and could cause an interpretation problem if not properly noted. Intrusive stocks are displayed in pastel colors of pink and light blue within the pit areas (F). The paleozoic limestone sequence (C) is distinct, appearing bluish/red. The color is due to high ratio values for limestone from the 0.44/1.015 ratio pair. Also, the leaching ponds (D) appear yellow. The coloration is due to high ratio values for both 1.65/2.20 (red) and 0.72/1.015 (green) ratio pairs.

The chromaticity diagram for CRC Set 1 compares favorably with the CRC image (Figure 7.20, page 61, Ratio Set 3). Separation of rock units and alteration assemblages was successfully determined by plotting

Figure 8.1 CRC Set 1.

the normalized ratio values in a ternary/chromaticity diagram. General colorations as defined by the chromaticity diagram are seen in the CRC image. Areas of clay mineralization appear reddish orange in the image and match color designations for clay rich rocks plotted in the diagram (Figure 7.20, page 61, Ratio Set 3). Also, vegetation was correctly defined as red in the diagram and appears as such in the image. The limestone color designation in the diagram, an orange-pink, does not match well with the color in the image. Spectral variability of the rock could account for the color variations.

In general, the overall coloration of the CRC image, that of an orange-red, matches the overall color designations for the sampled rocks used in the study. The bluish areas in and around the pit are not represented in the chromaticity diagram. Therefore, use of the chromaticity diagram proved successful for ratio pair selection, rock unit separation and alteration zone detection for CRC Set 1.

CRC Set 2 Analysis

CRC Set 2 consists of the ratio pairs 0.44/0.56 (Ch 1,11/4,11), 0.72/0.44 (Ch 8,11/1,11) and 1.65/2.20 (Ch 6,8/7,8). The three primary colors assigned to each ratio pair were: blue = 0.44/0.56, green = 0.72/0.44 and red = 1.65/2.20. CRC Set 2 exhibits moderate alteration discrimination between phyllic and propylitic rocks. Altered rocks are easily distinguished form unaltered rocks. However, the color separation between the altered rocks is not as good as in CRC Set 1. Rock and alteration units, defined in the CRC image, are indicated on an acetate overlay (Figure 8.2, page 77). The paleozoic limestone (A)

appears blue-green to light blue-violet, and is easily distinguished from the altered rocks. The leaching ponds (B) are yellow. Propylitic altered rocks are noted in the outer portions of the image, varying from pale green to a dark blue. C1 denotes propylitically altered alaskite while C2 denotes propylitically altered dacite. The phyllically altered rocks (D1 and D2) dominate the central portion of the image. Their greenish-yellow appearance is due to surficial iron staining and clay minerals. This is indicated by high ratio values for the ratio pairs 0.72/0.44 (green) and 1.65/2.20 (red). The stocks within the mine are displayed as pink to purplish-pink (E). Monzonite dikes are noted by small, bright pink dots (F). Natural exposed areas of potassic altered rocks are visible at G, but are obscured within the pit. The approximate potassic altered area is noted by the dashed line. The chromaticity diagram (Figure 7.24, page 65, Ratio Set 5) for CRC Set 2 shows all the rock samples plotted in one region of the spectral locus. Separability of rock and alteration units is limited, therefore, color separation of the rock units is subtle. Actual discrimination between alaskite and dacite is noted in the diagram, but is hard to detect in the CRC image. Limestone plots in the greenish-yellow region of the diagram but appears blue-green to yellow in the image. Once again, spectral variabilty of the rock unit could account for color variabilty between the plotted and actual colors. In general, the plotted colors for each rock unit match the actual colors seen for each rock unit in the CRC image.

CRC Set 2 is good for distinguishing altered from unaltered rocks, but only adequate for discrimination of alteration assemblages.

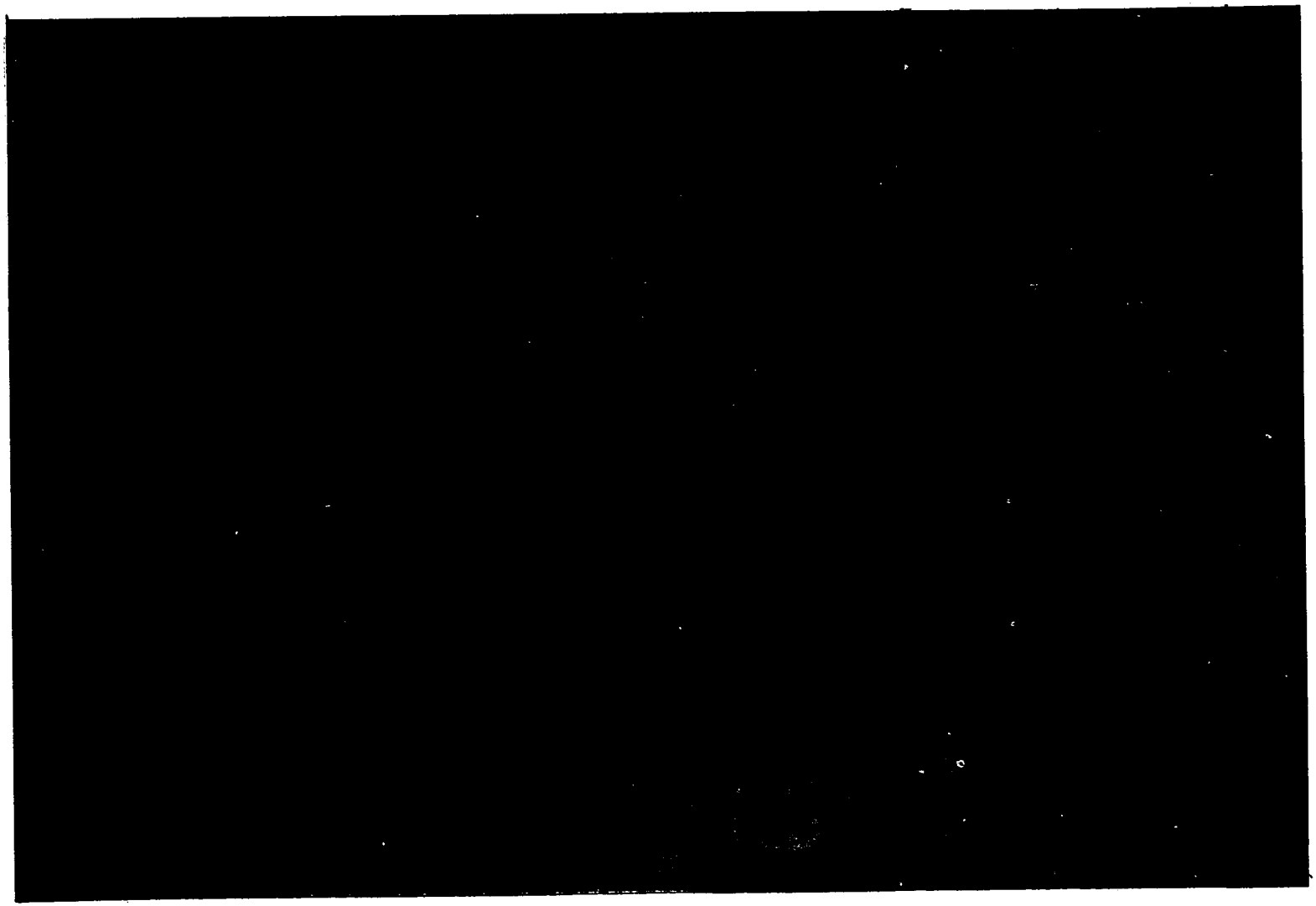

Figure 8.2 CRC Set 2.

The ternary/chromaticity diagram provides a qualitative method for determining color association with rock units in this ratio set. CRC Set 2 verifies the use of a ternary/chromaticity diagram for ratio pair selection, rock type separation and rock/color association.

CRC Set 3 Analysis

CRC Set 3 consists of the ratio pairs 0.44/0.56 (Ch 1,11/4,11), 0.72/0.56 (Ch 8,11/4,11) and 1.65/2.20 (Ch 6,8/7,8). The three primary colors assigned to each ratio pair were: blue = 0.44/0.56, green = 0.72/0.56 and red = 1.65/2.20. The third CRC set was selected to show how data clustering in a chromaticity diagram will produce a CRC image with uniform coloration and minimal rock type discrimination. The chromaticity diagram (Figure 7.16, page 57, Ratio Set 1) shows a clustering of the normalized ratio values within the green region of the spectral locus. Detection of altered versus unaltered rocks should be possible, but differentiation between altered rocks should be difficult due to overlap and clustering of the data points in the ternary diagram. The spectral band ratio of 0.72/0.56 should dominate over the other two ratio pairs, producing green to yellow-green CRC image.

The CRC image is green to yellow-green, verifying the color analysis indicated by the chromaticity diagram (Figure 8.3, page 79). The propylitically altered rocks (A) appear dark green to yellow green while the phyllically altered rocks (B) are green to yellow-green. The paleozoic rocks appear bluish to yellow-green (dashed area) outside the pit and deep blue within the pit. These colors are decidedly different than the colors for the altered rocks. Small patches of

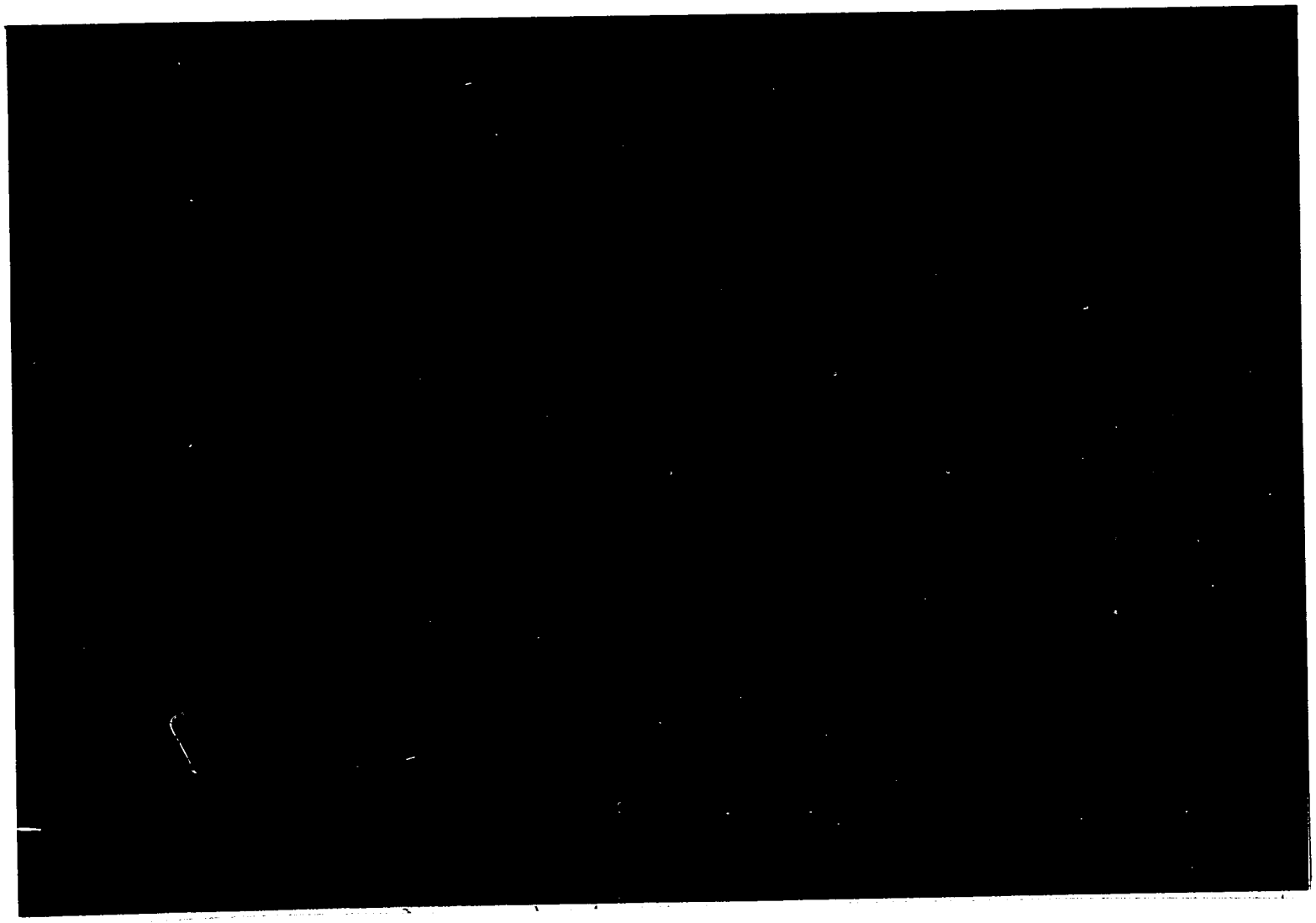

Figure 8.3 CRC Set 3.

bright pink dot the image indicating areas of clay mineralization (monzonite dikes). Actual rock type detection is very poor compared to CRC Sets 1 and 2. The contact between the alaskite and dacite in the northwest corner is very hard to detect, and the quartz monzonite stocks are also hard to detect. Only El Tiro stock appears visible with its light blue/pink shading.

Overall, the use of this CRC image for detection of alteration assemblages from unaltered units is good. However, identifying alteration zones within larger assemblages is not good. CRC Set 1 would be selected over this CRC image based upon spectral separability differences determined by comparing the chromaticity diagrams for each ratio set.

CHAPTER 9

RATIOS OF RATIO IMAGES

The use of spectral band ratios for rock type and alteration assemblage detection is well documented and has proved very successful in past remote sensing research work. By considering ratios of ratio images, one is refining the ratio technique. Material distinction can be further augmented by dividing one ratio image, that has high values for a specific material, by another ratio image, that has low ratio values for the same material. Then, by combining three such ratio/ratio images in a CRC, with each ratio/ratio image defining a specific material, the CRC image should depict each material in a specific color.

Another reason to conduct ratios of ratio images is that the two data sets can be combined into a single image. Previously, combination of two temporally different data sets in a ratio image was not possible due to illumination differences (Schowengerdt, 1983, p. 154). To circumvent this problem, the initial ratio analysis process, that of dividing spectral bands from the same scanner, effectively removed the temporal gain factor (illumination) present in each data set. Therefore, scene illumination differences between the two data sets, that initially kept them from being combined into a single ratio pair (refer to Ch 7, page 34), is effectively removed by the ratio process. So, once the ratio images were formed, combination of data sets into a single, ratio/ratio image was possible.

Selection of the Ratio/Ratio Image Pairs

The selection process for determining which ratio pairs would provide the best delineation of the rocks followed the same analysis methods used for determining spectral bands. Then, ratio/ratio pairs were selected that would highlight clay and iron-bearing minerals associated with each particular rock type. Ratio pairs selected were:

$\frac{\text{Ch 1,11}}{\text{Ch 4,11}} = \frac{0.44}{0.56}$, $\frac{\text{Ch 1,11}}{\text{Ch 10,11}} = \frac{0.44}{1.015}$, $\frac{\text{Ch 1,11}}{\text{Ch 8,11}} = \frac{0.44}{0.72}$, $\frac{\text{Ch 8,11}}{\text{Ch 4,11}} = \frac{0.72}{0.56}$,

$\frac{\text{Ch 8,11}}{\text{Ch 10,11}} = \frac{0.72}{1.015}$, and $\frac{\text{Ch 8,11}}{\text{Ch 1,11}} = \frac{0.72}{0.44}$.

Selection of ratio/ratio pairs from the ratio pairs was based upon three criterias. First, ratio/ratio pairs were selected to enhance clay and iron-bearing minerals. Second, ratio/ratio pairs were selected that would yield high ratio values, and therefore would appear bright in the ratio/ratio image. Third, each ratio/ratio pair was selected to highlight a particular lithologic unit. Therefore, the ratio/ratio pairs selected were:

1) $\frac{1.65/2.20 \text{ (Ch 6,8/7,8)}}{0.44/0.56 \text{ (Ch 1,11/4,11)}}$, 2) $\frac{0.72/0.56 \text{ (Ch 8,11/4,11)}}{1.65/2.20 \text{ (Ch 6,8/7,8)}}$,

3) $\frac{0.44/0.56 \text{ (Ch 1,11/4,11)}}{0.72/1.015 \text{ (Ch 8,11/10,11)}}$, 4) $\frac{0.44/1.015 \text{ (Ch 1,11/10,11)}}{0.72/1.015 \text{ (Ch 8,11/10,11)}}$,

5) $\frac{0.72/0.44 \text{ (Ch 8,11/1,11)}}{1.65/2.20 \text{ (Ch 6,8/7,8)}}$. Since ratio/ratio pair number 4 is the same as the ratio pair 0.44/0.72 (Ch 1,11/8,11) (6), the later was used as ratio/ratio pair number four in the analysis. Ratio/ratio values for each sample were calculated using the ratio values determined from each

ratio pair (Appendix G for ratio/ratio values). The average values for each ratio/ratio pair for each sample were tabulated (Table 2, page 84). Analysis of each average ratio/ratio value indicated that unique separation of the rocks could be determined by a combination of three ratio/ratio pairs in a CRC image. Four of the five ratio/ratio pairs (1,2,4 and 5) could effectively discriminate one rock type from all the others (see Table 2). Two of the four, 1 and 4, could effectively detect a single rock unit, number 1 for the dacite porphyry and number 4 for the limestone. The other two ratio/ratio pairs, 2 and 5, effectively detected the alaskite. The question remained as to which of these two was best for alaskite detection when combined with the ratio/ratio pairs 1 and 4. So, two ternary diagrams were constructed to determine the best possible three ratio/ratio set.

The first set consisted of the ratio/ratio pairs 1, 4 and 5. The second set consisted of the ratio/ratio pairs 1, 2 and 4. The two ternary diagrams and their respective chromaticity diagrams are seen in Figures 9.1 to 9.4, pages 85 through 88. Set number 1 separates the rock units better than set number 2, as an overlap of the rocks is noted in set two. Therefore, set number one was selected based upon the better separability of the rock units in the ternary diagram.

Table 2: Ratio/ratio values.
The numbers 1 to 5 in Table 2 represent the ratio/ratio pairs defined on page 69. The values in the table, under each numbered column, represent the ratio value for each material for that specific ratio/ratio pair.

	Ratio Values for Ratio/ratio pairs					
Material	1	2	3	4	5	6
Alaskite:						
Pot./Prop. 52405	2.01	1.40	0.71	0.34	2.00	0.33
Phyllic 52406	1.82	1.31	0.76	0.40	1.77	0.39
Propylitic 52603	1.73	1.36	0.72	0.42	2.22	0.41
Dacite Porphyry:						
Potassic 52604	2.41	1.04	0.71	0.38	1.64	0.38
Phyllic 52605	2.43	1.01	0.80	0.41	1.59	0.41
Qtz Monzonite Porphyry:						
Propylitic 52602	1.63	1.19	0.75	0.52	1.66	0.50
Limestone:						
52403	1.36	1.11	0.86	0.64	1.33	0.64
Vegetation:						
Manzanita 98	1.73	1.45	1.31	0.39	1.81	0.40
Lt. Clrd. Bush 99	1.89	1.14	1.11	0.46	1.62	0.47
Palo Verde 911	2.58	1.10	0.84	0.35	1.65	0.35

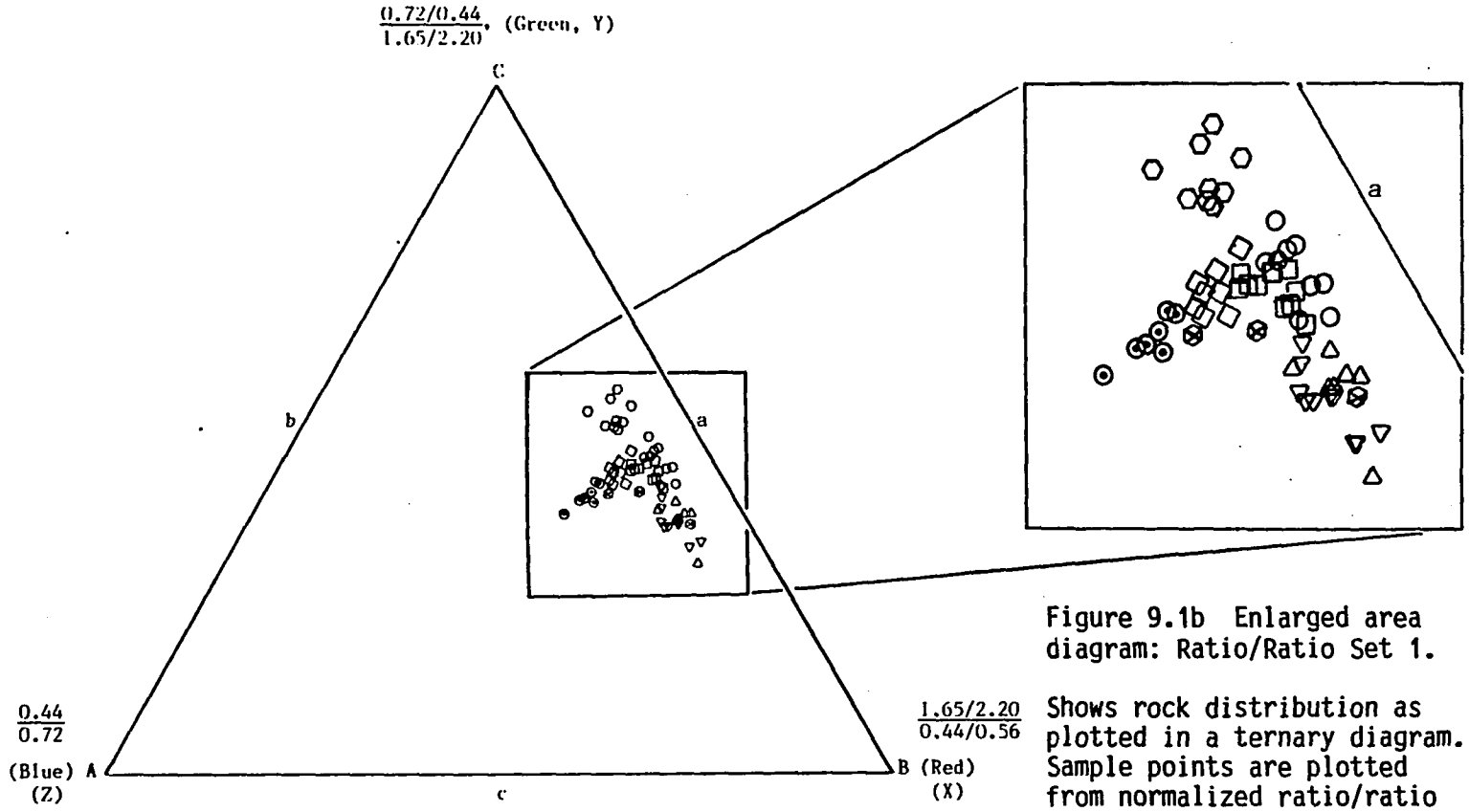

Figure 9.1a Ternary Diagram/Chromaticity Diagram: Ratio/Ratio Set 1.

Figure 9.1b Enlarged area diagram: Ratio/Ratio Set 1.

Shows rock distribution as plotted in a ternary diagram. Sample points are plotted from normalized ratio/ratio values (Refer to App. G).

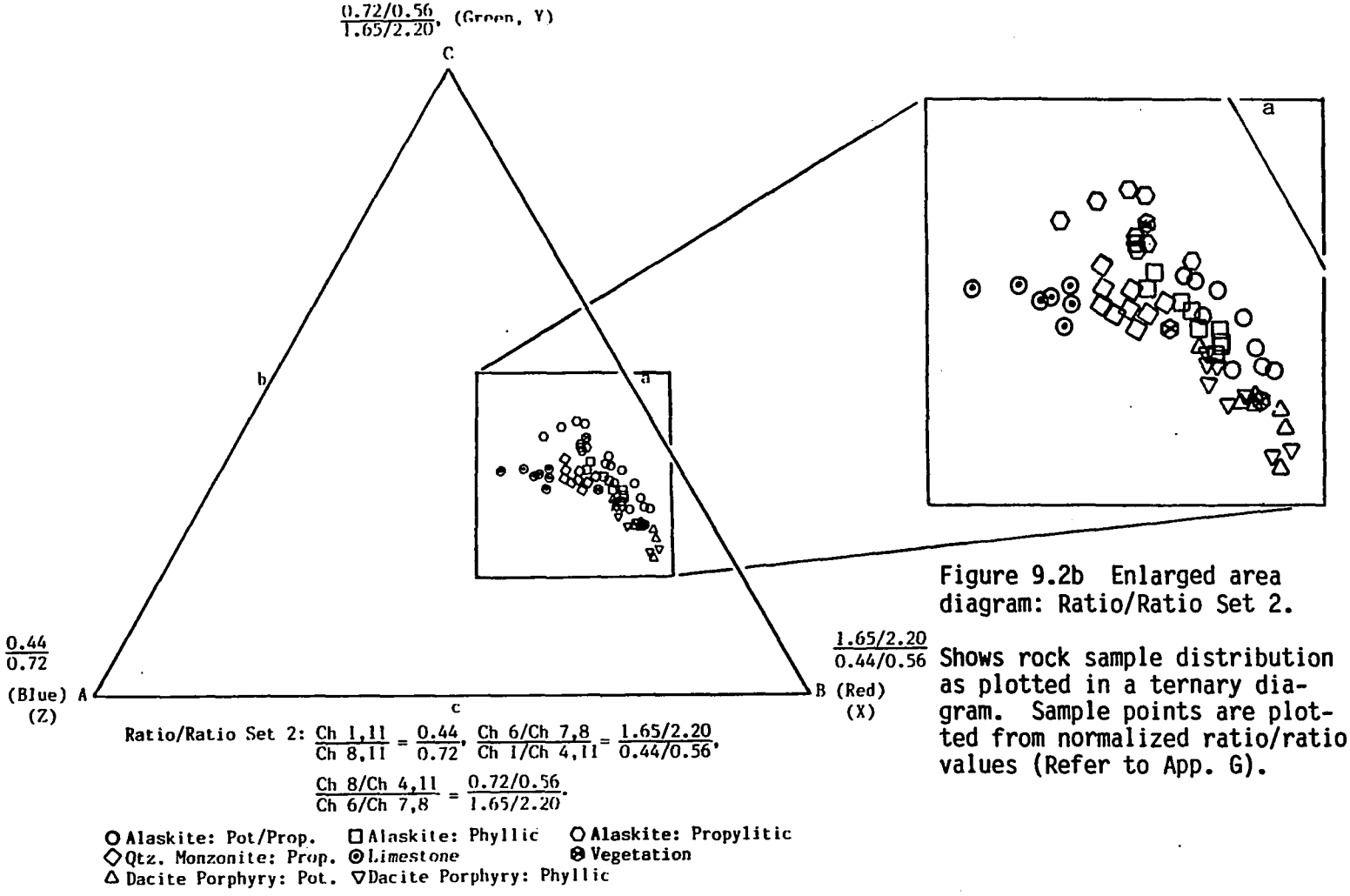

Figure 9.2a Ternary Diagram/Chromaticity Diagram: Ratio/Ratio Set 2.

Figure 9.2b Enlarged area diagram: Ratio/Ratio Set 2.

Shows rock sample distribution as plotted in a ternary diagram. Sample points are plotted from normalized ratio/ratio values (Refer to App. G).

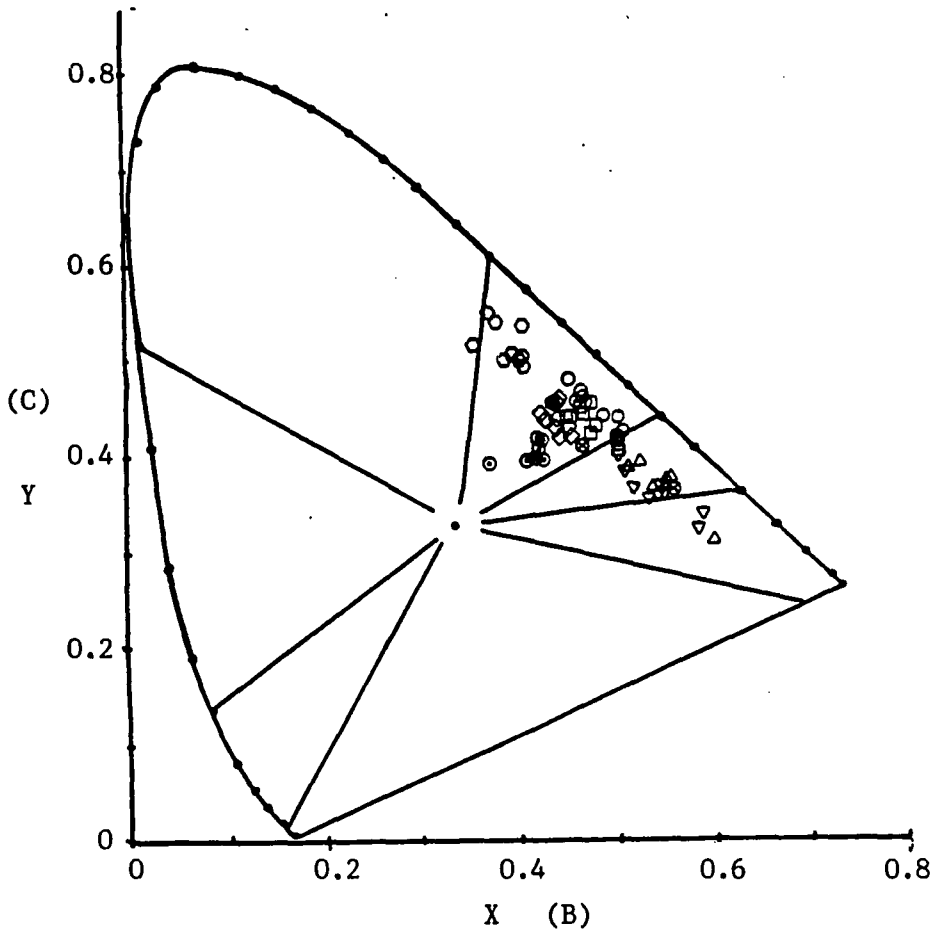

Ratio/Ratio Set 1:

$$\frac{\text{Ch } 1,11}{\text{Ch } 8,11} = \frac{0.44}{0.72}, \quad \frac{\text{Ch } 6,8/7,8}{\text{Ch } 1,11/4,11} = \frac{1.65/2.20}{0.44/0.56}, \quad \frac{\text{Ch } 8,11/1,11}{\text{Ch } 6,8/7,8} = \frac{0.72/0.44}{1.65/2.20}.$$

- ○ Alaskite: Pot./Prop.
- □ Alaskite: Phyllic
- ⬡ Alaskite: Propylitic
- ◇ Qtz. Monzonite: Prop.
- △ Dacite Porphyry: Potassic
- ▽ Dacite Porphyry: Phyllic
- ⊙ Limestone
- ⊗ Vegetation

Figure 9.3 Rectilinear Chromaticity Diagram: Ratio/Ratio Set 1. Data plotted from normalized ratio/ratio values (Refer to App. G).

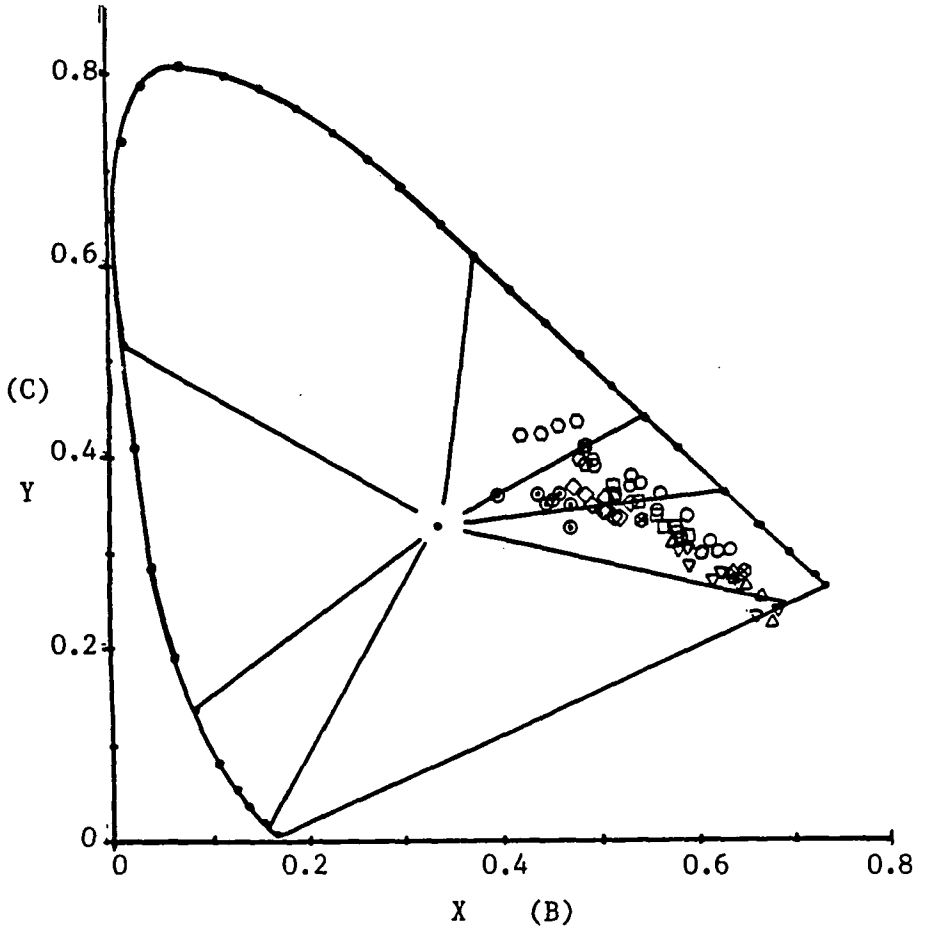

Ratio/Ratio Set 2:

$$\frac{\text{Ch } 1,11}{\text{Ch } 8,11} = \frac{0.44}{0.72},\ \frac{\text{Ch } 6,8/7,8}{\text{Ch } 1,11/4,11} = \frac{1.65/2.20}{0.44/0.56},\ \frac{\text{Ch } 8,11/4,11}{\text{Ch } 6,8/7,8} = \frac{0.72/0.56}{1.65/2.20}.$$

- ○ Alaskite: Pot./Prop.
- □ Alaskite: Phyllic
- ⬡ Alaskite: Propylitic
- ◇ Qtz. Monzonite: Prop.
- △ Dacite Porphyry: Potassic
- ▽ Dacite Porphyry: Phyllic
- ◉ Limestone
- ⊗ Vegetation

Figure 9.4 Rectilinear Chromaticity Diagram: Ratio/Ratio Set 2. Data plotted from normalized ratio/ratio values (Refer to App. G).

CRC Combination

The ratio images 1.65/2.20(Ch 6,8/7,8), 0.44/0.56(Ch 1,11/4,11), 0.72/0.44(Ch 8,11/1,11) and 0.44/0.72(Ch 1,11/8,11) were used in the ratio process to form the ratio/ratio images for combination into the CRC image. The computer program RATIO1 was used to compute each ratio/ratio image. A scale factor of 25.0 was determined as a satisfactory value for providing quality visual enhancement of each new ratio/ratio image. Two of the three ratio/ratio images, Figures 9.5 and 9.6, appear on pages 90 to 91, the third image, Figure 7.28, appears on page 71. The computer program CRC2 was used to compile ratio/ratio CRC image. The final CRC image is given as Figure 9.7 on page 92.

CRC Analysis

The ratio/ratio CRC image exhibits good separation of the major lithologic units in the study area (Figure 9.7). The alaskite appears yellow to yellowish green (APh), with darker greens noted for the propylitically altered areas (Ap). The dacite porphyry appears yellowish-orange to orange-red where phyllically altered (DPph), and yellow-green to green where propylitically altered (DPp). The paleozoic limestone (Ps), appears green to greenish-yellow, to areas of blue within the pit. The blue areas outside the pit in the alaskite region represent paleozoic waste material. Differentiation between the alaskite and dacite porphyry is noted, but the actual contact between the two is hidden within the pit area. A dashed line represents the probable contact area based upon comparisons with the geologic map (Figure 3.2). The reddish areas represent surface materials high in

Figure 9.5 Ratio/Ratio Image 1. $\frac{1.65/2.20}{0.44/0.56}$.

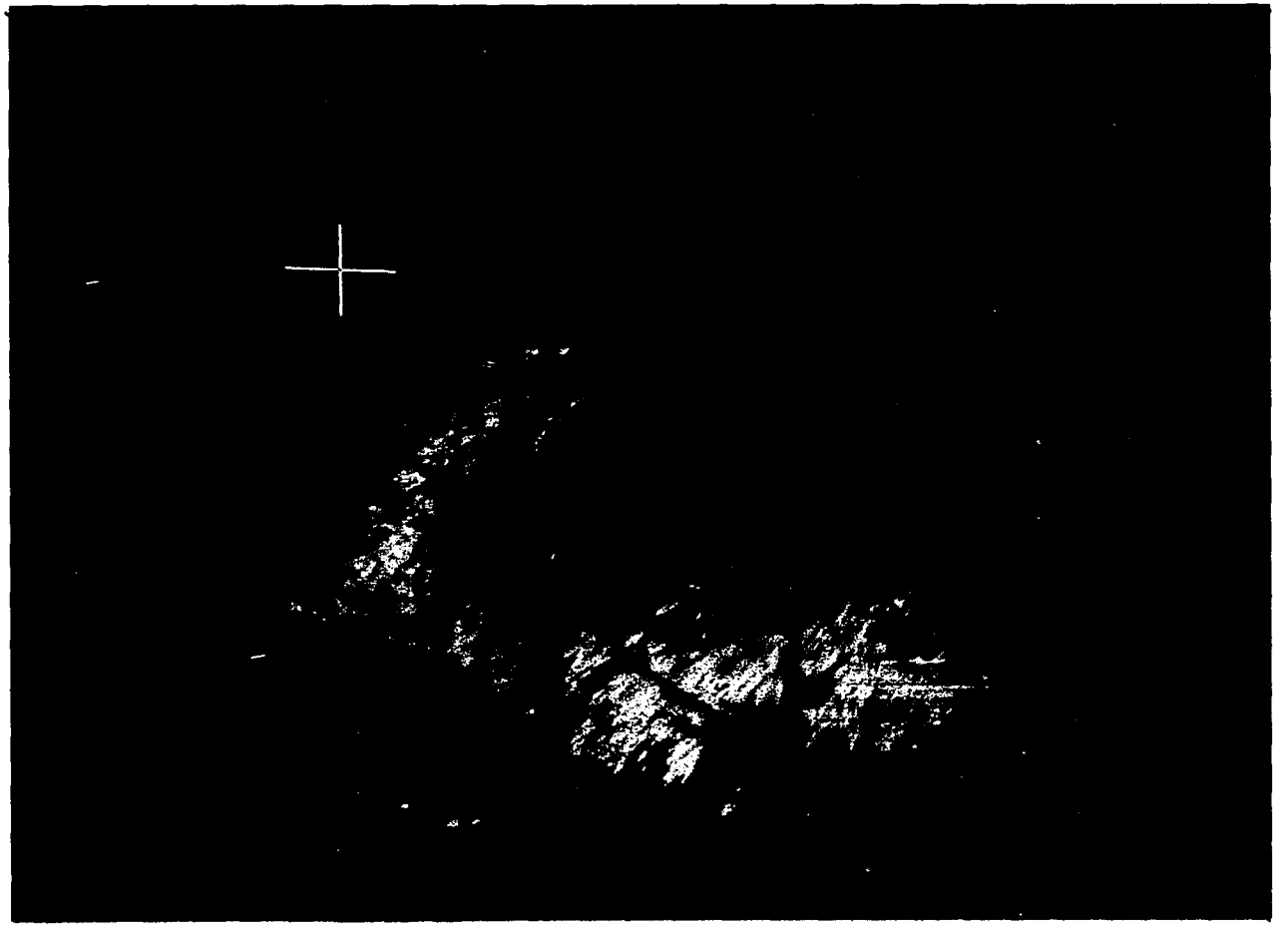

Figure 9.6 Ratio/Ratio Image 2. $\frac{0.72/0.44}{1.65/2.20}$.

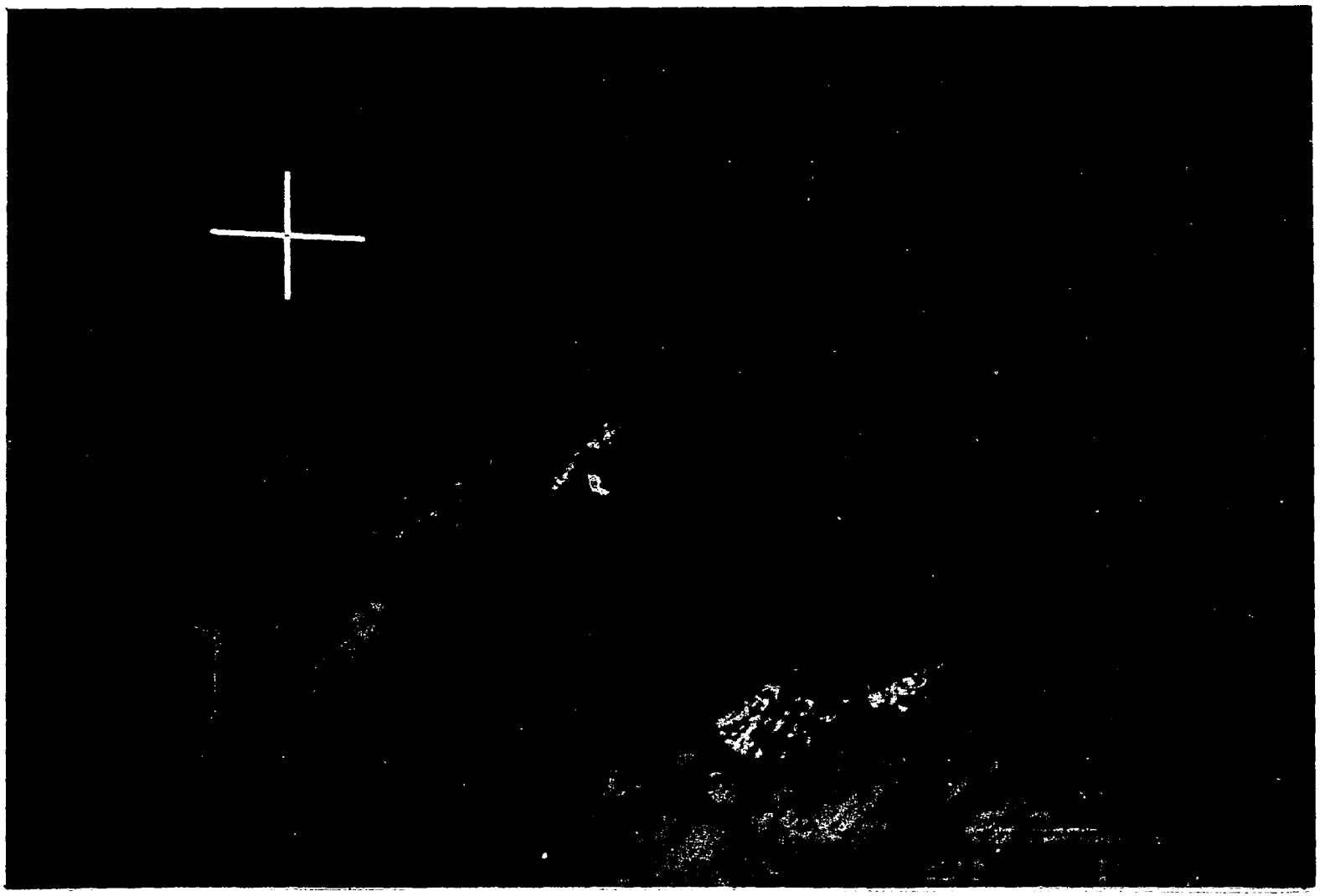

Figure 9.7 Ratio/Ratio CRC Image.

clay mineral concentration, due to high ratio values for ratio/ratio image number one (color coded red in the CRC image).

Chromaticity Diagram Analysis

The chromaticity diagram for this CRC image shows unique separation of the rock units (Figure 9.3). The normalized ratio values are spread over a wide range of regions between the red and green vertexes. The separability should provide unique colorations for each rock unit. A direct comparison of the CRC to the chromaticity diagram verifies the rock unit separability.

Overall, the CRC image matches the general color trend depicted by the chromaticity diagram. The CRC image appears yellowish-green, with areas of green dominating in the center and outer fringes of the image. The dacite porphyry appears yellowish-orange to orange-red which matches quite well with the predetermined colors of orange to reddish orange found in the chromaticity diagram. The alaskite appears yellow to yellowish-green to greenish-yellow in the image and also matches well with the colors presented in the chromaticity diagram. The paleozoic sedimentary sequence of limestones and quartzites appear green to greenish-yellow, and blue in the CRC image. Direct comparison of these rocks to their color designations in the chromaticity diagram shows that the limestone should appear yellow. The discrepency of color can be linked to the dominance of the 0.44/0.72 ratio image for the paleozoic sedimentary sequence. This ratio pair is color coded blue; therefore regions with only this rock unit exposed will appear blue. Also, since the limestone has the lowest ratio value for the green colored

ratio/ratio pair (number 5), it will appear dark green in the image. The combination of the two colors will make the limestone appear dark blue to blue-green. So, the chromaticity diagram was not useful for actual color designation of the limestone. However, the chromaticity diagram provided good spectral separability and good color designations for the rest of the rock units. Therefore, the chromaticity diagram proved useful as a qualitative tool for determining which rock unit discrimination in a CRC image.

Certain colors in the CRC image portray several lithologic units. One would tend to map similarly colored areas as one distinct lithologic unit without benefit of reference material for direct image comparison. Therefore, care must be taken for proper material identification when interpreting CRC images. Direct comparisons to other geologic data, such as geologic maps, will aid in the discrete differentiation and labeling of rock units. Use of ratio/ratio images in a CRC image should be conducted at a later stage in an exploration program, well after the initial ratio images are formed, interpreted and evaluated.

CHAPTER 10

CONCLUSIONS

In arid and semiarid regions, remote sensing data can be successfully used for detection and discrimination of rock and mineral units associated with hydrothermal alteration assemblages. By combining multiscanner data sets, the detectability and separability of rock and alteration units increase. The analyst can pick and choose spectral bands from both scanners that will effectively discriminate the desired materials. Spectral reflectance data generated from field samples provides the analyst with information necessary for spectral band selection.

A new technique for ratio pair selection in a CRC image has been proposed and has proved successful for determining spectral separability of materials. Through mathematical manipulation of ratio values, generated from field gathered spectral reflectance data, information can be derived that will determine spectral separability of materials based upon ratio pair combinations. The information is derived by plotting normalized ratio values for three ratio pairs in a ternary diagram. Spectral separability of the materials can be determined through use of this diagram.

Furthermore, a unique relationship between ternary diagrams and chromaticity diagrams has been proposed that effectively approximates the colors of each field-sampled material that will appear in the CRC image. This new qualitative approach of color assignment removes much of the ambiguity associated with color assignments in CRC images. However, high variability of spectral reflectance properties of materials leads to color variability in the CRC image. This color variability does not appear in the chromaticity diagram, mainly due to the limited field data samples used in generating the diagram. Overall, the ternary/chromaticity diagram method can qualitatively determine the approximate colorations for each material prior to actual CRC image compilation.

Finally, this new method provides the analyst a tool for predetermining which three-ratio set will produce the best CRC image based upon: 1) spectral reflectance values of materials, and 2) spectral separability of materials through spectral band ratios. This is very important, as it can decidedly cut down on computer time and cost associated with compiling CRC images in an analysis program.

APPENDIX A

COMPUTER PROGRAMS

ALL IMAGE PROCESSING WAS CONDUCTED AT THE DIGITAL IMAGE ANALYSIS LABORATORY (DIAL). COMPUTER PROGRAMS WERE WRITTEN OR MODIFIED FOR USE OF THE SADIE 3.0 SUBROUTINE LIBRARY.

Program RVERSE: Program for Geosat image reversal correction.

```
      PROGRAM RVERSE
      INTEGER BUF1(512),BUF2(512),FILE1(15),FILE2(15)
      INTEGER BUF3(512),BUF4(512)
      TYPE*, 'PROGRAM RVERSE IS DESIGNED TO CREATE A REVERSED'
      TYPE*, 'IMAGE OF A GEOSAT IMAGE.  THE NEW, REVERSED IMAGE'
      TYPE*, 'WILL BE GEOGRAPHICALLY CORRECT WITH RESPECT TO'
      TYPE*, 'THE EAST AND WEST DIRECTIONS.'
      TYPE*, 'INPUT FILE NAME: '
      READ(5,100) FILE1
  100 FORMAT(15A2)
      FILE1(15)=0
      OPEN(UNIT=1,NAME=FILE1,TYPE='OLD',FORM='UNFORMATTED')
      READ(1) NPIX,NLINE,NBAND
      TYPE*, 'OUTPUT FILE NAME: '
      READ(5,100) FILE2
      FILE2(15)=0
      OPEN(UNIT=2,NAME=FILE2,TYPE='NEW',FORM='UNFORMATTED')
      WRITE(2) NPIX,NLINE,NBAND
      NWRDS=NPIX/2
      LINE=NLINE*NBAND
C.....LINE LOOP
      DO 10 I=1,LINE
      TYPE*, I
      READ(1) (BUF1(II),II=1,NWRDS)
C.....UNPACK DATA
      DO 20 J=1,NWRDS
      BUF2(2*J-1)=BUF1(J).AND.'377
      BUF2(2*J)=ISHFT(BUF1(J),-8).AND.'377
   20 CONTINUE
C.....PIXEL LOOP
      DO 30 K=1,NPIX
      IPIX=NPIX+1
      BUF3(K)=BUF2(IPIX-K)
   30 CONTINUE
C.....PACK DATA AND OUTPUT
      DO 40 L=1,NWRDS
      I1=BUF3(2*L-1).AND.'377
      I2=BUF3(2*L)
      I3=ISHFT(I2,8)
      I3=I3.AND.'177400
      BUF4(L)=I1.OR.I3
   40 CONTINUE
      WRITE(2) (BUF4(JJ),JJ=1,NWRDS)
   10 CONTINUE
      WRITE(5,200) NBAND,FILE1
  200 FORMAT(I2' BAND INPUT FILE: '15A2)
      WRITE(5,300) NBAND,FILE2
  300 FORMAT(I2' BAND OUTPUT FILE CREATED: '15A2)
      CLOSE(UNIT=1)
```

```
      CLOSE(UNIT=2)
      STOP
      END
```

Program ALTER1: Computer program used for geometric warping of the 8 channel data set.

```
      PROGRAM ALTER1
      REAL X(18),Y(18),XP(18),YP(18)
      DATA XP/264,188,169,157,103,200,212,206,202,145,127,48,
     + 109,288,317,25,234,241/
      DATA YP/243,229,246,258,340,281,289,317,327,339,383,408,
     + 264,259,218,358,246,161/
      DATA X/205,273,307,330,435,311,307,339,351,404,449,506,
     + 376,197,117,492,241,142/
      DATA Y/138,351,349,348,270,196,143,80,63,175,98,224,427,
     + 26,66,385,207,391/
      CALL INIT
      CALL SCOEFF(X,Y,XP,YP,18,6)
      CALL GEOM(1,3,6,512,512,1.0)
      CALL FINI
      END
```

Program ALTER2: Program used for geometric warping of the 11 channel data set.

```
      PROGRAM ALTER2
      REAL X(18),Y(18),XP(18),YP(18)
      DATA XP/264,188,169,157,103,200,212,206,202,145,127,18,109,
     + 288,317,25,234,241/
      DATA YP/243,229,246,258,340,281,289,317,327,339,383,408,264,
     + 259,218,358,246,161/
      DATA Y/237,267,291,307,391,305,305,330,340,373,411,454,334,
     + 239,185,436,257,176/
      DATA Y/129,303,319,326,316,203,169,143,136,234,207,326,414,56,
     + 54,446,185,287/
      CALL INIT
      CALL SCOEFF(X,Y,XP,YP,18,6)
      CALL GEOM(1,3,6,512,512,1.0)
      CALL FINI
      END
```

Program MOD1: Program used for atmospheric correction for all data sets.

```
      PROGRAM MOD1
      EXTERNAL TFPIX
      COMMON/TOM/LUT(256)
      REAL VALUES(5)
      INTEGER IMIN1,IMAX1,IMIN2,IMAX2,IONE,ITWO,IHIST,IA
      TYPE 10
10    FORMAT(1X,'INPUT WF NUMBER = ',$)
      ACCEPT *, IONE
      TYPE 20
20    FORMAT(1X,'OUTPUT WF NUMBER = ' $)
      ACCEPT *, ITWO
      TYPE 30
30    FORMAT(1X,'NUMBER OF BINS FOR OUTPUT HISTOGRAM = ',$)
      ACCEPT *, IHIST
      TYPE 40
40    FORMAT(1X,'INPUT GL VALUE TO SUB FROM ALL PIXELS = ',$)
      ACCEPT *, IA
      TYPE 110
110   FORMAT(1X,'INPUT MIN GL VALUE TO = OUTPUT GL OF 0 = ',$)
      ACCEPT *, IMIN1
      TYPE *, ' '
      TYPE *, 'MAX GL BELOW SHOULD BE 1 UNIT LARGER THAN'
      TYPE *, 'THE GL VALUE TO SUB FROM ALL PIXELS'
      TYPE 120
120   FORMAT(1X,'INPUT MAX GL VALUE TO = OUTPUT GL OF 0 = ',$)
      ACCEPT *, IMAX1
      TYPE *, ' '
      TYPE *, 'THE NEXT TWO VARIABLES REPRESENT THE BIAS'
      TYPE *, 'SHIFT RANGE, MINIMUM AND MAXIMUM'
      TYPE 130
130   FORMAT(1X,'INPUT MIN GL TO SHIFT TO 0 = ',$)
      ACCEPT *, IMIN2
      TYPE 140
140   FORMAT(1X,"INPUT MAX GL TO BE SHIFTED = ",$)
      ACCEPT *, IMAX2
C.....SET UP LOOK-UP TABLE
      DO 100 I=IMIN1,IMAX1
      LUT(I)=0
100   CONTINUE
      DO 200 I=IMIN2,IMAX2
      LUT(I)=I-IA
200   CONTINUE
      LUT(256)=0
C.....CALL SADIE SUBROUTINES
      CALL INIT
      CALL STRETCH(IONE,ITWO,TFPIX)
      CALL STATS(ITWO,1,IHIST,VALUES)
      CALL FINI
      END
```

```
      SUBROUTINE TFPIX(A,N)
      DIMENSION A(1)
      COMMON/TOM/LUT(256)
C.....TRANSFORM ONE LINE AT A TIME
      DO 80 IPIX=1,N
      I=A(IPIX)
      IF(I.EQ.0) GOTO 5
      A(IPIX)=LUT(I)
      GOTO 80
5     A(IPIX)=LUT(256)
80    CONTINUE
      RETURN
      END
```

Program CRC2: Program used for compiling a CRC image from three ratio images.

```
      PROGRAM CRC2
      REAL VALUES(5)
      INTEGER IOUT, IHIST, NWFS, INWFS(3)
      DATA INWFS/1,2,3/
      TYPE 10
10    FORMAT(1X, '# OF INPUT WFS = ',$)
      ACCEPT *, NWFS
      TYPE 20
20    FORMAT(1X, 'OUTPUT WF NUMBER = ',$)
      ACCEPT *, IOUT
      TYPE 30
30    FORMAT(1X, '# OF BINS IN OUTPUT HISTOGRAM = ',$)
      ACCEPT *, IHIST
C.....CALL SADIE SUBROUTINES
      CALL INIT
      CALL LEAVE(INWFS,IOUT,NWFS)
      CALL STATS(IOUT,1,IHIST,VALUES)
      CALL FINI
      END
```

Program RATIO1: Program used for dividing one image by another.

```
      PROGRAM RATIO1
      REAL A, VALUES(5)
      INTEGER IONE1,IONE2,ITWO,IHIST
      TYPE *, 'PROGRAM RATIO1 DIVIDES ONE IMAGE BY ANOTHER.'
      TYPE *, 'IT FORMS A PIXEL-BY-PIXEL QUOTIENT OF THE TWO'
      TYPE *, 'IMAGES. THE EQUATION USED IS:'
      TYPE *, '     OUT = A*IN1/IN2
      TYPE *, ' '
      TYPE 10
10    FORMAT(1X,'INPUT NUMERATOR WF NUMBER (IN1) = ',$)
      ACCEPT *, IONE
      TYPE 20
20    FORMAT(1X,'INPUT DENOMINATOR WF NUMBER (IN2) = ',$)
      ACCEPT *, IONE2
      TYPE 30
30    FORMAT(1X,'OUTPUT WF NUMBER (OUT) = ',$)
      ACCEPT *, ITWO
      TYPE 40
40    FORMAT(1X,'NUMBER OF BINS FOR OUTPUT HISTOGRAM = ',$)
      ACCEPT *, IHIST
      TYPE *, ' '
      TYPE *, 'SCALE FACTOR AND QUOTIENT SWITCH "A" MUST BE'
      TYPE *, 'A NEGATIVE NUMBER.'
      TYPE *, ' '
      TYPE 50
50    FORMAT(1X,'SCALE FACTOR "A" FOR RATIO (REAL) = ',$)
      ACCEPT *, A
      TYPE *, ' '
C.....CALL SADIE SUBROUTINES
      CALL INIT
      CALL PROQUO(IONE1,IONE2,ITWO,A)
      CALL STATS(ITWO,1,IHIST,VALUES)
      CALL FINI
      END
```

APPENDIX B

CONTROL POINT DATA

PART A: INITIAL CONTROL POINT COORDINATE DATA FOR BOTH DATA SETS

PART B: FINAL CONTROL POINT COORDINATES FOR BOTH DATA SETS

PART A. CONTROL POINT COORDINATE DATA:
8 Channel Data Set, First Iteration

Control Point	MATCH IMAGE X	MATCH IMAGE Y	REFERENCE IMAGE (XP)	REFERENCE IMAGE (YP)
1	204.00	139.00	264.00	243.00
2	271.00	353.00	188.00	229.00
3	308.00	343.00	169.00	246.00
4	329.00	350.00	157.00	258.00
5	439.00	270.00	103.00	340.00
6	339.00	214.00	181.00	293.00
7	307.00	143.00	212.00	289.00
8	339.00	80.00	206.00	317.00
9	353.00	63.00	202.00	327.00
10	404.00	175.00	145.00	339.00
11	449.00	98.00	127.00	383.00
12	504.00	224.00	48.00	408.00
13	376.00	427.00	109.00	264.00
14	196.00	26.00	288.00	259.00
15	117.00	66.00	317.00	218.00
16	109.00	392.00	254.00	148.00
17	53.00	413.00	275.00	119.00
18	492.00	385.00	25.00	358.00
19	241.00	207.00	234.00	246.00
20	141.00	391.00	241.00	161.00

X COORDINATE TRANSFORMATION

A=322.750
B= -1.351 XP
C= 0.590 YP
D= 0.002 XP*YP
E= -0.001 XP*XP
F= 0.000 YP*YP

Y COORDINATE TRANSFORMATION

G=673.250
H= 0.641 XP
I= 0.534 YP
J= -0.006 XP*YP
K= -0.003 XP*XP
L= -0.003 YP*YP

C.P.	X CALC	Y CALC	DELTA X	DELTA Y
1	206.54	137.99	-2.54	1.01
2	273.26	349.59	-2.26	3.41
3	307.84	350.36	0.16	-7.36
4	329.67	347.94	-0.67	2.06
5	435.69	270.45	3.31	-0.45
6	338.54	210.51	0.46	3.49
7	306.96	144.40	0.04	-1.40
8	339.03	80.23	-0.03	-0.23
9	351.71	61.59	1.29	1.41
10	405.87	175.64	-1.87	-0.64
11	450.89	98.55	-1.89	-0.55
12	507.01	223.23	-3.01	0.77
13	377.21	425.56	-1.21	1.44
14	198.52	25.35	-2.52	0.65
15	115.47	66.63	1.53	-0.63
16	111.91	392.79	-2.91	-0.79
17	49.60	412.04	3.40	0.96
18	492.69	385.18	-0.69	-0.18
19	242.02	205.61	-1.02	1.39
20	143.14	390.89	-2.14	0.11

Root Mean Square Error at Control Points = 2.936

PART A: CONTROL POINT COORDINATE DATA:
11 Channel Data Set, First Iteration

Control Point	MATCH IMAGE X	MATCH IMAGE Y	REFERENCE IMAGE XP	REFERENCE IMAGE YP	
1	237.00	129.00	264.00	243.00	X COORDINATE TRANSFORMATION
2	267.00	303.00	188.00	229.00	
3	291.00	326.00	169.00	246.00	A=205.375
4	307.00	326.00	157.00	258.00	B= -0.768 XP
5	392.00	310.00	103.00	340.00	C= 0.773 YP
6	323.00	228.00	181.00	293.00	D= 0.001 XP*YP
7	305.00	169.00	212.00	289.00	E= 0.000 XP*XP
8	330.00	143.00	206.00	317.00	F= 0.000 YP*YP
9	340.00	136.00	202.00	327.00	
10	373.00	234.00	145.00	339.00	
11	411.00	207.00	127.00	383.00	X COORDINATE TRANSFORMATION
12	454.00	326.00	48.00	408.00	
13	334.00	412.00	109.00	264.00	
14	239.00	56.00	288.00	259.00	G=993.750
15	185.00	54.00	317.00	218.00	H= -2.034 XP
16	146.00	273.00	254.00	148.00	I= -1.302 YP
17	119.00	275.00	275.00	119.00	J= 0.000 XP*YP
18	436.00	446.00	25.00	358.00	K= 0.000 XP*XP
19	257.00	185.00	234.00	246.00	L= 0.000 YP*YP
20	178.00	287.00	241.00	161.00	

C.P.	X CALC	Y CALC	DELTA X	DELTA Y
1	237.06	127.96	-0.06	1.04
2	266.03	302.93	0.97	0.07
3	290.12	317.92	0.88	8.08
4	305.87	325.43	1.13	0.57
5	391.01	316.57	0.99	-6.57
6	321.52	227.27	1.48	0.73
7	303.39	170.00	1.61	-1.00
8	328.94	142.37	1.06	0.63
9	338.69	136.15	1.31	-0.15
10	372.54	233.83	0.46	0.17
11	410.60	205.44	0.40	1.56
12	454.84	325.05	-0.84	0.95
13	334.72	413.93	-0.72	-1.93
14	238.94	56.46	0.06	-0.46
15	184.23	52.83	0.77	1.17
16	154.73	277.55	-8.73	-4.55
17	112.86	272.39	6.14	2.61
18	434.18	445.18	1.82	0.82
19	255.77	185.35	1.23	-0.35
20	175.14	287.02	2.86	-0.02

Root Mean Square Error at Control Points = 3.804

PART B. CONTROL POINT COORDINATE DATA:
8 Channel Data Set, Seventh Iteration

Control Point	MATCH IMAGE X	MATCH IMAGE Y	REFERENCE IMAGE XP	REFERENCE IMAGE YP
1	205.00	138.00	478.00	236.00
2	273.00	351.00	326.00	208.00
3	307.00	349.00	288.00	242.00
4	330.00	348.00	264.00	266.00
5	435.00	270.00	156.00	430.00
6	311.00	196.00	350.00	312.00
7	307.00	143.00	374.00	328.00
8	339.00	80.00	362.00	384.00
9	351.00	63.00	354.00	404.00
10	404.00	175.00	240.00	428.00
11	449.00	98.00	204.00	516.00
12	506.00	224.00	46.00	566.00
13	376.00	427.00	168.00	278.00
14	197.00	26.00	526.00	268.00
15	117.00	66.00	584.00	186.00
16	492.00	385.00	0.00	466.00
17	241.00	207.00	418.00	242.00
18	142.00	391.00	432.00	72.00

X COORDINATE TRANSFORMATION

A=355.969
B= -0.517 XP
C= 0.338 YP
D= 0.001 XP*YP
E= 0.000 XP*XP
F= 0.000 YP*YP

Y COORDINATE TRANSFORMATION

G=692.672
H= -0.191 XP
I= -0.279 YP
J= -0.002 XP*YP
K= -0.001 XP*XP
L= -0.001 YP*YP

C.P.	X CALC	Y CALC	DELTA X	DELTA Y
1	206.50	137.83	-1.50	0.17
2	272.79	349.74	0.21	1.26
3	307.36	350.49	-0.36	-1.49
4	329.19	348.04	0.81	-0.04
5	435.07	270.24	-0.07	-0.24
6	310.08	195.93	0.92	0.07
7	306.51	144.26	0.49	-1.26
8	338.11	80.33	0.89	-0.33
9	350.60	61.79	0.40	1.21
10	405.03	175.46	-1.03	-0.46
11	449.24	98.65	-0.24	-0.65
12	505.81	223.01	0.19	0.99
13	376.34	426.30	-0.34	0.70
14	198.19	25.61	-1.19	0.39
15	115.68	66.66	1.32	-0.66
16	492.12	385.45	-0.12	-0.45
17	241.93	205.37	-0.93	1.63
18	142.23	391.47	-0.23	-0.47

Root Mean Square Error at Control Points = 1.138

PART B. CONTROL POINT COORDINATE DATA:
11 Channel Data Set, Seventh Iteration

Control Point	MATCH IMAGE X	MATCH IMAGE Y	REFERENCE IMAGE XP	REFERENCE IMAGE YP
1	237.00	129.00	478.00	236.00
2	267.00	303.00	326.00	208.00
3	291.00	319.00	288.00	242.00
4	307.00	326.00	264.00	266.00
5	391.00	316.00	156.00	430.00
6	305.00	204.00	350.00	312.00
7	305.00	169.00	374.00	328.00
8	330.00	143.00	362.00	384.00
9	340.00	136.00	354.00	404.00
10	373.00	234.00	240.00	428.00
11	411.00	207.00	204.00	516.00
12	454.00	326.00	46.00	566.00
13	334.00	414.00	168.00	278.00
14	239.00	56.00	526.00	268.00
15	185.00	54.00	584.00	186.00
16	436.00	446.00	0.00	466.00
17	257.00	185.00	418.00	242.00
18	176.00	287.00	432.00	72.00

X COORDINATE TRANSFORMATION

A=274.906
B= -0.298 XP
C= 0.392 YP
D= 0.000 XP*YP
E= 0.000 XP*XP
F= 0.000 YP*YP

Y COORDINATE TRANSFORMATION

G=784.609
H= -1.033 XP
I= -0.712 YP
J= 0.000 XP*YP
K= 0.000 XP*XP
J= 0.000 YP*YP

C.P.	X CALC	Y CALC	DELTA X	DELTA Y
1	238.00	127.87	-1.00	1.13
2	266.97	302.81	0.03	0.19
3	291.09	317.74	-0.09	1.26
4	306.86	325.22	0.14	0.78
5	391.78	316.57	-0.78	-0.57
6	303.74	205.36	1.26	-1.36
7	304.32	169.75	0.68	-0.75
8	329.56	142.37	0.44	0.63
9	339.18	136.26	0.82	-0.26
10	373.26	233.76	-0.26	0.24
11	410.69	206.00	0.31	1.00
12	454.83	326.04	-0.83	-0.04
13	335.34	414.17	-1.34	-0.17
14	239.51	56.76	-0.51	-0.76
15	184.87	53.27	0.13	0.73
16	434.47	446.01	1.53	-0.01
17	256.84	185.07	0.16	-0.07
18	175.51	287.72	0.49	-0.72

Root Mean Square Error at Control Points = 1.041

APPENDIX C

REFLECTANCE CURVES FOR FIELD DATA

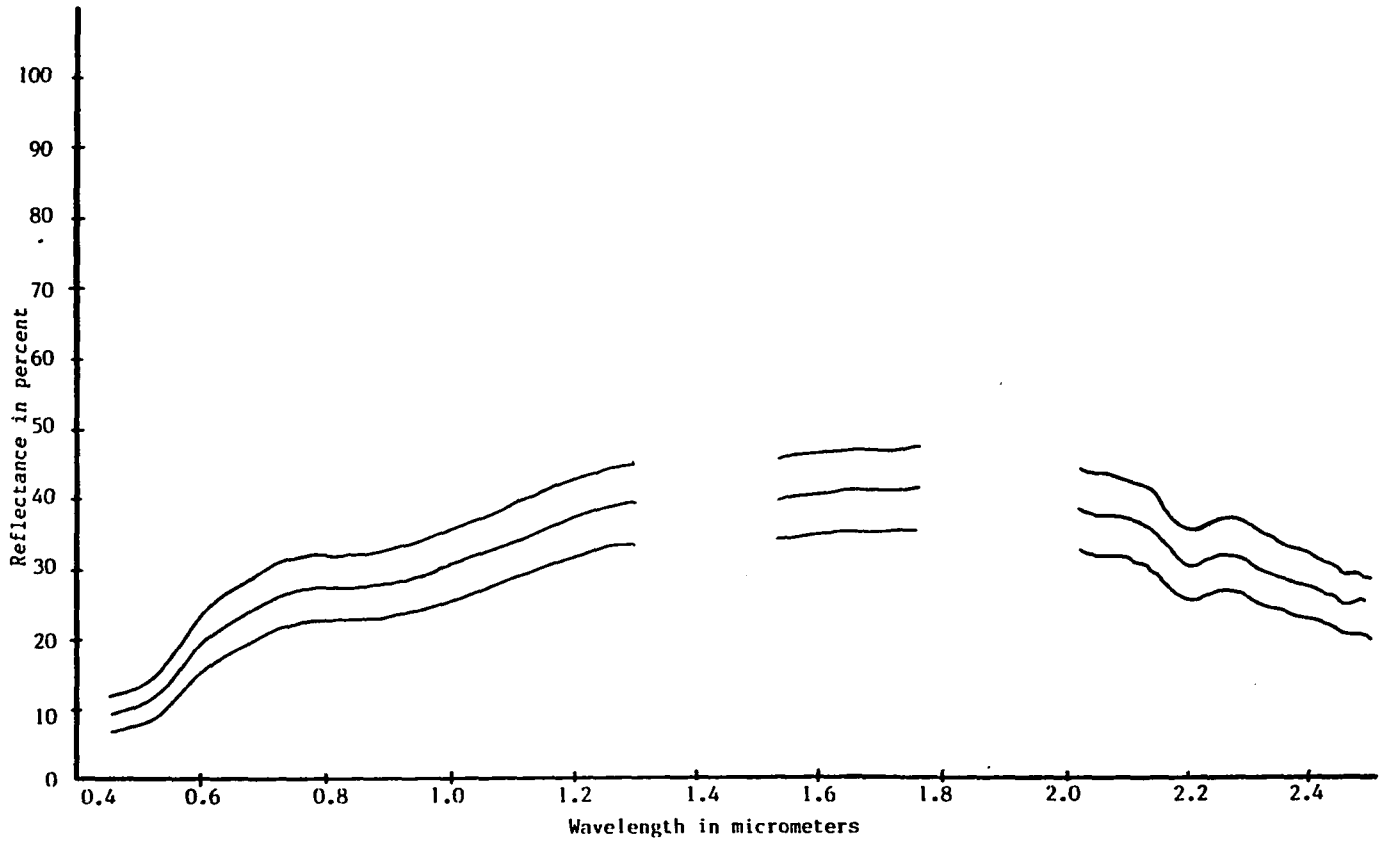

Figure C1. Alaskite: Potassic/Propylitic, Sample # 52405.

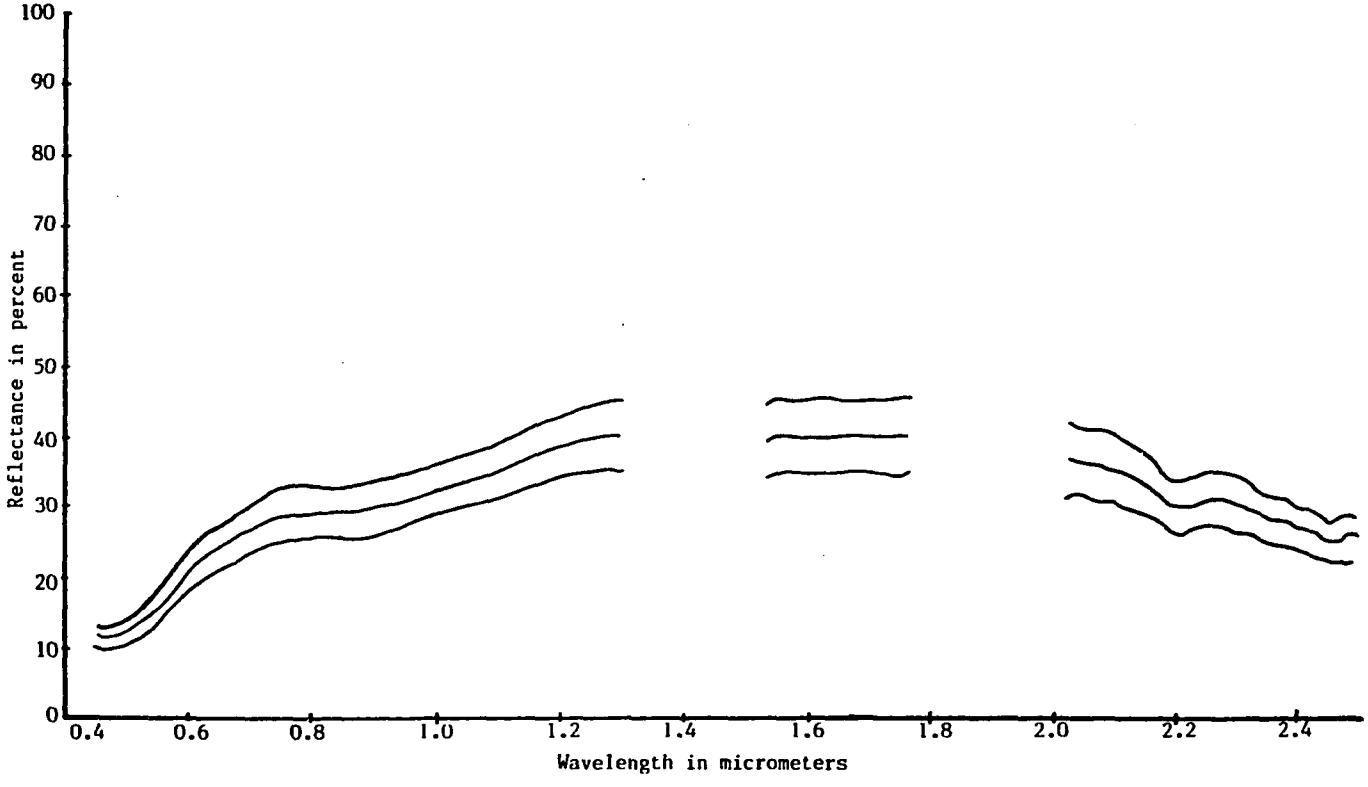

Figure C2. Alaskite: Phyllic, Sample # 52406.

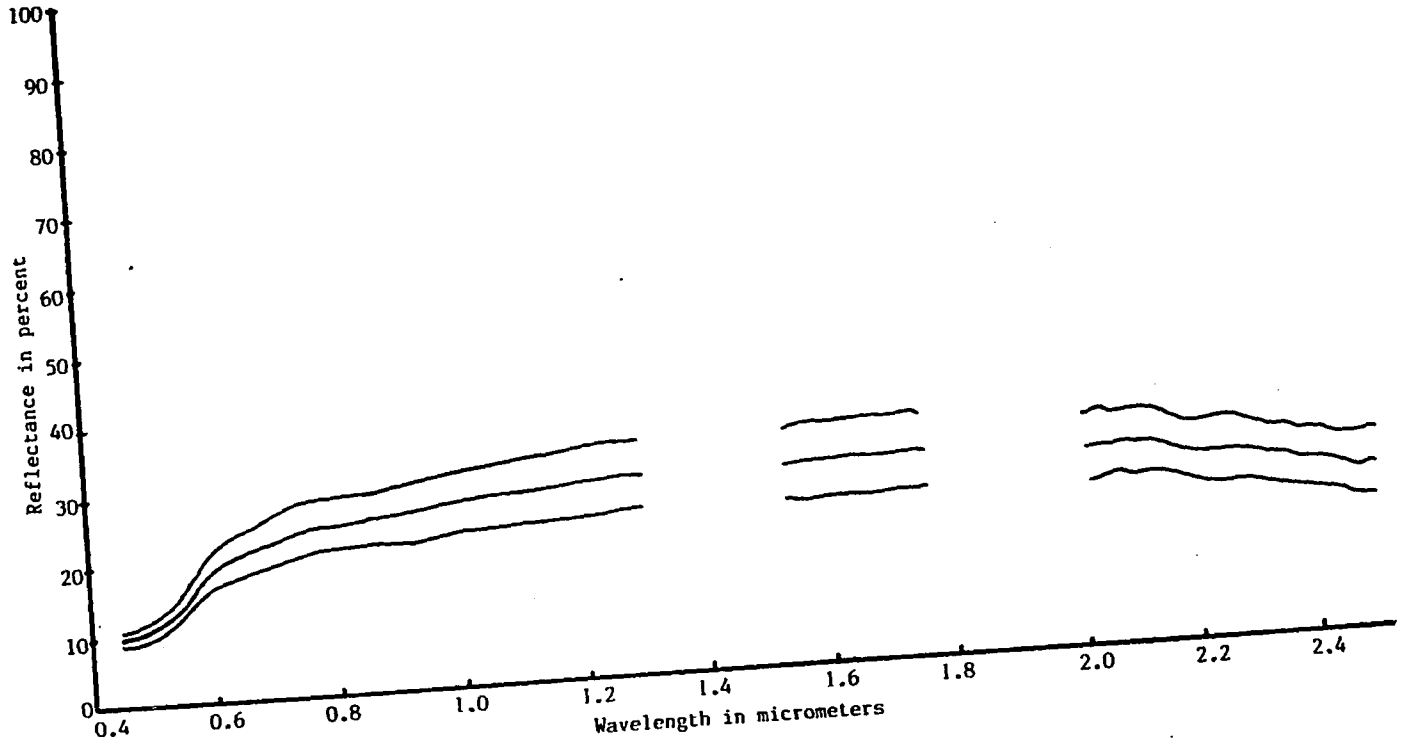

Figure C3. Alaskite: Propylitic, Sample # 52603.

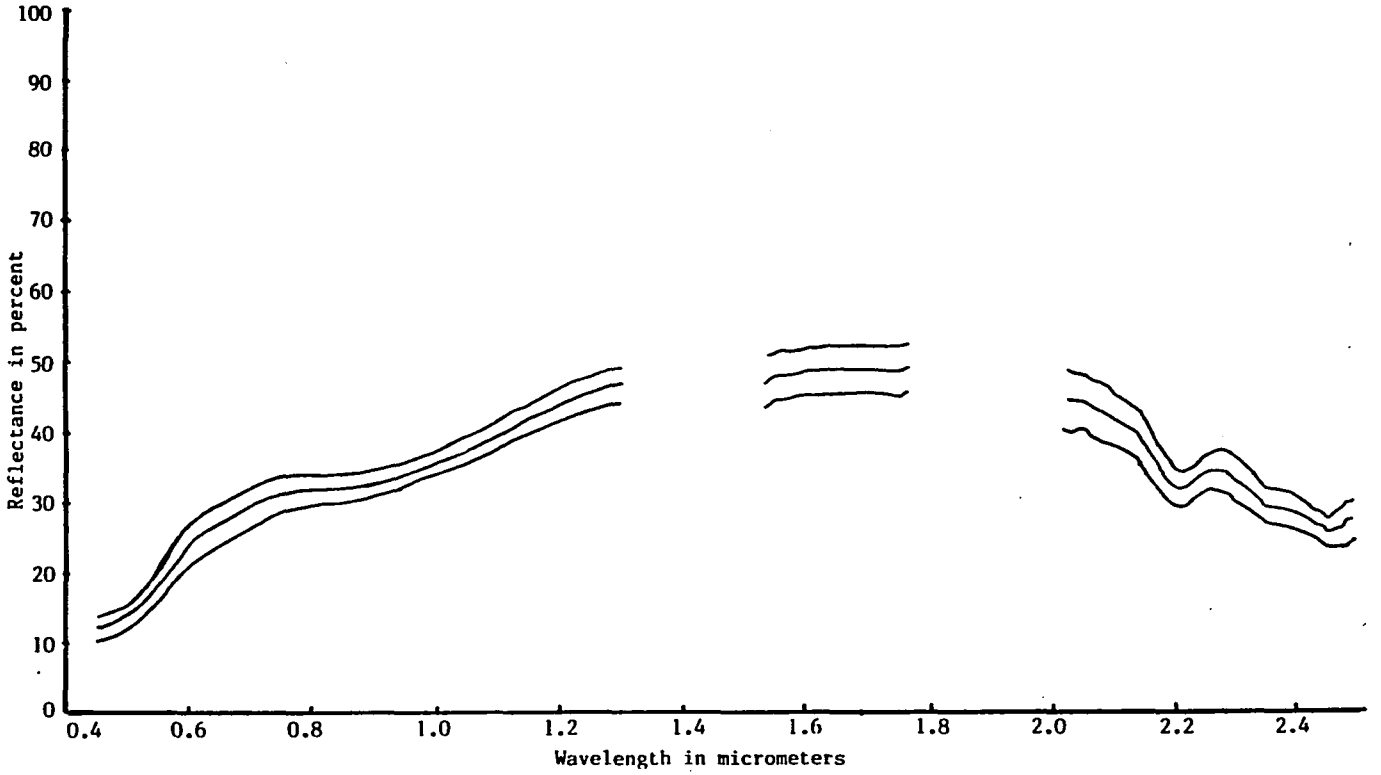

Figure C4. Dacite Porphyry: Potassic, Sample # 52604.

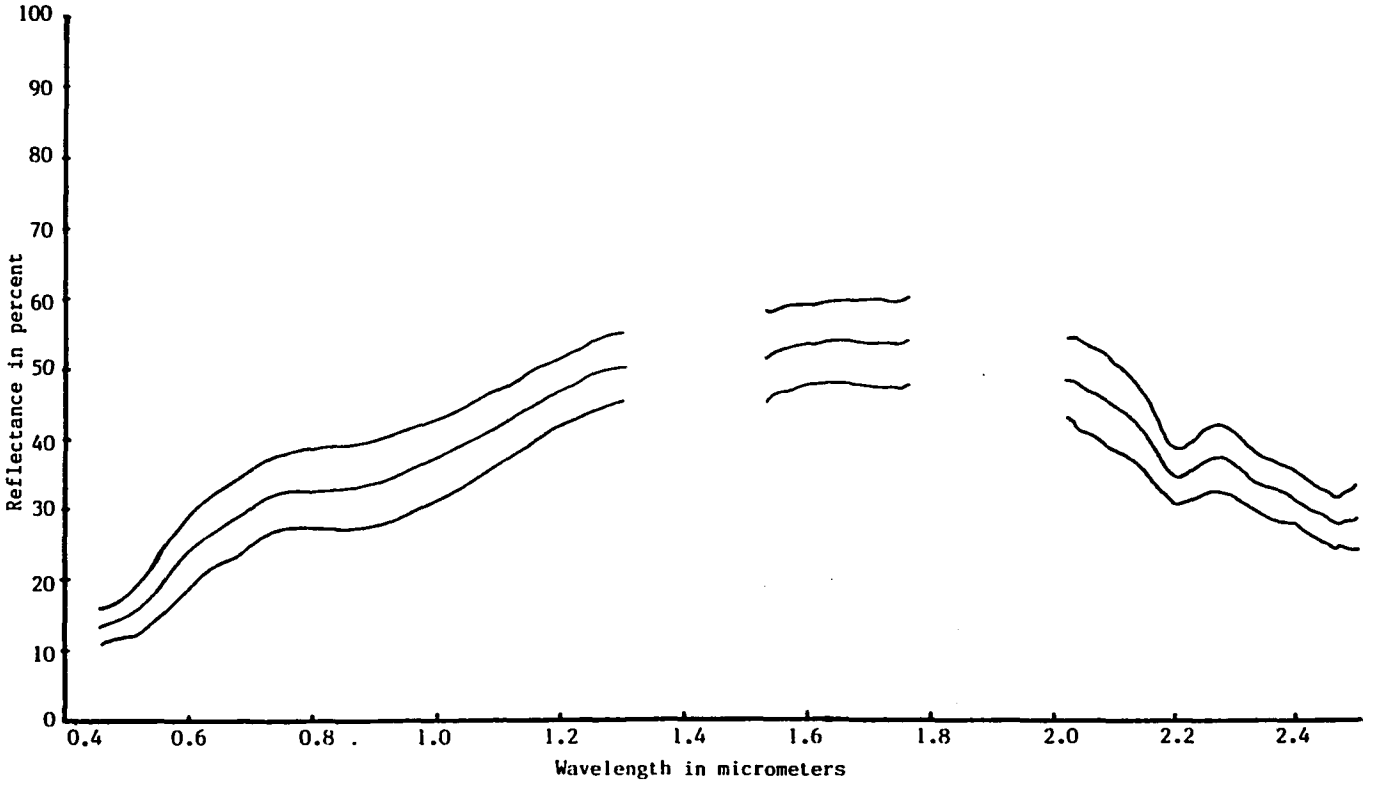

Figure C5. Dacite Porphyry: Phyllic, Sample # 52605.

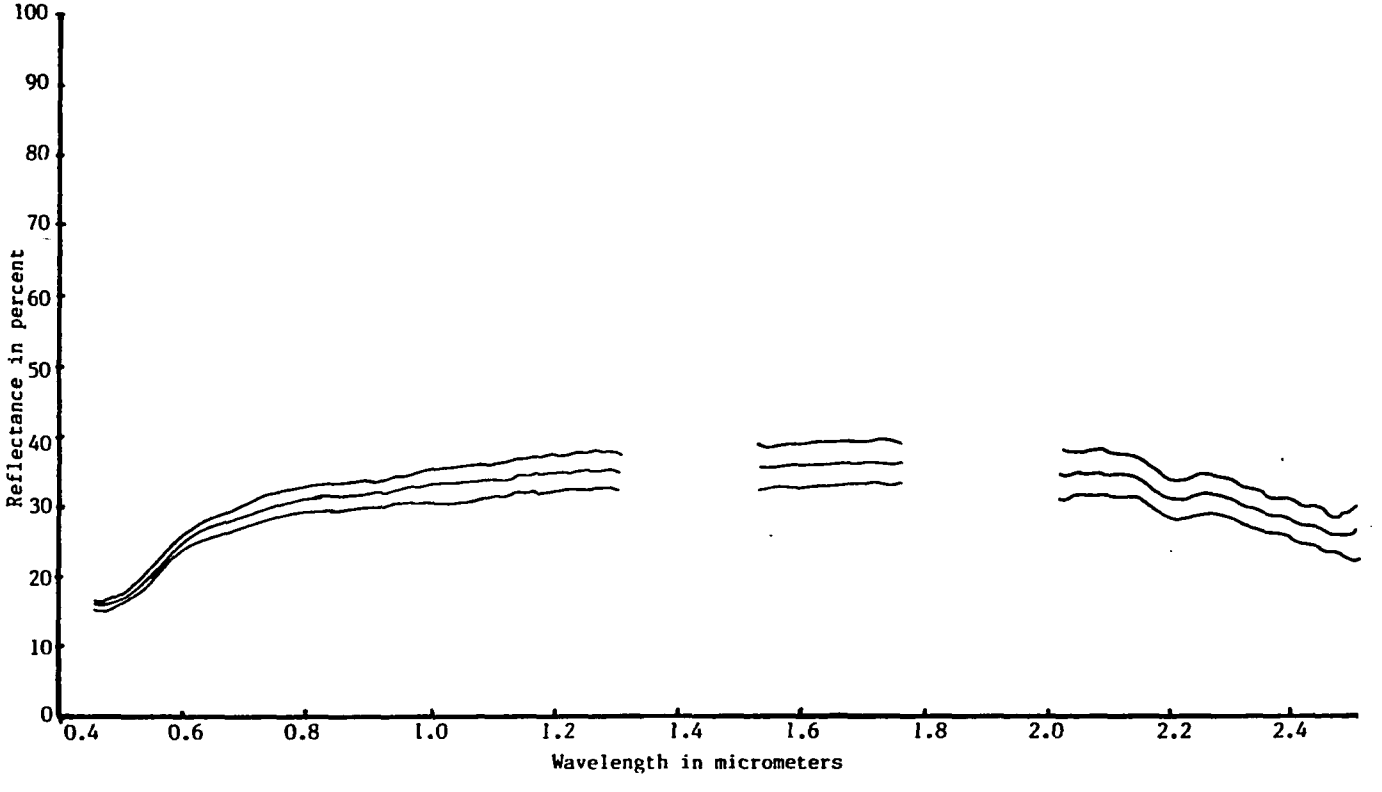

Figure C6. Quartz Monzonite: Propylitic, Sample # 52602.

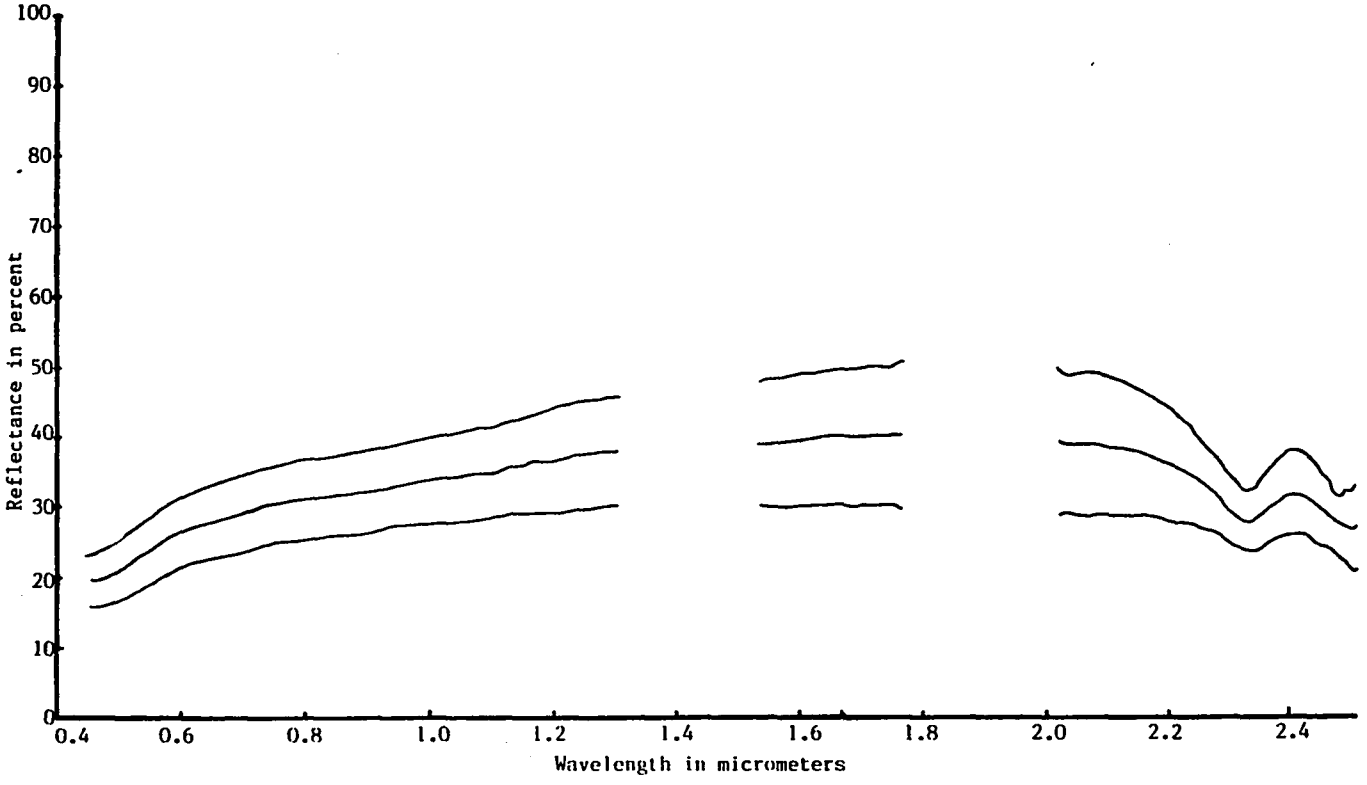

Figure C7. Limestone, Sample # 52403.

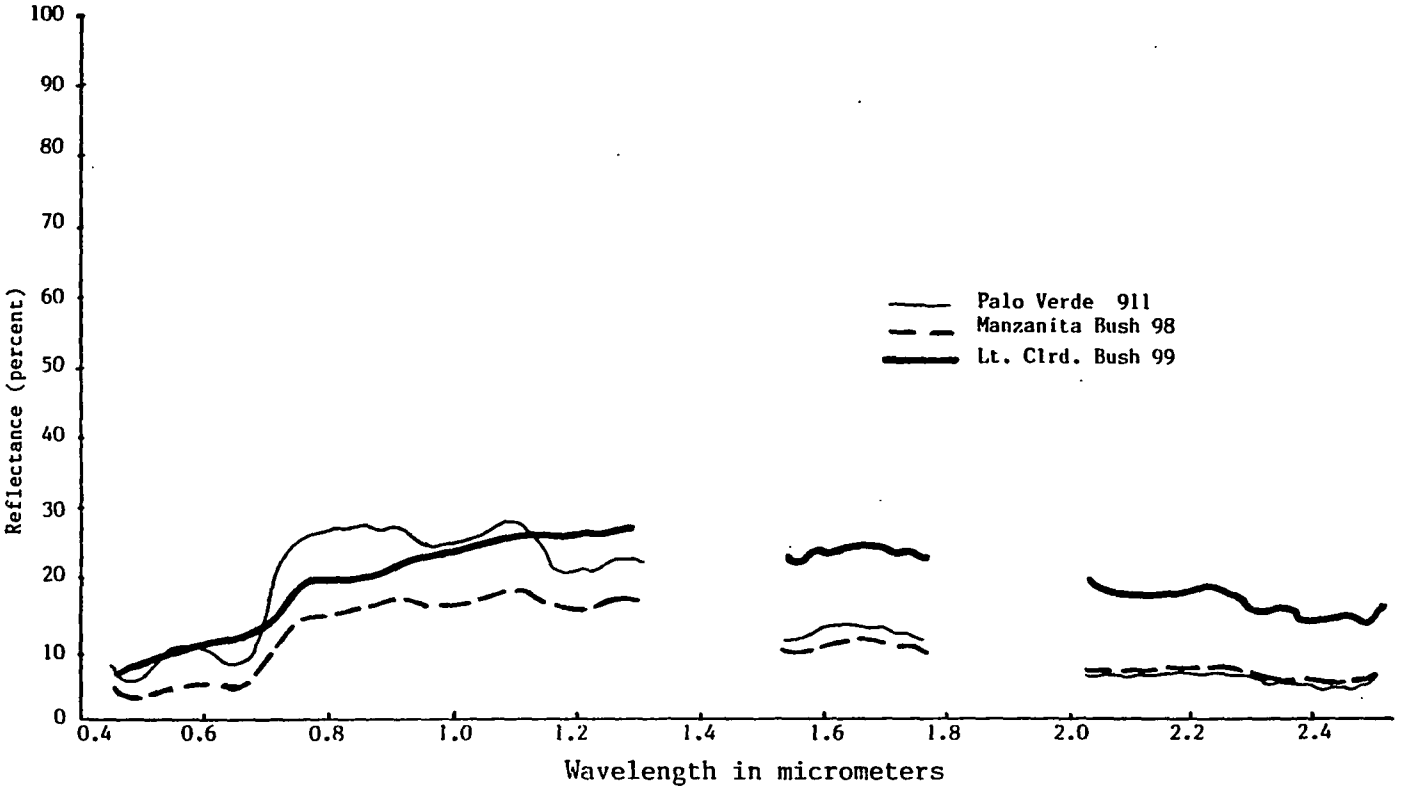

Figure C8. Vegetation Samples: Palo Verde, Manzanita and Lt. Clrd. Bush.

APPENDIX D

REFLECTANCE VALUES FROM FIELD DATA

APPENDIX D

Reflectance Values for Field Data at Specific Wavelengths

Columns 1 through 8 show percent reflectance values at specific wavelengths for each sample.

Column 1 = 0.44 micrometer
Column 2 = 0.56 micrometer
Column 3 = 0.68 micrometer
Column 4 = 0.72 micrometer
Column 5 = 0.815 micrometer
Column 6 = 1.015 micrometer
Column 7 = 1.65 micrometer
Column 8 = 2.20 micrometer

Alaskite: Potassic/Propylitic Alteration

Sample #	1	2	3	4	5	6	7	8
52405	9.5	14.0	23.5	26.0	27.0	30.0	41.0	30.0
5240501	10.0	17.5	24.0	26.0	27.5	30.5	40.0	30.0
5240502	8.0	15.0	25.0	27.5	29.0	32.5	44.0	30.5
5240503	10.0	18.0	30.0	32.0	33.0	38.0	46.0	35.0
5240504	12.0	20.0	30.0	33.0	34.0	38.0	49.0	38.0
5240505	7.0	12.0	20.0	22.0	22.0	24.0	34.5	23.0
5240506	7.0	12.0	21.0	22.5	23.0	26.0	34.0	26.0
5240507	7.0	12.5	19.0	22.0	24.0	27.5	35.0	25.0
5240508	8.0	12.0	21.5	23.0	24.0	28.0	43.0	31.0

Alaskite: Phyllic Alteration

Sample #	1	2	3	4	5	6	7	8
52406	11.5	15.5	25.0	27.5	29.0	32.0	40.5	30.0
5240601	10.0	16.0	24.0	26.0	27.0	29.0	34.5	26.5
5240602	10.0	16.5	25.5	27.5	29.0	32.5	41.0	30.0
5240603	11.0	17.0	25.5	27.5	29.5	32.5	37.5	27.5
5240604	9.0	14.0	22.0	24.5	24.5	27.5	37.0	25.5
5240605	10.0	15.0	23.0	24.5	25.5	30.0	38.0	29.0
5240606	12.0	21.0	31.5	34.0	35.0	38.0	45.5	35.0
5240607	13.0	20.0	30.0	32.5	34.0	36.5	50.0	35.0
5240608	12.0	17.0	24.5	27.0	30.0	32.0	37.0	29.0

Alaskite: Propylitic Alteration

Sample #	1	2	3	4	5	6	7	8
52603	9.5	15.0	22.0	23.0	24.5	26.0	29.0	26.5
5260301	10.0	14.5	21.0	22.0	23.0	24.5	27.0	25.0
5260302	10.0	16.0	22.5	23.5	25.0	27.5	31.5	29.0
5260303	7.5	12.0	17.5	19.0	20.5	22.0	25.5	22.5
5260304	8.0	15.0	23.0	24.0	26.0	29.0	33.0	30.0
5260305	10.0	15.5	25.0	26.0	28.0	30.0	33.0	30.5
5260306	9.0	13.5	17.5	18.0	19.0	20.0	19.0	20.0
5260307	10.0	16.5	26.5	29.0	30.5	32.5	35.0	32.0
5260308	9.5	14.5	21.0	22.5	23.5	25.0	27.0	24.0

Quartz Monzonite: Propylitic Alteration

Sample #	1	2	3	4	5	6	7	8
52602	15.0	21.0	27.5	29.0	30.5	32.5	36.0	31.0
5260201	15.0	21.0	27.0	28.0	29.5	31.5	32.5	28.0
5260202	15.0	22.5	28.0	30.0	32.0	34.0	36.0	31.0
5260203	14.0	21.0	29.0	30.5	32.0	34.5	40.0	32.5
5260204	14.0	21.0	28.0	29.0	30.5	32.5	35.5	31.0
5260205	14.0	20.0	25.0	26.0	27.0	28.0	31.5	27.0
5260206	15.0	22.5	28.0	29.5	31.0	32.5	34.5	29.0
5260207	13.0	22.0	29.0	31.0	32.5	35.0	39.0	34.0
5260208	15.0	21.0	28.0	30.0	31.5	34.0	39.0	34.5

Dacite Porphyry: Potassic Alteration

Sample #	1	2	3	4	5	6	7	8
52604	12.0	19.0	28.0	30.0	32.0	35.0	48.5	32.0
5260401	14.0	22.0	31.0	33.0	34.0	37.5	53.0	30.5
5260402	12.0	17.0	26.5	28.5	31.0	35.0	48.0	32.0
5260403	10.0	16.0	24.0	26.0	28.5	33.0	44.0	28.0
5260446	11.0	20.0	29.0	32.0	32.5	36.0	50.0	32.5
5260447	12.0	21.0	31.0	32.5	34.5	37.5	51.0	35.5
5260448	10.0	17.5	25.5	28.0	29.5	33.0	45.0	29.5

Dacite Porphyry: Phyllic Alteration

Sample #	1	2	3	4	5	6	7	8
52605	12.5	20.0	29.0	31.0	32.5	37.5	53.5	35.0
5260551	17.5	27.0	37.5	40.0	42.0	46.0	60.0	40.0
5260552	12.5	21.0	27.5	30.0	32.0	35.0	48.0	30.0
5260553	12.5	18.0	25.5	28.0	31.0	35.0	48.0	32.0
5260554	10.0	15.0	22.5	24.0	29.0	35.5	47.5	32.5
5260555	14.0	21.0	33.0	35.5	35.0	40.0	60.5	37.5
5260556	12.5	21.0	32.0	33.5	34.0	37.0	50.0	29.5
5260557	10.0	13.0	21.0	23.0	22.5	27.5	59.0	36.0
5260558	11.5	17.5	25.5	29.0	32.0	39.0	52.0	36.0

Limestone

Sample #	1	2	3	4	5	6	7	8
52403	20.0	24.0	28.0	30.0	31.0	33.0	40.0	35.5
5240301	20.0	25.0	30.0	31.0	32.5	34.0	40.0	35.5
5240302	18.0	23.0	27.5	29.0	30.5	33.0	40.0	35.5
5240303	18.0	21.0	23.0	24.0	25.0	25.5	26.0	25.0
5240304	21.0	29.0	34.5	35.5	37.0	40.0	45.0	41.0
5240305	14.0	18.0	23.0	24.5	27.0	30.0	34.0	29.0
5240306	24.0	32.0	36.5	37.5	40.0	44.0	56.5	50.0

Vegetation

Sample	1	2	3	4	5	6	7	8
Manzanita 98	4.0	5.0	5.0	10.0	15.0	16.5	11.0	8.0
Lt. Clrd. Bush 99	7.0	10.0	11.5	15.0	19.5	24.0	25.0	19.0
Palo Verde 911	7.0	10.5	8.0	20.0	27.0	25.0	13.0	7.5

APPENDIX E

RATIO VALUES FOR FIELD DATA. DATA COMPILED FROM WAVELENGTH REFLECTENCE VALUES (REFER TO APPENDIX D).

Columns 1 through 12 represent specific ratio pairs. Ratio values for each ratio pair are computed for each sample and are represented by the values in the tables.

Column 1 = Ratio Values for Ratio Pair 0.44/0.56

Column 2 = Ratio Values for Ratio Pair 0.72/0.56

Column 3 = Ratio Values for Ratio Pair 0.815/0.56

Column 4 = Ratio Values for Ratio Pair 1.015/0.56

Column 5 = Ratio Values for Ratio Pair 0.44/1.015

Column 6 = Ratio Values for Ratio Pair 0.56/1.015

Column 7 = Ratio Values for Ratio Pair 0.68/1.015

Column 8 = Ratio Values for Ratio Pair 0.72/1.015

Column 9 = Ratio Values for Ratio Pair 0.815/1.015

Column 10 = Ratio Values for Ratio Pair 0.44/0.72

Column 11 = Ratio Values for Ratio Pair 0.72/0.44

Column 12 = Ratio Values for Ratio Pair 1.65/2.20

Alaskite: Potassic/Propylitic Alteration

Sample #	1	2	3	4	5	6
52405	0.68	1.86	1.93	2.14	0.32	0.47
5240501	0.57	1.49	1.57	1.74	0.33	0.57
5240502	0.53	1.83	1.93	2.17	0.25	0.46
5240503	0.56	1.78	1.83	2.11	0.26	0.47
5240504	0.60	1.65	1.70	1.90	0.32	0.53
5240505	0.58	1.83	1.83	2.00	0.29	0.50
5240506	0.58	1.88	1.92	2.17	0.27	0.46
5240507	0.56	1.76	1.92	2.20	0.25	0.45
5240508	0.67	1.92	2.00	2.33	0.29	0.43
	7	8	9	10	11	12
52405	0.79	0.87	0.90	0.37	2.74	1.37
5240501	0.79	0.85	0.90	0.38	2.60	1.33
5240502	0.77	0.85	0.89	0.29	3.44	1.44
5240503	0.79	0.84	0.87	0.31	3.20	1.31
5240504	0.79	0.87	0.89	0.36	2.75	1.29
5240505	0.83	0.92	0.92	0.32	3.14	1.50
5240506	0.81	0.87	0.88	0.31	3.21	1.31
5240507	0.69	0.80	0.87	0.32	3.14	1.40
5240508	0.77	0.82	0.86	0.35	2.88	1.39

Vegetation

Sample	1	2	3	4	5	6
Manzanita 98	0.80	2.00	3.00	3.30	0.24	0.30
Lt. Clrd. Bush 99	0.70	1.50	1.95	2.40	0.29	0.42
Palo Verde 911	0.67	1.90	2.57	2.38	0.28	0.42
	7	8	9	10	11	12
Manzanita 98	0.30	0.61	0.91	0.40	2.50	1.38
Lt. Clrd. Bush 99	0.48	0.63	0.81	0.47	2.14	1.32
Palo Verde 911	0.32	0.80	1.08	0.35	2.86	1.73

Alaskite: Phyllic Alteration

Sample #	1	2	3	4	5	6
52406	0.74	1.77	1.87	2.06	0.36	0.48
5240601	0.63	1.63	1.69	1.81	0.34	0.55
5240602	0.61	1.67	1.76	1.97	0.31	0.51
5240603	0.65	1.62	1.74	1.91	0.34	0.52
5240604	0.64	1.75	1.75	1.96	0.33	0.51
5240605	0.67	1.63	1.70	2.00	0.33	0.50
5240606	0.57	1.62	1.67	1.81	0.32	0.55
5240607	0.65	1.63	1.70	1.83	0.36	0.55
5240608	0.71	1.59	1.76	1.88	0.38	0.53

	7	8	9	10	11	12
52406	0.78	0.86	0.91	0.42	2.39	1.35
5240601	0.83	0.90	0.93	0.38	2.69	1.30
5240602	0.78	0.85	0.89	0.36	2.75	1.37
5240603	0.78	0.85	0.91	0.40	2.50	1.36
5240604	0.80	0.89	0.89	0.37	2.72	1.45
5240605	0.77	0.82	0.85	0.41	2.45	1.31
5240606	0.83	0.89	0.92	0.35	2.83	1.30
5240607	0.82	0.89	0.93	0.40	2.50	1.43
5240608	0.77	0.84	0.94	0.44	2.25	1.28

Alaskite: Propylitic Alteration

Sample #	1	2	3	4	5	6
52603	0.63	1.53	1.63	1.73	0.37	0.58
5260301	0.69	1.62	1.59	1.69	0.41	0.59
5260302	0.63	1.47	1.56	1.72	0.36	0.58
5260303	0.63	1.58	1.71	1.83	0.34	0.55
5260304	0.53	1.60	1.73	1.93	0.28	0.52
5260305	0.65	1.68	1.81	1.94	0.33	0.52
5260306	0.67	1.33	1.41	1.48	0.50	0.68
5260307	0.61	1.76	1.85	1.97	0.31	0.51
5260308	0.66	1.55	1.62	1.72	0.38	0.58

	7	8	9	10	11	12
52603	0.85	0.88	0.94	0.41	2.42	1.09
5260301	0.86	0.90	0.94	0.45	2.20	1.08
5260302	0.82	0.85	0.91	0.43	2.35	1.09
5260303	0.80	0.86	0.93	0.39	2.53	1.13
5260304	0.79	0.83	0.90	0.33	3.00	1.10
5260305	0.83	0.87	0.93	0.38	2.60	1.08
5260306	0.88	0.90	0.95	0.50	2.00	0.95
5260307	0.82	0.89	0.94	0.34	2.90	1.09
5260308	0.84	0.90	0.94	0.42	2.37	1.13

Quartz Monzonite: Prpoylitic Alteration

Sample #	1	2	3	4	5	6
52602	0.71	1.38	1.45	1.55	0.46	0.65
5260201	0.71	1.33	1.40	1.50	0.48	0.67
5260202	0.67	1.33	1.42	1.51	0.44	0.66
5260203	0.67	1.45	1.52	1.64	0.41	0.61
5260204	0.67	1.38	1.45	1.55	0.43	0.65
5260205	0.70	1.30	1.35	1.40	0.50	0.71
5260206	0.67	1.31	1.38	1.44	0.46	0.69
5260207	0.59	1.41	1.48	1.59	0.37	0.63
5260208	0.71	1.43	1.50	1.62	0.44	0.62
	7	8	9	10	11	12
52602	0.85	0.89	0.94	0.52	1.93	1.16
5260201	0.86	0.89	0.94	0.54	1.87	1.16
5260202	0.82	0.88	0.94	0.50	2.00	1.16
5260203	0.84	0.88	0.93	0.46	2.18	1.23
5260204	0.86	0.89	0.94	0.48	2.07	1.15
5260205	0.89	0.93	0.96	0.54	1.86	1.17
5260206	0.86	0.91	0.95	0.51	1.97	1.19
5260207	0.83	0.89	0.93	0.42	2.38	1.15
5260208	0.82	0.88	0.93	0.50	2.00	1.13

Limestone

Sample #	1	2	3	4	5	6
52403	0.83	1.25	1.29	1.38	0.61	0.73
5240301	0.80	1.24	1.30	1.36	0.59	0.74
5240302	0.78	1.26	1.33	1.43	0.55	0.70
5240303	0.86	1.14	1.19	1.21	0.71	0.82
5240304	0.72	1.22	1.28	1.38	0.53	0.73
5240305	0.78	1.36	1.50	1.67	0.47	0.60
5240306	0.75	1.17	1.25	1.38	0.55	0.73
	7	8	9	10	11	12
52403	0.85	0.91	0.94	0.67	1.50	1.13
5240301	0.88	0.91	0.96	0.65	1.55	1.13
5240302	0.83	0.88	0.92	0.62	1.61	1.13
5240303	0.90	0.94	0.98	0.75	1.33	1.04
5240304	0.86	0.89	0.93	0.59	1.69	1.10
5240305	0.77	0.82	0.90	0.57	1.75	1.17
5240306	0.83	0.85	0.91	0.64	1.56	1.13

Dacite Porphyry: Potassic Alteration

Sample #	1	2	3	4	5	6
52604	0.63	1.58	1.68	1.84	0.34	0.54
5260401	0.64	1.50	1.55	1.70	0.37	0.59
5260402	0.71	1.68	1.82	2.06	0.34	0.49
5260403	0.63	1.63	1.78	2.06	0.30	0.48
5260446	0.55	1.60	1.63	1.80	0.31	0.56
5260447	0.57	1.55	1.64	1.79	0.32	0.56
5260448	0.57	1.60	1.69	1.89	0.30	0.53

	7	8	9	10	11	12
52604	0.80	0.86	0.91	0.40	2.50	1.52
5260401	0.83	0.88	0.91	0.42	2.37	1.74
5260402	0.76	0.81	0.89	0.42	2.38	1.50
5260403	0.73	0.79	0.86	0.38	2.60	1.57
5260446	0.81	0.89	0.90	0.34	2.91	1.54
5260447	0.83	0.87	0.92	0.37	2.71	1.44
5260448	0.77	0.85	0.89	0.36	2.80	1.53

Dacite Porphyry: Phyllic Alteration

Sample #	1	2	3	4	5	6
52605	0.63	1.55	1.63	1.88	0.33	0.53
5260551	0.65	1.48	1.56	1.70	0.38	0.59
5260552	0.60	1.43	1.52	1.67	0.36	0.60
5260553	0.69	1.56	1.72	1.94	0.36	0.51
5260554	0.67	1.60	1.93	2.37	0.28	0.42
5260555	0.67	1.69	1.67	1.90	0.35	0.53
5260556	0.60	1.60	1.62	1.76	0.34	0.57
5260557	0.77	1.77	1.73	2.12	0.36	0.47
5260558	0.66	1.66	1.83	2.23	0.29	0.45

	7	8	9	10	11	12
52605	0.77	0.83	0.87	0.40	2.50	1.53
5260551	0.82	0.87	0.91	0.44	2.29	1.50
5260552	0.79	0.86	0.91	0.42	2.40	1.60
5260553	0.73	0.80	0.89	0.45	2.24	1.50
5260554	0.63	0.68	0.82	0.42	2.40	1.46
5260555	0.83	0.89	0.88	0.39	2.54	1.61
5260556	0.86	0.91	0.92	0.37	2.68	1.69
5260557	0.76	0.84	0.82	0.43	2.30	1.64
5260558	0.65	0.74	0.82	0.40	2.52	1.44

APPENDIX F

NORMALIZATION OF RATIO VALUES FOR 5 RATIO SETS

Ratio Value Normalization Process

Mathematical Relationships:

$$a = \frac{d}{d+e+f}(100), \quad b = \frac{e}{d+e+f}(100), \quad c = \frac{f}{d+e+f}(100),$$

$$SUM = a + b + c$$

Ratio Set 1. 0.44/0.56, 1.65/2.20, 0.72/0.56

d = Ratio Value for $\frac{0.44}{0.56}$, a = normalized value for $\frac{0.44}{0.56}$ = Vertex A in Ternary Diagram

e = Ratio Value for $\frac{1.65}{2.20}$, b = normalized value for $\frac{1.65}{2.20}$ = Vertex B in Ternary Diagram

f = Ratio Value for $\frac{0.72}{0.56}$, c = normalized value for $\frac{0.72}{0.56}$ = Vertex C in Ternary Diagram

---

Ratio Set 2. 0.44/0.56, 0.72/0.56, 1.015/0.56

d = Ratio Value for $\frac{0.44}{0.56}$, a = normalized value for $\frac{0.44}{0.56}$ = Vertex A in Ternary Diagram

e = Ratio Value for $\frac{0.72}{0.56}$, b = normalized value for $\frac{0.72}{0.56}$ = Vertex B in Ternary Diagram

f = Ratio Value for $\frac{1.015}{0.56}$, c = normalized value for $\frac{1.015}{0.56}$ = Vertex C in Ternary Diagram

Ratio Set 3. 0.44/1.015, 1.65/2.20, 0.72/1.015

d = Ratio Value for $\frac{0.44}{1.015}$, a = normalized value for $\frac{0.44}{1.015}$ = Vertex A in Ternary Diagram

e = Ratio Value for $\frac{1.65}{2.20}$, b = normalized value for $\frac{1.65}{2.20}$ = Vertex B in Ternary Diagram

f = Ratio value for $\frac{0.72}{1.015}$, c = normalized value for $\frac{0.72}{1.015}$ = Vertex C in Ternary Diagram

---

Ratio Set 4. 0.44/0.56, 0.72/0.56, 0.72/1.015

d = Ratio value for $\frac{0.44}{0.56}$, a = normalized value for $\frac{0.44}{0.56}$ = Vertex A in Ternary Diagram

e = Ratio value for $\frac{0.72}{0.56}$, b = normalized value for $\frac{0.72}{0.56}$ = Vertex B in Ternary Diagram

f = Ratio value for $\frac{0.72}{1.015}$, c = normalized value for $\frac{0.72}{1.015}$ = Vertex C in Ternary Diagram

---

Ratio Set 5. 0.44/0.56, 1.65/2.20, 0.72/0.44

d = Ratio value for $\frac{0.44}{0.56}$, a = normalized value for $\frac{0.44}{0.56}$ = Vertex A in Ternary Diagram

e = Ratio value for $\frac{1.65}{2.20}$, b = normalized value for $\frac{1.65}{2.20}$ = Vertex B in Ternary Diagram

f = Ratio value for $\frac{0.72}{0.44}$, c = normalized value for $\frac{0.72}{0.44}$ = Vertex C in Ternary Diagram

Actual and Normalized Reflectance Ratio Values: Ratio Set 1

Alaskite Sample:

Pot./Prop	d	e	f	SUM	a	b	c
52405	0.68	1.32	1.86	3.86	17.6	34.2	48.2
5240501	0.57	1.33	1.49	3.39	16.8	39.2	44.0
5240502	0.53	1.44	1.83	3.80	13.9	37.9	48.2
5240503	0.56	1.31	1.78	3.65	15.3	35.9	48.8
5240504	0.60	1.29	1.65	3.54	16.9	36.4	46.6
5240505	0.58	1.50	1.83	3.91	14.8	38.4	46.8
5240506	0.58	1.31	1.77	3.66	15.8	35.8	48.4
5240507	0.56	1.40	1.76	3.72	15.1	37.6	47.3
5240508	0.67	1.39	1.92	3.98	16.8	34.9	48.2

Phyllic	d	e	f	SUM	a	b	c
52406	0.74	1.35	1.77	3.86	19.2	35.0	45.9
5240601	0.63	1.30	1.63	3.56	17.7	36.5	45.8
5240602	0.61	1.37	1.67	3.65	16.7	37.5	45.8
5240603	0.65	1.36	1.62	3.63	17.9	37.5	44.6
5240604	0.64	1.45	1.75	3.84	16.7	37.8	45.6
5240605	0.67	1.31	1.63	3.61	18.6	36.3	45.2
5240606	0.57	1.30	1.62	3.49	16.3	37.2	46.4
5240607	0.65	1.43	1.63	3.71	17.5	38.5	43.9
5240608	0.71	1.28	1.59	3.58	19.8	35.8	44.4

Prop.	d	e	f	SUM	a	b	c
52603	0.63	1.09	1.53	3.25	19.4	33.5	47.1
5260301	0.69	1.08	1.62	3.39	20.4	31.9	47.8
5260302	0.63	1.09	1.47	3.19	19.7	34.2	46.1
5260303	0.63	1.13	1.58	3.34	18.9	33.8	47.3
5260304	0.53	1.10	1.60	3.23	16.4	34.1	49.5
5260305	0.65	1.08	1.68	3.41	19.1	31.7	49.3
5260306	0.67	0.95	1.33	2.95	22.7	32.2	45.1
5260307	0.61	1.09	1.76	3.46	17.6	31.5	50.9
5260308	0.66	1.13	1.55	3.34	19.8	33.8	46.4

Vegetation	d	e	f	SUM	a	b	c
Manzanita 98	0.80	1.38	2.00	4.18	19.1	33.0	47.9
Lt. Clrd. Bush	0.70	1.32	1.50	3.52	19.9	37.5	42.6
Palo Verde 911	0.67	1.73	1.90	4.30	15.6	40.2	44.2

Actual and Normalized Reflectance Ratio Values: Ratio Set 1

Quartz Monzonite Sample:

Prop.	d	e	f	SUM	a	b	c
52602	0.71	1.16	1.38	3.25	21.8	35.7	42.5
5260201	0.71	1.16	1.33	3.20	22.2	36.3	41.6
5260202	0.67	1.16	1.33	3.16	21.2	36.7	42.1
5260203	0.67	1.23	1.45	3.35	20.0	36.7	43.3
5260204	0.67	1.15	1.38	3.20	20.9	35.9	43.1
5260205	0.70	1.17	1.30	3.17	22.1	36.9	41.0
5260206	0.67	1.19	1.31	3.17	21.1	37.5	41.3
5260207	0.59	1.15	1.41	3.15	18.7	36.5	44.8
5260208	0.71	1.13	1.43	3.27	21.7	34.6	43.7

Dacite Porphyry Sample:

Potassic	d	e	f	SUM	a	b	c
52604	0.63	1.52	1.58	3.73	16.9	40.8	42.4
5260401	0.64	1.74	1.50	3.88	16.5	44.8	38.7
5260402	0.71	1.50	1.68	3.89	18.3	38.6	43.2
5260403	0.63	1.57	1.63	3.83	16.4	41.0	42.6
5260446	0.55	1.54	1.60	3.69	14.9	41.7	43.4
5260447	0.57	1.44	1.55	3.56	16.0	40.4	43.5
5240608	0.57	1.53	1.60	3.70	15.4	41.4	43.2
Phyllic	**d**	**e**	**f**	**SUM**	**a**	**b**	**c**
52605	0.63	1.53	1.55	3.71	17.0	41.2	41.8
5260551	0.65	1.50	1.48	3.63	17.9	41.3	40.8
5260552	0.60	1.60	1.43	3.63	16.5	44.1	39.4
5260553	0.69	1.50	1.56	3.75	18.4	40.0	41.6
5260554	0.67	1.46	1.60	3.73	18.0	39.1	42.9
5260555	0.67	1.61	1.69	3.97	16.9	40.6	42.6
5260556	0.60	1.69	1.60	3.89	15.4	43.4	41.1
5260557	0.77	1.64	1.77	4.18	18.4	39.2	42.3
5260558	0.66	1.44	1.66	3.76	17.6	38.3	44.1

Limestone Sample:	d	e	f	SUM	a	b	c
52403	0.83	1.13	1.25	3.21	25.9	35.2	38.9
5240301	0.80	1.13	1.24	3.17	25.2	35.6	39.1
5240302	0.78	1.13	1.26	3.17	24.6	35.6	39.7
5240303	0.86	1.04	1.14	3.04	28.3	34.2	37.5
5240304	0.72	1.10	1.22	3.04	23.7	36.2	40.1
5240305	0.78	1.17	1.36	3.31	23.6	35.3	41.1
5240306	0.75	1.13	1.17	3.05	24.6	37.0	38.4

Actual and Normalized Reflectance Ratio Values: Ratio Set 2

Alaskite Sample:

Pot./Prop.	d	e	f	SUM	a	b	c
52405	0.68	1.86	2.14	4.68	14.5	39.7	45.7
5240501	0.57	1.49	1.74	3.80	15.0	39.2	45.8
5240502	0.53	1.83	2.17	4.53	11.7	40.4	47.9
5240503	0.56	1.78	2.11	4.45	12.6	40.0	47.4
5240504	0.60	1.65	1.90	4.15	14.5	39.8	45.8
5240505	0.58	1.83	2.00	4.41	13.2	41.5	45.4
5240506	0.58	1.88	2.17	4.63	12.5	40.6	46.9
5240507	0.56	1.76	2.20	4.52	12.4	38.9	48.7
5240508	0.67	1.92	2.33	4.92	13.6	39.0	47.4

Phyllic	d	e	f	SUM	a	b	c
52406	0.74	1.77	2.06	4.57	16.2	38.7	45.1
5240601	0.63	1.63	1.81	4.07	15.5	40.0	44.5
5240602	0.61	1.67	1.97	4.25	14.4	39.3	46.4
5240603	0.65	1.62	1.91	4.18	15.6	38.8	45.7
5240604	0.64	1.75	1.96	4.35	14.7	40.2	45.1
5240605	0.67	1.62	2.00	4.29	15.6	37.8	46.6
5240606	0.57	1.62	1.81	4.00	14.3	40.5	45.3
5240607	0.65	1.63	1.83	4.11	15.8	39.7	44.5
5240608	0.71	1.59	1.88	4.18	17.0	38.0	45.0

Prop.	d	e	f	SUM	a	b	c
52603	0.63	1.53	1.73	3.89	16.2	39.3	44.5
5260301	0.69	1.62	1.69	4.00	17.3	40.5	42.3
5260302	0.63	1.47	1.72	3.82	16.5	38.5	45.0
5260303	0.63	1.58	1.83	4.04	15.6	39.1	45.3
5260304	0.53	1.60	1.93	4.06	13.1	39.4	47.5
5260305	0.65	1.68	1.94	4.27	15.2	39.3	45.4
5260306	0.67	1.33	1.48	3.48	19.3	38.2	42.5
5260307	0.61	1.76	1.97	4.34	14.1	40.6	45.4
5260308	0.66	1.55	1.72	3.93	16.8	39.4	43.8

Vegetation	d	e	f	SUM	a	b	c
Manzanita 98	0.80	2.00	3.30	6.10	13.1	32.8	54.1
Lt. Clrd. Bush 99	0.70	1.50	2.40	4.60	15.2	32.6	52.2
Palo Verde 911	0.67	1.90	2.38	4.95	13.5	38.4	48.1

Actual and Normalized Reflectance Ratio Values: Ratio Set 2

Quartz Monzonite Sample:

Prop.	d	e	f	SUM	a	b	c
52602	0.71	1.38	1.55	3.64	19.5	37.9	42.6
5260201	0.71	1.33	1.50	3.54	20.1	37.6	42.4
5260202	0.67	1.33	1.51	3.51	19.1	37.9	43.0
5260203	0.67	1.45	1.64	3.76	17.8	38.6	43.6
5260204	0.67	1.38	1.55	3.60	18.6	38.3	43.1
5260205	0.70	1.30	1.40	3.40	20.6	38.2	41.2
5260206	0.67	1.31	1.44	3.42	19.6	38.3	42.1
5260207	0.59	1.41	1.59	3.59	16.4	39.3	44.3
5260208	0.71	1.43	1.62	3.76	18.9	38.0	43.1

Dacite Porphyry Sample:

Potassic	d	e	f	SUM	a	b	c
52604	0.63	1.58	1.84	4.05	15.6	39.0	45.4
5260401	0.64	1.50	1.70	3.84	16.7	39.1	44.3
5260402	0.71	1.68	2.06	4.45	16.0	37.8	46.3
5260403	0.63	1.63	2.06	4.32	14.6	37.7	47.7
5260446	0.55	1.60	1.80	3.95	13.9	40.5	45.6
5260447	0.57	1.55	1.79	3.91	14.6	39.6	45.8
5260448	0.57	1.60	1.89	4.06	14.0	39.4	46.6
Phyllic	**d**	**e**	**f**	**SUM**	**a**	**b**	**c**
52605	0.63	1.55	1.88	4.06	15.5	38.2	46.3
5260551	0.65	1.48	1.70	3.83	17.0	38.6	44.4
5260552	0.60	1.43	1.67	3.70	16.2	38.6	45.1
5260553	0.69	1.56	1.94	4.19	16.5	37.2	46.3
5260554	0.67	1.60	2.37	4.64	14.4	34.5	51.1
5260555	0.67	1.69	1.90	4.26	15.7	39.7	44.6
5260556	0.60	1.60	1.76	3.96	15.2	40.4	44.4
5260557	0.77	1.77	2.12	4.66	16.5	38.0	45.5
5260558	0.66	1.66	2.23	4.55	14.5	36.5	49.0

Limestone Sample:	d	e	f	SUM	a	b	c
52403	0.83	1.25	1.38	3.46	24.0	36.1	39.9
5240301	0.80	1.24	1.36	3.40	23.5	36.5	40.0
5240302	0.78	1.26	1.43	3.47	22.5	36.3	41.2
5240303	0.86	1.14	1.21	3.21	26.8	35.5	37.7
5240304	0.72	1.22	1.38	3.32	21.7	36.7	41.6
5240305	0.78	1.36	1.67	3.81	20.5	35.7	43.8
5240306	0.75	1.17	1.38	3.30	22.7	35.5	41.8

Actual and Normalized Reflectance Ratio Values: Ratio Set 3

Alaskite Sample:

Pot./Prop.	d	e	f	SUM	a	b	c
52405	0.32	1.32	0.87	2.51	12.7	52.6	34.7
5240501	0.33	1.33	0.85	2.51	13.1	53.0	33.9
5240502	0.25	1.44	0.85	2.54	9.8	56.7	33.5
5240503	0.26	1.31	0.84	2.41	10.8	54.4	34.9
5240504	0.32	1.29	0.87	2.48	12.9	52.0	35.1
5240505	0.29	1.50	0.92	2.71	10.7	55.4	33.9
5240506	0.27	1.31	0.87	2.45	11.0	53.5	35.5
5240507	0.25	1.40	0.80	2.45	10.2	57.1	32.7
5240508	0.29	1.39	0.82	2.50	11.6	55.6	32.8

Phyllic	d	e	f	SUM	a	b	c
52406	0.36	1.35	0.86	2.57	14.0	52.5	33.5
5240601	0.34	1.30	0.90	2.54	13.4	51.2	35.4
5240602	0.31	1.37	0.85	2.53	12.3	54.2	33.6
5240603	0.34	1.36	0.85	2.55	13.3	53.3	33.3
5240604	0.33	1.45	0.89	2.67	12.4	54.3	33.3
5240605	0.33	1.31	0.82	2.46	13.4	53.3	33.3
5240606	0.32	1.30	0.89	2.51	12.7	51.8	35.5
5240607	0.36	1.43	0.89	2.68	13.4	53.4	33.2
5240608	0.38	1.28	0.84	2.50	15.2	51.2	33.6

Prop.	d	e	f	SUM	a	b	
52603	0.37	1.09	0.88	2.34	15.8	46.6	37.6
5260301	0.41	1.08	0.90	2.39	17.2	45.2	37.7
5260302	0.36	1.09	0.85	2.30	15.7	47.4	37.0
5260303	0.34	1.13	0.86	2.33	14.6	48.5	36.9
5260304	0.28	1.10	0.83	2.21	12.7	49.8	37.6
5260305	0.33	1.08	0.87	2.28	14.5	47.4	38.2
5260306	0.50	0.95	0.90	2.35	21.3	40.4	38.3
5260307	0.31	1.09	0.89	2.29	13.5	47.6	38.9
5260308	0.38	1.13	0.90	2.41	15.8	46.9	37.3

Vegetation	d	e	f	SUM	a	b	c
Manzanita 98	0.24	1.38	0.61	2.23	10.8	61.9	27.3
Lt. Clrd. 99	0.29	1.32	0.63	2.24	12.9	59.0	28.1
Palo Verde 911	0.28	1.73	0.80	2.81	10.0	61.6	28.4

Actual and Normalized Reflectance Ratio Values: Ratio Set 3

Quartz Monzonite Sample:

Prop.	d	e	f	SUM	a	b	c
52602	0.46	1.16	0.89	2.51	18.3	46.2	35.5
5260201	0.48	1.16	0.89	2.53	19.0	45.8	35.2
5260202	0.44	1.16	0.88	2.48	17.7	46.8	35.5
5260203	0.41	1.23	0.88	2.52	16.3	48.8	34.9
5260204	0.43	1.15	0.89	2.47	17.4	46.6	36.0
5260205	0.50	1.17	0.93	2.60	19.2	45.0	35.8
5260206	0.46	1.19	0.91	2.56	18.0	46.5	35.5
5260207	0.37	1.15	0.89	2.41	15.4	47.7	36.9
5260208	0.44	1.13	0.88	2.45	18.0	46.1	35.9

Dacite Porphyry Sample:

Potassic	d	e	f	SUM	a	b	c
52604	0.34	1.52	0.86	2.72	12.5	55.9	31.6
5260401	0.37	1.74	0.88	2.99	12.4	58.2	29.4
5260402	0.34	1.50	0.81	2.65	12.8	56.6	30.6
5260403	0.30	1.57	0.79	2.66	11.3	59.0	29.7
5260446	0.31	1.54	0.89	2.74	11.3	56.2	32.5
5260447	0.32	1.44	0.87	2.63	12.2	54.8	33.1
5260448	0.30	1.53	0.85	2.68	11.2	57.1	31.7
Phyllic	d	e	f	SUM	a	b	c
52605	0.33	1.53	0.83	2.69	12.3	56.9	30.9
5260551	0.38	1.50	0.87	2.75	13.8	54.5	31.6
5260552	0.36	1.60	0.86	2.82	12.8	56.7	30.5
5260553	0.36	1.50	0.80	2.66	13.5	56.4	30.1
5260554	0.28	1.46	0.68	2.42	11.6	60.3	28.1
5260555	0.35	1.61	0.89	2.85	12.3	56.5	31.2
5260556	0.34	1.69	0.91	2.94	11.6	57.5	31.0
5260557	0.36	1.64	0.84	2.84	12.7	57.7	29.6
5260558	0.29	1.44	0.74	2.47	11.7	58.3	30.0

Limestone Sample:	d	e	f	SUM	a	b	c
52403	0.61	1.13	0.91	2.65	23.0	42.6	34.4
5240301	0.59	1.13	0.91	2.63	22.4	43.0	34.6
5240302	0.55	1.13	0.88	2.56	21.5	44.1	34.4
5240303	0.71	1.04	0.94	2.69	26.4	38.7	34.9
5240304	0.53	1.10	0.89	2.52	21.0	43.7	35.3
5240305	0.47	1.17	0.82	2.46	19.1	47.6	33.3
5240306	0.55	1.13	0.85	2.53	21.7	44.7	33.6

Actual and Normalized Reflectance Ratio Values: Ratio Set 4

Alaskite Sample:

Pot./Prop.	d	e	f	SUM	a	b	c
52405	0.68	1.86	0.87	3.41	19.9	54.5	25.5
5240501	0.57	1.49	0.85	2.91	19.6	51.2	29.2
5240502	0.53	1.83	0.85	3.21	16.5	57.0	26.5
5240503	0.56	1.78	0.84	3.18	17.6	56.0	26.4
5240504	0.60	1.65	0.87	3.12	19.2	52.9	27.9
5240505	0.58	1.83	0.92	3.33	17.4	55.0	27.6
5240506	0.58	1.88	0.87	3.33	17.4	56.5	26.1
5240507	0.56	1.72	0.80	3.08	18.2	55.8	26.0
5240508	0.67	1.92	0.82	3.41	19.6	56.3	24.1
Phyllic	d	e	f	SUM	a	b	c
52406	0.74	1.77	0.86	3.37	22.0	52.5	25.5
5240601	0.63	1.63	0.90	3.16	19.9	51.6	28.5
5240602	0.61	1.67	0.85	3.13	19.5	53.4	27.1
5240603	0.65	1.62	0.85	3.12	20.8	51.9	27.2
5240604	0.64	1.72	0.89	3.25	19.7	52.9	27.4
5240605	0.67	1.63	0.82	3.12	21.5	52.2	26.3
5240606	0.57	1.62	0.89	3.08	18.5	52.6	28.9
5240607	0.65	1.63	0.89	3.17	20.5	51.4	28.1
5240608	0.71	1.59	0.84	3.14	22.6	50.6	26.8
Prop.	d	e	f	SUM	a	b	c
52603	0.63	1.53	0.88	3.04	20.7	50.3	29.0
5260301	0.69	1.62	0.90	3.21	21.5	50.5	28.0
5260302	0.63	1.47	0.85	2.95	21.4	49.8	28.8
5260303	0.63	1.58	0.86	3.07	20.5	51.5	28.0
5260304	0.53	1.60	0.83	2.96	17.9	54.1	28.0
5260305	0.65	1.68	0.87	3.20	20.3	52.5	27.2
5260306	0.67	1.33	0.90	2.90	23.1	45.9	31.0
5260307	0.61	1.76	0.89	3.26	18.7	54.0	27.3
5260308	0.66	1.55	0.90	3.11	21.2	49.8	28.9
Vegetation	d	e	f	SUM	a	b	c
Manzanita 98	0.80	2.00	0.61	3.41	23.5	58.6	17.9
Lt. Clrd. Bush 99	0.70	1.50	0.63	2.83	24.7	53.0	22.3
Palo Verde 911	0.67	1.90	0.80	3.37	19.9	56.4	23.7

Actual and Normalized Reflectance Ratio Values: Ratio Set 4

Quartz Monzonite Sample:

Prop.	d	e	f	SUM	a	b	c
52602	0.71	1.38	0.89	2.98	23.8	46.3	29.9
5260201	0.71	1.33	0.89	2.93	24.2	45.4	30.4
5260202	0.67	1.33	0.88	2.88	23.3	46.2	30.5
5260203	0.67	1.45	0.88	3.00	22.3	48.3	29.4
5260204	0.67	1.38	0.89	2.94	22.8	46.9	30.3
5260205	0.70	1.30	0.93	2.93	23.9	44.4	31.7
5260206	0.67	1.31	0.91	2.89	23.2	45.3	31.5
5260207	0.59	1.41	0.89	2.89	20.4	48.8	30.8
5260208	0.71	1.43	0.88	3.02	23.5	47.4	29.1

Dacite Porphyry Sample:

Potassic	d	e	f	SUM	a	b	c
52406	0.63	1.58	0.86	3.07	20.5	51.5	28.0
5240601	0.64	1.50	0.88	3.02	21.2	49.7	29.1
5240602	0.71	1.68	0.81	3.20	22.2	52.5	25.3
5240603	0.63	1.63	0.79	3.05	20.7	53.4	25.9
5240646	0.55	1.60	0.89	3.04	18.1	52.6	29.3
5240647	0.57	1.55	0.87	2.99	19.1	51.8	29.1
5240648	0.57	1.60	0.85	3.02	18.9	53.0	28.1

Phyllic	d	e	f	SUM	a	b	c
52605	0.63	1.55	0.83	3.01	20.9	51.5	27.6
5260551	0.65	1.48	0.87	3.00	21.7	49.3	29.0
5260552	0.60	1.43	0.86	2.89	20.8	49.5	29.7
5260553	0.69	1.56	0.80	3.05	22.6	51.1	26.2
5260554	0.67	1.60	0.68	2.95	22.7	54.2	23.1
5260555	0.67	1.69	0.89	3.25	20.6	52.0	27.4
5260556	0.60	1.60	0.91	3.11	19.3	51.4	29.3
5260557	0.77	1.77	0.84	3.38	22.8	52.4	24.8
5260558	0.66	1.66	0.74	3.06	21.6	54.2	24.2

Limestone Sample:	d	e	f	SUM	a	b	c
52403	0.83	1.25	0.91	2.99	27.8	41.8	30.4
5240301	0.80	1.24	0.91	2.95	27.1	42.0	30.9
5240302	0.78	1.26	0.88	2.92	26.7	43.2	30.1
5240303	0.86	1.14	0.94	2.94	29.3	38.8	32.0
5240304	0.72	1.22	0.89	2.83	25.4	43.1	31.5
5240305	0.78	1.36	0.82	2.96	26.4	45.9	27.7
5240306	0.75	1.17	0.85	2.77	27.1	42.2	30.7

Actual and Normalized Reflectance Ratio Values: Ratio Set 5

Alaskite Sample:

Pot./Prop.	d	e	f	SUM	a	b	c
52405	0.68	1.37	2.74	4.79	14.2	28.6	57.2
5240501	0.57	1.33	2.60	4.50	12.7	29.6	57.8
5240502	0.53	1.44	3.44	5.41	9.8	26.6	63.6
5240503	0.56	1.31	3.20	5.07	11.0	25.8	63.1
5240504	0.60	1.29	2.75	4.64	12.9	27.8	59.3
5240505	0.58	1.50	3.14	5.22	11.1	28.7	60.2
5240506	0.58	1.31	3.21	5.10	11.4	25.7	62.9
5240507	0.56	1.40	3.14	5.10	11.0	27.5	61.6
5240508	0.67	1.39	2.88	4.94	13.6	28.1	58.3
Phyllic	d	e	f	SUM	a	b	c
52406	0.74	1.35	2.39	4.48	16.5	30.1	53.4
5240601	0.63	1.30	2.60	4.53	13.9	28.7	57.4
5240602	0.61	1.37	2.75	4.73	12.9	29.0	58.1
5240603	0.65	1.36	2.50	4.51	14.4	30.2	55.4
5240604	0.64	1.45	2.72	4.81	13.3	30.1	56.6
5240605	0.67	1.31	2.45	4.43	15.1	29.6	55.3
5240606	0.57	1.30	2.83	4.70	12.1	27.7	60.2
5240607	0.65	1.43	2.50	4.58	14.2	31.2	54.6
5240608	0.71	1.28	2.75	4.74	15.0	27.0	58.0
Prop.	d	e	f	SUM	a	b	c
52603	0.63	1.09	2.42	4.14	15.2	26.3	58.5
5260301	0.69	1.08	2.20	3.97	17.4	27.2	55.4
5260302	0.63	1.09	2.35	4.07	15.5	26.8	57.7
5260303	0.63	1.13	2.53	4.29	14.7	26.3	59.0
5260304	0.53	1.10	3.00	4.63	11.4	23.8	64.8
5260305	0.65	1.08	2.60	4.33	15.0	24.9	60.1
5260306	0.67	0.95	2.00	3.62	18.5	26.2	55.3
5260307	0.61	1.09	2.90	4.60	13.3	23.7	63.0
5260308	0.66	1.13	2.37	4.16	15.9	27.2	57.0
Vegetation	d	e	f	SUM	a	b	c
Manzanita 98	0.80	1.38	2.50	4.68	17.1	29.5	53.4
Lt. Clrd. Bush 99	0.70	1.32	2.14	4.16	16.8	31.7	51.5
Palo Verde 911	0.67	1.73	2.86	5.26	12.7	32.9	54.4

Actual and Normalized Reflectance Ratio Values: Ratio Set 5

Quartz Monzonite Sample:

Prop.	d	e	f	SUM	a	b	c
52602	0.71	1.16	1.93	3.80	18.7	30.5	50.8
5260201	0.71	1.16	1.87	3.74	19.0	31.0	50.0
5260202	0.67	1.16	2.00	3.83	17.5	30.3	52.2
5260203	0.60	1.23	2.18	4.01	15.0	30.7	54.4
5260204	0.67	1.15	2.07	3.89	17.2	29.6	53.2
5260205	0.70	1.17	1.86	3.73	18.8	31.4	49.9
5260206	0.67	1.19	1.97	3.83	17.5	31.1	51.4
5260207	0.59	1.15	2.38	4.12	14.3	27.9	57.8
5260208	0.71	1.13	2.00	3.84	18.5	29.4	52.1

Dacite Porphyry Sample:

Potassic	d	e	f	SUM	a	b	c
52604	0.63	1.52	2.50	4.65	13.5	32.7	53.8
5260401	0.64	1.74	2.36	4.74	13.5	36.7	49.8
5260402	0.71	1.50	2.38	4.59	15.5	32.7	51.8
5260403	0.63	1.57	2.60	4.80	13.1	32.7	54.2
5260446	0.55	1.54	2.91	5.00	11.0	30.8	58.2
5260447	0.57	1.44	2.71	4.72	12.1	30.5	57.4
5260448	0.57	1.53	2.80	4.90	11.6	31.2	57.1
Phyllic	d	e	f	SUM	a		c
52605	0.63	1.53	2.48	4.64	13.6	33.0	53.4
5260551	0.65	1.50	2.29	4.44	14.6	33.8	51.6
5260552	0.60	1.60	2.40	4.60	13.0	34.8	52.2
5260553	0.69	1.50	2.24	4.43	15.6	33.9	50.6
5260554	0.67	1.46	2.40	4.53	14.8	32.2	53.0
5260555	0.67	1.61	2.54	4.82	13.9	33.4	52.7
5260556	0.60	1.69	2.68	4.97	12.1	34.0	53.9
5260557	0.77	1.64	2.30	4.71	16.3	34.8	48.8
5260558	0.66	1.44	2.52	4.62	14.3	31.2	54.5

Limestone Sample:	d	e	f	SUM	a	b	c
52403	0.83	1.13	1.50	3.46	24.0	32.7	43.4
5240301	0.80	1.13	1.55	3.48	23.0	32.5	44.5
5240302	0.78	1.13	1.61	3.52	22.2	32.1	45.7
5240303	0.86	1.04	1.33	3.23	26.6	32.2	41.2
5240304	0.72	1.10	1.69	3.51	20.5	31.3	48.2
5240305	0.78	1.17	1.75	3.70	21.1	31.6	47.3
5240306	0.75	1.13	1.56	3.44	21.8	32.8	45.4

APPENDIX G

RATIO VALUES FOR RATIO/RATIO SETS 1 AND 2

Ratio/Ratio Set 1. $\frac{0.44}{0.72}$, $\frac{1.65/2.20}{0.44/0.56}$ and $\frac{0.72/0.44}{1.65/2.20}$

d = Ratio value for $\frac{0.44}{0.72}$, $a = \frac{d}{d+e+f}(100)$ = Vertex A in Ternary Diagram

e = Ratio value for $\frac{1.65/2.20}{0.44/0.56}$, $b = \frac{e}{d+e+f}(100)$ = Vertex B in Ternary Diagram

f = Ratio value for $\frac{0.72/0.44}{1.65/2.20}$, $c = \frac{f}{d+e+f}(100)$ = Vertex C in Ternary Diagram

---

Ratio/Ratio Set 2. $\frac{0.44}{0.72}$, $\frac{1.65/2.20}{0.44/0.56}$ and $\frac{0.72/0.56}{1.65/2.20}$

d = Ratio value for $\frac{0.44}{0.72}$, $a = \frac{d}{d+e+f}(100)$ = Vertex A in Ternary Diagram

e = Ratio value for $\frac{1.65/2.20}{0.44/0.56}$, $b = \frac{e}{d+e+f}(100)$ = Vertex B in Ternary Diagram

f = Ratio value for $\frac{0.72/0.56}{1.65/2.20}$, $c = \frac{f}{d+e+f}(100)$ = Vertex C in Ternary Diagram

Actual and Normalized Reflectance Ratio Values.

Ratio/Ratio Set 1:

Alaskite Sample:

Pot./Prop.	d	e	f	SUM	a	b	c
52405	0.37	2.01	2.00	4.38	8.4	45.9	45.7
5240501	0.38	2.33	1.95	4.66	8.2	50.0	41.8
5240502	0.29	2.72	2.39	5.40	5.4	50.4	44.3
5240503	0.31	2.43	2.44	5.18	6.0	46.9	47.1
5240504	0.36	2.15	2.13	4.64	7.8	46.3	45.9
5240505	0.32	2.59	2.10	5.01	6.4	51.7	41.9
5240506	0.31	2.26	2.45	5.02	6.2	45.0	48.8
5240507	0.32	2.50	2.24	5.06	6.3	49.4	44.3
5240508	0.35	2.07	2.07	4.49	7.8	46.1	46.1
Phyllic	d	e	f	SUM	a	b	c
52406	0.42	1.82	1.77	4.01	10.5	45.4	44.1
5240601	0.38	2.06	2.00	4.44	8.6	46.4	45.0
5240602	0.36	2.25	2.01	4.62	7.8	48.7	43.5
5240603	0.40	2.09	1.84	4.33	9.2	48.3	42.5
5240604	0.37	2.27	1.88	4.52	8.2	50.2	41.6
5240605	0.41	1.96	1.87	4.24	9.7	46.2	44.1
5240606	0.35	2.28	2.18	4.81	7.3	47.4	45.3
5240607	0.40	2.20	1.75	4.35	9.2	50.6	40.2
5240608	0.44	1.80	1.76	4.00	11.0	45.0	44.0
Prop.	d	e	f	SUM	a	b	c
52603	0.41	1.73	2.22	4.36	9.4	39.7	50.9
5260301	0.45	1.57	2.04	4.06	11.1	38.7	50.2
5260302	0.43	1.73	2.16	4.32	10.0	40.0	50.0
5260303	0.39	1.79	2.24	4.42	8.8	40.5	50.7
5260304	0.33	2.08	2.73	5.14	6.4	40.5	53.1
5260305	0.38	1.66	2.41	4.45	8.5	37.3	54.2
5260306	0.50	1.42	2.11	4.03	12.4	35.2	52.4
5260307	0.34	1.79	2.66	4.79	7.1	37.4	55.5
5260308	0.42	1.71	2.10	4.23	9.9	40.4	49.7
Vegetation Sample:	d	e	f	SUM	a	b	c
Manzanita 98	0.40	1.73	1.81	3.94	10.2	43.9	45.9
Lt. Clrd. Bush 99	0.47	1.89	1.62	3.98	11.8	47.5	40.7
Palo Verde 911	0.35	2.58	1.65	4.58	7.7	56.3	36.0

Actual and Normalized Reflectance Ratio Values.

Ratio/Ratio Set 1:

Quartz Monzonite Sample:

Prop.	d	e	f	SUM	a	b	c
52602	0.52	1.63	1.67	3.82	13.6	42.7	43.7
5260201	0.54	1.63	1.61	3.78	14.3	43.1	42.6
5260202	0.50	1.73	1.72	3.95	12.7	43.8	43.5
5260203	0.46	1.84	1.77	4.07	11.3	45.2	43.5
5260204	0.48	1.72	1.80	4.00	12.0	43.0	45.0
5260205	0.54	1.67	1.59	3.80	14.2	43.9	41.8
5260206	0.51	1.78	1.65	3.94	12.9	45.2	41.9
5260207	0.42	1.95	2.07	4.44	9.5	43.9	46.6
5260208	0.50	1.59	1.65	3.74	13.4	42.5	44.1

Dacite Porphyry Sample:

Potassic	d	e	f	SUM	a	b	c
52604	0.40	2.43	1.64	4.47	8.9	54.4	36.7
5260401	0.42	2.72	1.36	4.50	9.3	60.4	30.3
5260402	0.42	2.11	1.59	4.12	10.2	51.2	38.6
5260403	0.38	2.49	1.66	4.53	8.4	55.0	36.6
5260446	0.34	2.80	1.89	5.03	6.8	55.7	37.6
5260447	0.37	2.53	1.88	4.78	7.7	52.9	39.3
5260448	0.36	2.68	1.83	4.87	7.4	55.0	37.6

Phyllic	d	e	f	SUM	a	b	c
52605	0.40	2.43	1.62	4.45	9.0	54.6	36.4
5260551	0.44	2.31	1.52	4.27	10.3	54.1	35.6
5260552	0.42	2.67	1.50	4.59	9.2	58.2	32.7
5260553	0.45	2.17	1.49	4.11	10.9	52.8	36.3
5260554	0.42	2.18	1.64	4.24	9.9	51.4	38.7
5260555	0.39	2.40	1.57	4.36	8.9	55.0	36.0
5260556	0.37	2.82	1.59	4.78	7.7	59.0	33.3
5260557	0.43	2.13	1.40	3.96	10.9	53.8	35.4
5260558	0.40	2.18	1.75	4.33	9.2	50.3	40.4

Limestone Sample:	d	e	f	SUM	a	b	c
52403	0.67	1.36	1.33	3.36	19.9	40.5	39.6
5240301	0.65	1.41	1.37	3.43	19.0	41.1	39.9
5240302	0.62	1.45	1.43	3.50	17.7	41.4	40.9
5240303	0.75	1.21	1.28	3.24	23.1	37.3	39.5
5240304	0.59	1.53	1.54	3.66	16.1	41.8	42.1
5240305	0.57	1.50	1.50	3.57	16.0	42.0	42.0
5240306	0.64	1.51	1.38	3.53	18.1	42.8	39.1

Actual and Normalized Reflectance Ratio Values.

Ratio/Ratio Set 2:

Alaskite Sample:

Pot./Prop.	d	e	f	SUM	a	b	c
52405	0.37	2.01	1.36	3.74	9.9	53.7	36.4
5240501	0.39	2.33	1.12	3.84	10.2	60.7	29.2
5240502	0.29	2.72	1.27	4.28	6.8	63.6	29.7
5240503	0.31	2.43	1.36	4.10	7.6	59.3	33.2
5240504	0.37	2.15	1.28	3.80	9.7	56.6	33.7
5240505	0.32	2.59	1.22	4.13	7.7	62.7	29.5
5240506	0.31	2.26	1.44	4.01	7.7	56.4	35.9
5240507	0.31	2.50	1.26	4.07	7.6	61.4	31.0
5240508	0.35	2.07	1.38	3.80	9.2	54.5	36.3
Phyllic	d	e	f	SUM	a	b	c
52406	0.42	1.82	1.31	3.55	11.8	51.3	36.9
5240601	0.38	2.06	1.25	3.69	10.3	55.8	33.9
5240602	0.36	2.25	1.22	3.83	9.4	58.7	31.9
5240603	0.40	2.09	1.19	3.68	10.9	56.8	32.3
5240604	0.37	2.27	1.21	3.85	9.6	59.0	31.4
5240605	0.40	1.96	1.24	3.60	11.1	54.4	34.5
5240606	0.36	2.28	1.25	3.89	9.3	58.6	32.1
5240607	0.40	2.20	1.14	3.74	10.7	58.8	30.5
5240608	0.45	1.80	1.24	3.49	12.9	51.6	35.5
Prop.	d	e	f	SUM	a	b	c
52603	0.42	1.73	1.40	3.55	11.8	48.7	39.4
5260301	0.46	1.57	1.50	3.53	13.0	44.5	42.5
5260302	0.42	1.73	1.35	3.50	12.0	49.4	38.6
5260303	0.40	1.79	1.40	3.59	11.1	49.9	39.0
5260304	0.34	2.08	1.45	3.87	8.8	53.7	37.5
5260305	0.38	1.66	1.56	3.60	10.6	46.1	43.3
5260306	0.50	1.42	1.40	3.32	15.1	42.8	42.1
5260307	0.35	1.79	1.61	3.75	9.3	47.7	43.0
5260308	0.42	1.71	1.37	3.50	12.0	48.9	39.1
Vegetation Sample:	d	e	f	SUM	a	b	c
Manzanita 98	0.39	1.73	1.45	3.57	10.9	48.5	40.6
Lt. Clrd. Bush 99	0.46	1.89	1.14	3.49	13.2	54.1	32.7
Palo Verde 911	0.35	2.58	1.10	4.03	8.7	64.0	27.3

Actual and Normalized Reflectance Ratio Values.

Ratio/Ratio Set 2:

Quartz Monzonite Sample:

Prop.	d	e	f	SUM	a	b	c
52602	0.52	1.63	1.19	3.34	15.6	48.8	35.6
5260201	0.54	1.63	1.15	3.32	16.3	49.1	34.6
5260202	0.50	1.73	1.15	3.38	14.8	51.2	34.0
5260203	0.47	1.84	1.18	3.49	13.5	52.7	33.8
5260204	0.48	1.72	1.20	3.40	14.1	50.6	35.3
5260205	0.54	1.67	1.11	3.32	16.3	50.3	33.4
5260206	0.51	1.78	1.10	3.39	15.0	52.5	32.5
5260207	0.42	1.95	1.23	3.60	11.7	54.2	34.2
5260208	0.50	1.59	1.27	3.36	14.9	47.3	37.8

Dacite Porphyry Sample:

Potassic	d	e	f	SUM	a	b	c
52604	0.40	2.43	1.04	3.87	10.3	62.8	26.9
5260401	0.42	2.72	0.86	4.00	10.5	68.0	21.5
5260402	0.42	2.11	1.12	3.65	11.5	57.8	30.7
5260403	0.38	2.49	1.04	3.91	9.7	63.7	26.6
5260446	0.35	2.80	1.04	4.19	8.4	66.8	24.8
5260447	0.37	2.53	1.08	3.98	9.3	63.6	27.1
5260448	0.35	2.68	1.05	4.08	8.6	65.7	25.7

Phyllic	d	e	f	SUM	a	b	c
52605	0.40	2.43	1.01	3.84	10.4	63.3	26.3
5260551	0.44	2.31	0.99	3.74	11.8	61.8	26.5
5260552	0.42	2.67	0.89	3.98	10.6	67.1	22.4
5260553	0.45	2.17	1.04	3.66	12.3	59.3	28.4
5260554	0.41	2.18	1.10	3.69	11.1	59.1	29.8
5260555	0.39	2.40	1.05	3.84	10.2	62.5	27.3
5260556	0.37	2.82	0.95	4.14	8.9	68.1	23.0
5260557	0.43	2.13	1.08	3.64	11.8	58.5	29.7
5260558	0.39	2.18	1.15	3.72	10.5	58.6	30.9

Limestone Sample:	d	e	f	SUM	a	b	c
52403	0.67	1.36	1.11	3.14	21.3	43.3	35.4
5240301	0.65	1.41	1.10	3.16	20.6	44.6	34.8
5240302	0.63	1.45	1.12	3.20	19.7	45.3	35.0
5240303	0.76	1.21	1.10	3.07	24.8	39.4	35.8
5240304	0.60	1.53	1.11	3.24	18.5	47.2	34.3
5240305	0.57	1.50	1.16	3.23	17.6	46.4	35.9
5240306	0.65	1.51	1.04	3.20	20.3	47.2	32.5

REFERENCES

Abrams, M.J., Brown, D., Lepley, L., and Sadowsky, R., 1983, Remote sensing for porphyry copper deposits in southern Arizona: Econ. Geol., v. 78, pp. 591 - 604.

Bouma, P.J., 1971, Physical Aspects of Colour, de Groot, W., Kruithof, A.A., and Ouweltjes, J.L., eds., 2nd ed., MacMillan and Co., LTD., London, England, 280p.

Buckingham. F., and Sommer, S.E., 1983, Mineralogical characterization of rock surfaces formed by hydrothermal alteration and weathering-application to remote sensing: Econ. Geol., v. 78, pp. 664 - 674.

Clulow, F.W., 1972 Color: Its Principles and Their Applications, Morgan and Morgan Inc., New York, NY, 236p.

Goetz, A.F.H., Rock, B.N., and Rowan, L.C., 1983, Remote sensing for exploration: An overview : Econ. Geol., v. 78, pp. 573 - 590.

Graybeal, F.T., 1982, Geology of the El Tiro area, In, Titley, S.F., ed., Advances in Geology of the Porphyry Copper Deposits: Tucson, Univ. of Ariz. Press, pp. 487 - 505.

Hunt, G.R., Salisbury, J.W., and Lenhoff, C.J., 1971a, Visible and near infrared spectra of minerals and rocks: III. oxides and hydroxides: Modern Geology, v. 2, pp. 195 - 205.

_____, 1971b, Visible and near infrared spectra of minerals and rocks-IV: sulphides and sulphates: Modern Geology, v. 3, pp. 1 - 14.

_____, 1973a, Visible and near infrared spectra of minerals and rocks: VII. acidic igneous rocks: Modern Geology, v. 4, pp. 217 - 224.

_____, 1973b, Visible and near infrared spectra of minerals and rocks: VIII. Intermediate igneous rocks: Modern Geology, v. 4, pp. 237 - 244.

_____, 1974, Visible and near infrared spectra of minerals and rocks: IX. Basic and ultrabasic igneous rocks: Modern Geology, v. 5, pp. 15 - 22.

Hunt, G.R., and Salisbury, J.W., 1976a, Visible and near infrared spectra of minerals and rocks: XI. Sedimentary rocks: Modern Geology, v. 5, pp. 211 - 217.

_____, 1976b, Visible and near infrared spectra of minerals and rocks: XII. Metamorphic rocks: Modern Geology, v. 5, pp. 219 - 228.

Hunt, G.R., 1977, Spectral signatures of particulate minerals in the visible and near infrared: Geophysics, v. 42, no. 3, pp. 501 - 513.

_____, and Salisbury, J.W., 1978, Assessment of Landsat filters for rock type discrimination, based on intrinsic information in laboratory spectra: Geophysics, v. 43, no. 4, pp. 738 - 747.

Hunt, G.R., and Ashley, R.P., 1979, Spectra of altered rocks in the visible and near infrared: Econ. Geol., v.74, pp. 1613 - 1629.

Judd, D.B., and Wyszechi,G., 1975, Color in Business, Science and Industry, 3rd ed., John Wiley & Sons, New York, 553p.

Kerr, P.F., 1951, Alteration features at Silver Bell, Arizona: Geol. Soc. America Bull., v. 62, pp. 452 - 480.

Lillesand, T.M., and Kieffer, R.W., 1979, Remote Sensing and Image Interpretation, John Wiley & Sons, New York, 612p.

Loghry, J.D., 1972, Characteristics of favorable cappings from several southwestern porphyry copper deposits: Unpub. M.S. Thesis, Univ. of Az., Tucson, 112p.

Prost, G., 1980, Alteration mapping with airborne multispectral scanners: Econ Geol., v. 75, pp. 894 - 906.

Realmuto, V.J., 1984, Application of digital imagery to mineral exploration: Lone Star mining district, Graham County, Arizona: Unpub. M.S Thesis, Univ. of Ariz., Tucson, 89p.

Richard, K., and Courtright, J., 1966, Structure and mineralization at Silver Bell, Arizona, In Titley, S.R., and Hicks, C., eds., Geology of the Porphyry Copper Deposits: Univ. of Arizona Press, Tucson, Ariz., 560p.

Rowan, L.C., Goetz, A.F.H., and Ashley, R.P., 1977, Discrimination of hydrothermally altered and unaltered rocks in visible and near infrared multispectral images: Geophysics, v. 42, no. 3, pp. 522 - 535.

Schowengerdt, R.A., 1983, Techniques for Image Processing and Classification in Remote Sensing, Academic Press, New York, NY, 249p.

Siegal, B.S., and Gillespie, A.R., 1980, Remote Sensing in Geology, John Wiley & Sons, New York, NY, 702p.

Slater, P.N., 1985, Survey of multispectral imaging systems for earth observations: Remote Sensing of Environment, v. 17, no.1, pp. 85 - 102.

Vaca Hills NE Quadrangle, Arizona-Pima Co., 7.5 Minute Orthophotoquad, 1972, U.S.G.S.

Whitney, C.G., Abrams, M.J., and Goetz, A.F.H., 1983, Mineral discrimination using a portable ratio-determining radiometer: Econ. Geol., v. 78, pp. 688-698.